Università degli Studi di Cagliari

# PhD DEGREE IN
# MOLECULAR AND TRANSLATIONAL MEDICINE

Cycle XXXII

# SPATIAL ORGANIZATION OF LAMIN A/C

# IN HODGKIN'S LYMPHOMA AND MULTIPLE MYELOMA

BIO/13 APPLIED BIOLOGY

PhD Student:                                    Fabio Contu

Coordinator of the
PhD Program:                                   Prof. Sebastiano Banni

Supervisors:                                   Prof. Roberta Vanni
                                               Prof. Sabine Mai

Final exam. Academic Year 2018 – 2019
Thesis defence: January-February 2020 Session

*This work is dedicated to my brother Luca,*
*Hodgkin's Lymphoma survivor, and to all cancer patients out there.*
*This is for you who are still fighting,*
*for you who won the battle, and for you who lost it.*

# THESIS INDEX

# LIST OF ABBREVIATIONS

2D – Two-dimensional

3D – Three-dimensional

Ab – antibody

ABVD - Doxorubicin, bleomycin, vinblastine, dacarbazine

Akt/PKB - Protein Kinase B

ALT - Alternative Lengthening of Telomeres

AP1 – Activator protein 1

ATM – ATM serine/threonine kinase

ATR - ATR serine/threonine kinase

AWS - Atypical Werner Syndrome

BAF - Barrier-to-autointegration factor

BCA - Bicinchoninic Acid

BCL-2 - B-cell lymphoma 2

BCL-6 - B-cell lymphoma 6

BCMA - B-cell maturation antigen

BCR – B-cell Receptor

BFB - breakage-bridge-fusion

BM - Bone Marrow

BOB.1 - Oct-binding factor-1

BRAF – B- RAF Proto-Oncogene Serine/Threonine-Protein Kinase

BSA - Bovine serum albumin

BubR1/BUB1B - Budding Uninhibited By Benzimidazoles 1

CAMs - Cell Adhesion Molecules

Cas9 - CRISPR associated protein 9

CD - Cluster of Differentiation

CD95L - Cluster of Differentiation 95 Ligand

CENP-E - Centromere protein E

ChIP–qPCR - Chromatin Immunoprecipitation Quantitative Reverse Transcription PCR

CHK1 - Checkpoint kinase 1

CHK2 - Checkpoint kinase 2

cHL – Classical Hodgkin's Lymphoma

CHLVPP - Chlorambucil, vinblastine, procarbazine, prednisone

CIN – Chromosomal Instability

$CO_2$ – Carbon Dioxide

CREB – cAMP response elements binding transcription factor

CRISPR - Clustered Regularly Interspaced Short Palindromic Repeats

CSR – Class Switch Recombination

CTCs - Circulating tumor cells

CTLs – Cytotoxic T-Lymphocytes

Cy3 – Cyanine 3

Cy5 – Cyanine 5

DAPI - 4′,6-diamidino-2-phenylindole

DDR - DNA-damage response

DHFR - Dihydrofolate Reductase

DMD - Duchenne muscular dystrophy

DNA - Deoxyribonucleic acid

DSBs - Double-Strand Breaks

dsDNA - Double-stranded DNA

DZ – Dark Zone

EBER - Epstein-Barr encoded small RNAs

EBF - Early B cell factor

EBV - Epstein-Barr Virus

EDMD - Emery-Dreifuss muscular dystrophy

ER - Endoplasmic reticulum

EtOH – Ethanol

ETS - E26 transformation-specific

FBS - Fetal bovine serum

FGF1/2 - Fibroblast Growth Factors ½

FGFR3 - Fibroblast Growth Factor 3

FICTION - Fluorescence immune-phenotyping and interphase cytogenetics analysis

FITC - Fluorescein isothiocyanate

FoxO - Forkhead box O

GAPDH - Glyceraldehyde 3-phosphate dehydrogenase

GC – Germinal Center

GF - Growth Factor

GFP - Green Fluorescent Protein

GLUT1 - Glucose Transporter 1

H – Hodgkin

H&E - Haemotoxylin and Eosin

H2A – Histone Protein 2A

H2B – Histone Protein 2A

H3 – Histone Protein 3

H3K9me3 - Histone H3 at position lysine 9

H4 – Histone Protein 4

Ha95 – Homologue of A-kinase anchor protein 8-like

HCl - Hydrochloric acid

HGPS - Hutchinson Gilford Progeria Syndrome

HL – Hodgkin's Lymphoma

H-MM - Hyperdiploid Multiple Myeloma

HP1 - Heterochromatin Protein 1

hTERT – Human Telomerase Reverse Transcriptase

hTR – Human Telomerase RNA

$I_e$ - External lamin A/C intensity

IgH – Heavy Chain of the Immunoglobulin

IgL – Light Chain of the Immunoglobulin

IgV – Variable portion of the Immunoglobulin

IHC – Immunohistochemistry

$I_i$ - Internal lamin A/C intensity

IKK - IκB kinase

IL – Interleukin

INM – Inner Nuclear Membrane

ITLs - Interstitial t-loops

ITSs - Interstitial telomeric sequences

kD – Kilo Dalton

L&H - Lymphocytic and Histiocytic cells

LADs - Lamina-associated domains

LAMP1 - Lamina-associated proteins 1

LAMP2 - Lamina-associated proteins 2

LBR – Lamin B Receptor

LC - Light Chain

LDCHL - Lymphocyte Depleted Classical Hodgkin's Lymphoma

LKB1 - Liver Kinase B1

LMP1 - Latent Membrane Protein-1

LMP2 - Latent Membrane Protein-2

LP - Lymphocyte Predominant

LPS – Lipopolysaccharide

LRCHL - Lymphocyte Rich Classical Hodgkin's Lymphoma

Mad1 - Mitotic arrest-deficient 1

Mad2 - Mitotic arrest-deficient 2

MAFs - Musculoaponeurotic Fibrosarcoma

MAN1 - Membrane Protein 1

MAPK - Mitogen-Activated Protein Kinase

MCCHL - Mixed Cellularity Classical Hodgkin's Lymphoma

MDM2 - Mouse double minute 2 homolog

MEFs - Mouse embryo fibroblast

MGUS - Monoclonal Gammopathy of unknown significance

MM – Multiple Myeloma

MMR - Mismatch Repair

mRNA - Messenger Ribonucleic acid

MSI – Microsatellite Instability

mTOR - Mammalian Target of Rapamycin

mTORC1 - mechanistic target of rapamycin complex 1

mTORC2 - mechanistic target of rapamycin complex 2

MYCC – Cellular MYC Proto-oncogene

NaCl - Sodium chloride

NBEA - Neurobeachin

nCIN – Numerical Chromosomal Instability

NEMO - Inhibitor of Nuclear Factor Kappa B Kinase

NF-κB - Nuclear Factor κ B

NH-MM – Non Hyperdiploid Multiple Myeloma

NIH - National Institute of Health

NK – Natural Killer

NLPHL - Nodular Lymphocyte Predominant Hodgkin's Lymphoma

NPC - Nuclear Pore Complexes

NSCHL - Nodular Sclerosis Classical Hodgkin's Lymphoma

OCT-2 - Organic cation transporter 2

p21 – Protein 21

p53 – Protein 53

PAX5 - Paired Box 5

PBLs - Peripheral blood lymphocytes

PBS - Phosphate-buffered saline

PD1 - Programmed Death 1

PDGF - Platelet-derived Growth Factor

PD-L1 - Programmed Death-Ligand 1

PD-L2 - Programmed Death-Ligand 2

PI3K - Phosphoinositide 3-Kinase

PIP3 - Phosphatidylinositol (3,4,5)-trisphosphate

PNA - Peptide nucleic acid

POT1 - Protection of telomeres 1

pRb/RB1 - Retinoblastoma Protein

PSF - Point spread function

PTEN - Phosphatase And Tensin Homolog

Q-FISH - Quantitative Fluorescent in situ hybridization

qRT-PCR - Real-Time Quantitative Reverse Transcription PCR

RAF - RAF Proto-Oncogene Serine/Threonine-Protein Kinase

RANK - Receptor Activator of Nuclear Factor κ B

RAP1 - Ortholog of yeast Rap1

RAS - RAS Proto-Oncogene GTPase

REL - REL Proto-Oncogene NF- κB Subunit

RI – Refractive Index

RIPA - Radioimmunoprecipitation assay buffer

RNA - Ribonucleic acid

RPMI - Roswell Park Memorial Institute

RS – Reed-Sternberg

RT – Room Temperature

S.D. – Standard Deviation

sCIN – Structural Chromosomal Instability

SDS - Sodium dodecyl sulfate

SFLC - Serum Free Light Chain

SIM – Structured Illumination Microscopy

siRNA - Silencing Ribonucleic acid

siRNA – Silencing Ribonucleic acid

SKY – Spectral Karyotyping

SMM – Smoldering Multiple Myeloma

SOS - Son of Sevenless

Sp1 - Specificity Protein 1

Sp3 - Specificity Protein 3

Src - Proto-oncogene tyrosine-protein kinase Src

SSBs - Single-Strand Breaks

SSC - Saline Sodium Citrate

ssDNA - Single-stranded DNA

SUN - Sad1/Unc-84 Protein

Suv39h1 - Suppressor of Variegation 3-9 Homolog 1

TACI - Transmembrane activator and CAML interactor

TAs – Telomere Aggregates

TBST - Tris-buffered saline Tween 20

TCF3 - Transcription factor 3

TCR – T Cell Receptor

TERRA - Telomeric Repeat-containing RNA

TF – Transcription Factor

TGFα - Tumor Growth Factor α

TGFβ - Tumor Growth Factor β

Th1 – T Helper 1

TIN2 - TRF1-interacting nuclear factor 1

TP53 - Tumor Protein 53

TPP1 - Telomere Protection Protein 1

TRF1 - Telomeric repeat-binding factor 1

TRF2 - Telomeric repeat-binding factor 2

TSC 1 - Tuberous sclerosis 1

TSC 2 - Tuberous sclerosis 2

UV - Ultra-Violet

VEGF - Vascular Endothelial Growth Factor

WB - Western Blot

WHO - World Health Organization

Wnt - Wingless-Type

# **ABSTRACT**

Genomic Instability is a complex phenomenon observed both at the DNA and the chromosome level. It is responsible for the generation of mutations and chromosomal rearrangements, which can potentially lead to tumor development. A common genomic instability feature found in some malignant tumors is the shortening of the telomeres, the end of the chromosomes. Shortening of telomeres leads to the formation of anaphase bridges, subsequent breakage and initiation new breakage-bridge-fusion (BFB) cycles. Classical Hodgkin's lymphoma (cHL) and Multiple Myeloma (MM) are two blood tumor both characterized by genomic instability. cHL is a B-Cell lymphoma comprised of mononuclear Hodgkin cells (H) and bi- to multi-nucleated Reed-Sternberg (RS) cells, both characterized by numerical (nCIN) and structural chromosomal instability (sCIN). Transition from H to RS cells is correlated with aberrant number of mitotic spindles, aberrant 3D telomere organization, increase in the number of telomere aggregates and telomere loss. Advanced shortening of telomeres leads disruption of 3D interaction of the telomere with TRF2, a member of the shelterin proteins responsible for the protection of the chromosome ends from the DNA damage repair system. MM, an incurable plasma cell disorder, is also characterized by CIN, microsatellite instability (MSI), and telomere attrition. Lamin A/C, a nuclear envelope protein and component of the nuclear matrix, is important for the assembly of the mitotic spindles and for the maintenance of the 3D telomeres architecture by binding the shelterin protein TRF2. Due to lamin A/C involvement in the maintenance of genomic stability, our goal was to investigate lamin A/C 3D spatial organization in cHL and MM, and understand whether the localized uncapping of TRF2 from telomeres leads to their detachment from the nuclear matrix component lamin A/C causing genomic instability. Western blot analysis and qRT-PCR analysis revealed that H and RS are characterized by an overall overexpression of lamin A/C when compared to the B-lymphocytes control. Three dimensional (3D) fluorescent microscopy in cHL and MM cells revealed that the regular homogeneous lamin A/C pattern identified in normal activated B-lymphocytes, was replaced by an aberrant lamin A/C 3D spatial distribution characterized by the presence of internal lamin A/C structures. Different lamin A/C patterns where observed where the internal lamin A/C sub-divided the nucleus in to two or multiple compartments, suggesting a possible involvement of lamin A/C in the multi-nucleation process. To investigate lamin A/C involvement in the multinucleation process and transition from H to RS, the downregulation of lamin A/C with siRNA was performed. Downregulation of lamin A/C affected the transition from H to RS cells, as the number of RS cells found after lamin silencing was decreased. Telomere 3D structure and nuclear organization were also affected by the deregulation of lamin A/C. H and RS cells were also characterized by unbinding of telomere-TRF2-lamin A/C when compared to the healthy control.

Lack of co-localization of telomere-TRF2-lamin A/C confirms lamin A/C involvement in genomic instability, and suggests that localized absence of TRF2 could be causal to the genome remodeling in cHL.

# <u>INTRODUCTION</u>

**HALLMARKS OF CANCER AND GENOMIC INSTABILITY**

<u>Hallmarks of Cancer</u>

During malignant cellular transformation, the accumulation of mutations in cellular proto-oncogenes generates oncogenes with dominant gain of function, whereas mutations in tumor suppressor genes are responsible for recessive loss of function (Hanahan and Weinberg, 2000). In the early 2000, Hanahan and Weinberg predicted that despite the complexity and differences among different tumors, oncogenesis could be described in terms of a small number of common underlying principles which became known as the six "hallmarks of cancer". These include self-sufficiency in growth signals, insensitivity to growth-inhibitory (antigrowth) signals, evasion of programmed cell death (apoptosis), limitless replicative potential, sustained angiogenesis, and tissue invasion reflect genetic alterations that drive the progressive and metastasis (Hanahan and Weinberg, 2000). Later in 2011, Hanahan and Weinberg updated the list with the latest progresses made in the field, adding other two hallmarks, *i.e.* the reprogramming of energy metabolism and the evasion from immune destruction, and the characterization of two enabling tumor characteristics which facilitate the acquisition of both the core and emerging hallmarks, *i.e.* genomic instability and tumor promoting inflammation (Hanahan and Weinberg, 2011).

While normal cells require growth factor (GF) stimulation from the microenvironment to proliferate, tumor cells show reduced dependence on external GF due to the acquired ability to synthetize endogenous GFs such as platelet-derived growth factor (PDGF) and tumor growth factor (TGFα) combined with GF receptor overexpression (Fedi et al., 1997). Another important pathway developed by cancer cells to acquire independence from GF stimulation is by alteration of the downstream SOS-RAS-RAF-MAPK pathway (Medema and Bos, 1993). The activation of this pathway has been found in cancer cells with mutations in BRAF and RAS (Davies and Samuels, 2010). Mutations of BRAF and RAS, as well as mutations in the catalytic subunit of phosphoinositide 3-kinase (PI3K) isoforms, lead to hyperactivate the PI3K signaling circuitry, including its key Akt/PKB signal transducer (Jiang and Liu, 2009; Yuan and Cantley, 2008).

In normal cells, cellular quiescence is maintained by balancing the activity of GFs and antiproliferative signals. During the cell cycle, molecules like the TGFβ allow hypophosphorylation of the retinoblastoma protein (pRb), causing a downstream block of the cell proliferation due to sequestration of the E2F transcription factors (Datto et al., 1997; Hannon and Beach, 1994; Weinberg,

1995). Cell-to-cell contacts mediate an antiproliferative effect suppressing further cell proliferation; however, such contact inhibition is abolished in various types of cancer cells, due to suppression of Merlin and LKB1 expression (Curto et al., 2007; Partanen et al., 2009).

Evasion from programmed cell death, or apoptosis, is a feature that allows tumor cells to proliferate without regulation. p53, encoded by tumor suppressor gene TP53, is a DNA damage checkpoint protein that responds to genotoxic- and oncogene-induced DNA damage and it is subject to selective pressure for the inactivation in cancer. Loss of p53 function, and early event which occurs in more than 50 percent of human cancers (Olivier et al., 2010), is correlated with the escape of the cell from apoptotic/senescence effects and oncogenesis (Bartkova et al., 2005, 2007; Di Micco et al., 2006; Gorgoulis et al., 2005). Upregulation of the oncogene *bcl-2* and *MYCC* have been correlated with anti-apoptotic effects (McDonnell and Korsmeyer, 1991; Vaux et al., 1988).

Growth signal autonomy, insensitivity to anti-growth signals and evasion from apoptosis lead to uncoupling of cell growth programs from the cellular microenvironment. However, these three components by themselves are not enough for expansive tumor growth due to limited cell multiplication capability (Hayflick, 1997). The telomeres, the ends of the chromosomes, are involved in the regulation of cellular replicative lifespan, since with every cell division the telomeres shorten, blocking further cell division and inducing senescence (Gilley and Blackburn, 1994). Hayflick termed this the definite life span of normal cells, which is since called the "Hayflick limit" (Hayflick, 1965; Hayflick and Moorhead, 1961).

It has been demonstrated, however, that malignant tumor cells show active telomere maintenance through upregulation of the telomerase enzyme (Bryan and Cech, 1999) and/or through the alternative lengthening of telomeres (ALT), which maintains telomeres through recombination-based intrachromosomal recombination (Bryan et al., 1995).

Sustained angiogenesis is another key feature acquired during the oncogenetic process. Even if the proliferative capability can initially overcome the absence of nutrients and oxygen provided by the blood vessels, in order to progress to a larger size, the tumor cells need to develop the angiogenic ability (Bouck et al., 1996; Hanahan and Folkman, 1996). Angiogenesis-initiating signals are exemplified by vascular endothelial growth factor (VEGF) and acidic and basic fibroblast growth factors (FGF1/2) are commonly overexpressed in tumor cells (Singh et al., 1995), while on the other hand, angiogenesis inhibitor like thrombospondin-1, are downregulated (Volpert et al., 1997). The sixth hallmark of cancer is the acquired capability of tissue invasiveness and metastasis, where cells shed from the primary tumor to invade other tissues. One of the main reasons behind the acquisition of the metastatic potential is the loss of the E-cadherin function due to mutational inactivation of the E-cadherin or β-catenin genes, transcriptional repression, or proteolysis of the extracellular cadherin

domain (Christofori and Semb, 1999). Changes in expression of cell adhesion molecules (CAMs) appear to play critical roles in the tumor invasion and metastasis (Johnson, 1991) by upregulating matrix-degrading proteases genes while downregulating protease inhibitor genes (Stetler-Stevenson, 1999; Werb, 1997).

The tendency of tumor cells to use the glycolysis as main source of glucose processing even in presence of oxygen, instead of the classic citric acid cycle performed by the normal cells, has been described by Warburg (Warburg, 1956a, 1956b). The loss of energy that is caused by this reprogramming of metabolism, is however countered by an increase in the upregulation glucose transporters, like GLUT1, which substantially increase glucose import into the cytoplasm (DeBerardinis et al., 2008; Hsu and Sabatini, 2008; Jones and Thompson, 2009). An increased glycolysis allows the cell to use the glycolytic intermediates in various biosynthetic pathways to generate molecules such as nucleosides and amino acids, important for the biosynthesis of the macromolecules and organelles required for assembling new cells (Vander Heiden et al., 2009).

The capability of tumor cells to evade the destruction by the immune-system is currently one of the hot topics in cancer research. It has been demonstrated that mice deficient in the development or function of CD8+ cytotoxic T lymphocytes (CTLs), CD4+ Th1 helper T cells, or natural killer (NK) cells present with an increase in tumor incidence, meaning that both innate and adaptive immune system contribute to immune surveillance and tumor eradication (Kim et al., 2007; Teng et al., 2008). Cancer cells, however, have the capability to suppress infiltrating CTLs and NK cells, by secreting immunosuppressive cytokines as IL10 and TGFß, express CD95, which can induce apoptosis in CD95L-positive CTLs, and PD-L1 and PD-L2, which inhibit the activity of PD1+ CTLs (Shields et al., 2010; Wein and Küppers, 2016; Yang et al., 2010).


Genomic Instability

In general the acquisition of the hallmarks described by Hanahan and Weinberg is made possible mainly by two enabling characteristics: i) an inflammatory state of premalignant and malignant lesions that is driven by cells of the immune system and ii) the development of genomic instability in cancer cells, which generates random and non random mutations including chromosomal rearrangements, some of which can lead to the development of a certain mutant genotype which confers selective advantage on subclones of cells, allowing their outgrowth in the tissue (Hanahan and Weinberg, 2011).

Genomic instability is a complex phenomenon observed both at the DNA nucleotide level and at the chromosome level. However, the existence of genetic alterations in a tumor, even when frequent, does not mean that the tumor is genetically unstable (Lengauer et al., 1998). Instability is, by

definition, a matter of rate, whereas the existence of a mutation is a state, providing no information about the rate of its occurrence. In fact, instability is a process. Cells become prone to an increased propensity for genomic alterations, which accumulate during the cell cycles. The presence of genomic instability can provide to cancer cells different types of advantages, from shorter cell cycle, to the possibility of bypassing intracellular and immunological control systems, resulting in a growth advantage when compared to normal cells (Wei Dai, 2014).

Different are the known causes which lead to genomic instability. Physical stresses (like the UV light) and chemical stresses (like oxygen free radicals) can induce the formation of DNA-adducts which disturb nucleotide-pairing, blocking DNA replication and transcription, and leading to the formation of DNA single-strand breaks (SSBs) and double-strand breaks (DSBs) (Jackson and Bartek, 2009). To sense, signal and repair DNA damage, the cells have developed different mechanisms, known as DNA-damage response (DDR), where a major role in the DDR-signaling is played by the protein kinases ATM and ATR (Harper and Elledge, 2007; Rouse and Jackson, 2002). Defects in the DDR lead to tumor development (Gorgoulis et al., 2005).

Lack of accuracy during DNA replication has also been associated with genomic instability, since sequence changes at DNA base, i. e. substitutions or deletions or insertions of a few nucleotides as observed in numerous cancers which involve a missing or damaged p53 gene or a mutated ATM (Bailey et al., 2018; Greenman et al., 2007). Normally, DNA base mismatch would be corrected by different DNA mismatch repair (MMR) proteins, however, mutations in MMR genes have been associated with cancer development, and loss of MMR is associated with a significant fraction of sporadic cancers (Hsieh and Yamane, 2008).

Epigenetic changes can lead to genomic instability, since DNA methylation has been implicated in affecting stability within the genome of the microsatellites, which are particularly susceptible to length change mutations. Microsatellite repeat instability (MSI) is found in many diseases such as Huntington's, myotonic dystrophy, and cancer and is often associated with defects in the MMR machinery (Putiri and Robertson, 2011).

Defects in the maintenance of chromosome ploidy and structure have been correlated with genomic instability, and have been described as chromosome instability (CIN). Alterations in chromosome number (nCIN), which leads to aneuploidy, has been recently anti-correlated with expression of immune signaling genes due to decreased leukocyte infiltrates in high-aneuploidy sample (Taylor et al., 2018). Structural chromosome changes (sCIN), such as translocation, inversions and deletions, generate gene fusions (Zhang et al., 2018). Theodor Boveri was the first scientist who, by observing abnormal development of sea urchin and ascaris embryos in presence of aberrant chromosome number, suggested that chromosomes played a role in cellular cooperation, and supposed that

disrupted growth patterns in human cancers may result from chromosomal aneuploidy (Boveri, 1902; Boveri, 1914; Cheng and Loeb, 1993). As demonstrated by the presence of increased rate of CIN in transformed CHO cells with increased ploidy, the aneuploidy destabilizes the genome by unbalancing genes required for mitosis, resulting in the autocatalytic formation of randomly generated karyotypes due to recurrent segregation errors (Duesberg et al., 1998). Defects in the mitotic spindle assembly checkpoint, result in numerical aneuploidy and CIN (Kops et al., 2005). Deregulation of the expression of the mitotic checkpoint components Mad1, Mad2, or CENP-E leads to missegregation of one or more chromosomes per division, resulting in tumorogenesis, especially when coupled with other tumor-promoting activity, such as reduced rate of cell death (Weaver and Cleveland, 2009). Interestingly, high rates of CIN caused by complete depletion of Mad2 or BubR1 have been shown to cause rapid death in tumor cells (Kops et al., 2004; Michel et al., 2004).

Ongoing nCIN or sCIN lead to the production of genetically distinct populations of daughter cells (Bayani et al., 2007; Lepage et al., 2019). CIN is responsible for the increased intratumoral heterogeneity which may confer a selective growth advantage to a subpopulation of cells like increased cell proliferation, metastatic potential, or intrinsic drug resistance (Lee et al., 2011). Selective pressures, like the one promoted by the chemotherapy, potentially induce unregulated proliferation of cells harboring specific growth advantages (such as drug resistance), producing a highly aggressive or drug-resistant tumor (Gerlinger and Swanton, 2010).

Deregulation of proto-oncogenes like *Ras*, *HER2* and/or *MYCC* is correlated with genomic instability (Hanahan and Weinberg, 2011). Proto-oncogenes are often involved in stimulating cell growth and proliferation during embryogenesis, and some of them proto-oncogenes also negatively regulate cell differentiation. Improper regulation of the proto-due to point mutation, gene amplification and/or chromosomal translocation may induce tumorigenesis (Anderson et al., 1992). Proto-oncogene *MYCC*, in particular, is frequently overexpressed in human cancers, leading to many of the hallmarks associated with tumorigenesis, including autonomous proliferation, increased biogenesis and altered metabolism (Gabay et al., 2014; Mai and Mushinski, 2003). Overexpression of *MYCC* in CHO cells results in amplification and rearrangements of the dihydrofolate reductase (DHFR) gene (Mai et al., 1996a), and causes locus-specific and karyotypic instability (Felsher and Bishop, 1999; Mai et al., 1996a, 1996b; Rockwood et al., 2002). Previous studies demonstrated that functional p53 allele counter formation of large lobular mammary hyperplasia in transgenic mice, in the context of *MYCC* overexpression (McCormack et al., 1998). *MYCC* deregulation has also been implicated in CIN since it affects the regulation of Mad2 and BUB1B of the spindle assembly checkpoint (Menssen et al., 2007; Sansregret et al., 2018). Moreover, *MYCC* deregulation induces formation of DNA breaks (Vafa et al., 2002) and alterations of DNA repair system (Hironaka et al., 2003; Karlsson et al., 2003).

**TELOMERES**

Organization and Replication of Telomeres

Telomeres, the ends of linear chromosomes, are formed by heterochromatic structures, protecting chromosomes from degradation and repair activities. Their integrity is essential to ensure chromosomal stability. The telomeric heterochromatin contains repetitive non-coding DNA sequences.

On average, human telomeres span 10-15 kB (Blasco, 2005), and are characterized by a longer hexanucleotidic 5'-(TTAGGG)$_n$-3' tandem repeat sequence on the "sense" strand, also known as "G-rich" strand, and its shorter complement 5'-(CCCTAA)$_n$-3' on the "antisense" strand, also known as "C-rich" strand (Makarov et al., 1997; Moyzis et al., 1988). The spatial organization of the telomeres has been investigated during the years, and the current accepted model is characterized by two particular structures formed by the extra nucleotides present in the G-rich strand: a "t-loop" end structure, whose formation is influenced by a complex of proteins called shelterines (de Lange, 2005), and a "d-loop" structure, also called displacement loop, where the excess portion of the G-rich strand undermines a guanine-rich region of the same strand in order to interact with a cytosine-rich region of the complementary strand and to hide chromosome termini from unrestricted protein recognition of telomere ends as double-strand breaks (Greider, 1999; Nečasová et al., 2017; Van Ly et al., 2018). The human shelterin complex is composed of six proteins: TRF1, TRF2, RAP1, TIN2, TPP1 and POT1 (de Lange, 2005). In addition to inducing the t-loop, the shelterin proteins, are important for two main purposes: chromosomal end protection from DNA damage response, and the prevention of genomic information loss at chromosome ends. Telomere double-stranded DNA (dsDNA) binding protein TRF2 and single-stranded DNA (ssDNA) binding protein POT1 are responsible for the protection from DNA damage responses induced by ATM and ATR kinases, activated by p53 (Denchi and de Lange, 2007; He et al., 2006; Okamoto et al., 2013). TRF2 in particular is the main regulator of the formation of the t-loop (Doksani et al., 2013). Also TRF1, with its DNA bending activity, contributes to the t-loop formation (Bianchi et al., 1997). Other functions of TRF1 are the regulation of telomere replication during the S phase of the cell cycle (Sfeir et al., 2009) and the regulation of the telomerase by negative feedback through the recruitment of the shelterin protein TIN2, binding to the TPP1-POT1 complex on the single-stranded G-overhang (Okamoto et al., 2008; Ye et al., 2004).

The human telomerase is a RNA-dependent DNA polymerase protein complex responsible for the replication of the telomeric ends by addition of guanine-rich repetitive sequences and is composed of

two subunits: i) hTR (gene located on chromosome 3, q26.2 position), the RNA subunit complementary to the hexanucleotide repeat sequences of the telomeric sense strand; ii) hTERT (gene located on chromosome 5, p15.33), the enzymatic subunit that catalyzes the reaction of reverse transcription required for the maintenance of telomere length (Weinrich et al., 1997), which can only be active in the presence of shelterines (Palm and de Lange, 2008).

While in stem cells and germ-line cells the hTR and hTERT genes are constitutively expressed, these genes are epigenetically down-regulated in differentiated cells. The down-regulation leads to a gradual shortening of the telomeric DNA after each replication cycle, which culminates in an event called "senescence", a state of permanent cell-cycle arrests when telomere length is below a critical length (the "Hayflick limit"), leading to growth arrest and/or cell death (Hayflick, 1965; Levy et al., 1992). Cells in senescence display molecular markers characteristic of cells bearing DSBs, suggesting that dysfunctional telomeres induce DDR (d'Adda di Fagagna et al., 2003). Dysfunctional telomeres are in fact recognized as DSBs, affecting the p53 and/or pRB tumor suppressor pathways to induce expression of their regulators p21 and p16 Ink4a to initiate replicative senescence (Kamijo et al., 1997; Sage et al., 2003; Wright and Shay, 1992).

The levels of hTERT mRNA in differentiated cells are under strong transcriptional control (Akıncılar et al., 2016). Different transcription factors (TFs) regulate hTERT RNA transcription. hsp90 and Sp1 have been found to actively promote hTERT transcription by direct binding at the level of the GC-box of the promoter, and by physical association of hsp90 to hTERT, promoting telomerase activity by increasing the affinity of the enzyme complex to telomeric ends. (Kim et al., 2008). Other important TFs oncogenes play an important role in the activation of the promoter, such as MYCC, which has been found to induce gene transcription together with Sp1 (Wang et al., 1998), and the transcription factors of the ETS family. hTERT expression has been reported in about 90% of malignant tumors. As the main underlying mechanisms of hTERT upregulation, mutations and methylation of the hTERT promoter have been described in many tumors. The most common mutations found in the promoter are -124 C/T (C228T) and -146 C/T (C250T) (Liu and Xing, 2016). While both the mutations inhibit the hTERT gene silencing process in embryonic stem cells resulting in tumorigenesis, only the -124 C/T mutation leads to the formation of a new binding site for the ETS transcription factors, causing an increased transcription of the hTERT gene (Chiba et al., 2015).

In addition to telomerase-dependent pathways, lengthening of the telomeres by alternative mechanisms (alternative lengthening of the telomeres, ALT) has been reported in numerous tumors especially those arising from mesenchymal tissues including bone, soft tissues, neuroendocrine systems, peripheral nervous system and central nervous system (De Vitis et al., 2018; Dilley and Greenberg, 2015; Heaphy et al., 2011; Henson and Reddel, 2010). The ALT pathway is characterized

by heterogeneous and long telomere DNA and the formation of ALT-associated promyelocytic leukemia (PML) body (APB) (Nabetani and Ishikawa, 2011).

When telomeres are transcribed, they give rise to a class of long noncoding RNA called telomeric repeat-containing RNAs, or TERRA (Azzalin et al., 2007; Schoeftner and Blasco, 2008). TERRA play a role as scaffold molecule, promoting the recruitment of proteins and enzymatic activities at chromosome ends, but they are also involved in chromatin regulation, telomere maintenance and genome stability (Bettin et al., 2019). TERRA regulate the epigenetic signature of chromatin and gene expression at subtelomeres as well as extratelomeric loci. TERRA transcripts interact with heterochromatic marks, including H3K9me3 and HP1 proteins (Deng et al., 2009), the histone methyltransferase Suv39h1 (Porro et al., 2014) and with chromatin remodeling complexes (Postepska-Igielska et al., 2013; Scheibe et al., 2013). TERRA has been found to interact with shelterin protein TRF1 and TRF2 (Deng et al., 2009), together with other proteins involved in the telomerase activity and in the DNA-metabolism (Deng et al., 2009). TERRA transcripts participate in telomere protection at multiple chromosome ends, since absence of TERRA showed increased DNA damage at chromosome ends, telomere fusions, and decreased telomere length (Montero et al., 2016). In addition, TERRA is a direct target of different proteins like p53 (Tutton et al., 2016) and Rb (Gonzalez-Vasconcellos et al., 2017).


Telomeres Alterations and Genomic Instability

Short telomeres and their maintenance are considered one of the hallmarks of malignant tumors (Hastie et al., 1990; de Lange et al., 1990). Cancer cells, however, are able to overcome the limit to cell division imposed by critically short telomeres through the activation of the telomerase and/or the activation of the ALT pathway. As mentioned before, critically short telomeres which can no longer exert end-protective functions are described as dysfunctional.

While dysfunctional telomeres in normal cells lead to cell senescence, in cancer cells they lead to chromosomal breakage-bridge-fusion (BFB) cycles that initiate ongoing genomic instability (Deng et al., 2008; Lansdorp, 2009; Misri et al., 2008). These chromosomal fusions are a basis of genomic instability associated with telomere dysfunction as they lead to anaphase bridges and subsequent breakage which requires further repair. When the damaged chromosome replicates there are two possible outcomes: i) sister chromatids fuse and form a bridge during the anaphase, and the two centromeres of the fused sister chromatids are pulled into opposite poles of the dividing cell. After the bridge breaks, the resulting daughter cells receive defective chromosomes that lack telomeres and can initiate new BFB cycles (Croll et al., 2013). ii) two different chromosomes fuse together generating a dicentric chromosomes at anaphase. Following breakage of the fused chromosomes, the

DNA from one chromosome can be transferred to the second chromosome. The two resulting chromosomes are characterized by the lack of telomeric signals at chromosomal ends and interstitial telomere signals as result of previous BFB cycles (Mai and Garini, 2006; Murnane, 2012).

In humans, BFB cycles play a significant role in cancer progression (Bailey and Murnane, 2006; Gisselsson et al., 2000; Thompson and Compton, 2011).

The analysis of the telomere spatial distribution within the nucleus in normal cells during cell cycle revealed that during the G0/G1 and S phase the telomeres are dispersed throughout the nuclear space, while in late G2 phase, they localize into a telomeric disk (Chuang et al., 2004). Tumor cells, on the other hand are also characterized by telomeric aggregates (TAs), which can be defined as clusters of telomeres that, at the Abbe resolution of 200 nm, cannot be resolved further (Danescu et al., 2013; Vermolen et al., 2005). The TAs generation does not require the presence of critically short telomere or the upregulation of hTERT, but it is often correlated with telomere uncapping and is independent of telomerase (Knecht et al., 2009; Louis et al., 2005).

Deregulation of the expression of the MYCC oncogene has been found to be a cause of the generation of TAs. The number of TA cycles was proportional to the time of MYCC deregulation, but even if MYCC was responsible for the initiation of the TA cycles, the oncoprotein was no longer required for the downstream effects of subsequent cycles of TA formation (Louis et al., 2005).


**HODGKIN'S LYMPHOMA**


Anatomopathology of Hodgkin's Lymphoma

According to the National Institute of Health (NIH), Hodgkin's Lymphoma (HL) is a relatively rare but highly curable blood tumor, representing 0.5% of all new cancer cases in the United States. In 2018, it was estimated that there will be 8,500 new cases of HL and an estimated 1,050 people would die of this disease. According to the World Health Organization (WHO), HL can be divided into two main entities: Classical Hodgkin's Lymphoma (cHL) and Nodular Lymphocyte Predominant Hodgkin's Lymphoma (NLPHL) (Swerdlow et al., 2016). In both the cases, the lymph node anatomical architecture is disrupted, with the neoplastic cell population, composed of both mononuclear and multi-nuclear cells, representing only a small percentage of the entire cell population.

In NLPHL the tumor cells are referred as lymphocyte predominant (LP) cells, also known as lymphocytic and histiocytic cells (L&H), characterized by large multilobulated nuclei (called "popcorn cell"). Immunohistochemically, LP cells show a B cell phenotype, with the expression of

CD20, CD45, CD75, CD79a and transcription factors BOB.1, OCT-2 and BCL-6 (Carbone et al., 1998; Greiner et al., 2005). LP cells are negative for CD30, CD15 and Epstein-Barr Virus (EBV).

cHL is characterized by the presence of two population of tumor cells: the mononuclear Hodgkin (H) cells, and the bi- to multi-nuclear Reed Sternberg (RS) cells (Küppers, 2009). H cells represent around 1% of the entire cell population of the lymph node, while the RS cells represents less than 1% of the tumor cell population (Swerdlow et al., 2016). H and RS cells are positive for CD30 and CD15, while B cell lineage markers such as CD20 and CD79a are usually downregulated (Swerdlow et al., 2016). Also BOB.1, OCT-2 and the Sp-1 proto-oncogene are downregulated in H and RS cells (Hertel et al., 2002; Jundt et al., 2002; Re et al., 2001a; Stein, 2001; Torlakovic et al., 2001). Positivity to EBV, determined by Latent Membrane Protein-1 (LMP1) staining or Epstein-Barr encoded small RNAs (EBER) in situ hybridization, is also common in cHL, where they represent around 40% of the cases (Massini et al., 2009). Positivity for CD30 and presence of RS cells among the tumor cell infiltrate in the lymph node, is used for the diagnosis of cHL.

cHL lymphoma can be further differentiated into four histological subtypes: Nodular Sclerosis Classical Hodgkin's Lymphoma (NSCHL), Mixed Cellularity Classical Hodgkin's Lymphoma (MCCHL), Lymphocyte Depleted Classical Hodgkin's Lymphoma (LDCHL) and Lymphocyte Rich Classical Hodgkin's Lymphoma (LRCHL).


Molecular Biology of cHL

For many years, the origin of H and RS cells remained unresolved. Somatic hypermutation have been found in the IgV genes of both H and RS. Analysis of the rearranged immunoglobulin heavy and light (IgH and IgL respectively) revealed identical IgV gene rearrangements in the H and RS cells of a given HL case, establishing the monoclonal nature of these cell, indicating them as tumor cells. Since the process of somatic hypermutation is specifically active in antigen-activated mature B cells proliferating in the germinal center (GC) of the lymph node (Küppers et al., 1992), it was clear that H and RS cells derived from post germinal center B cells (Küppers et al., 1994; Marafioti et al., 2000). More specifically, H cells originate from pre-apoptotic germinal center B cells which have been rescued from apoptosis by cellular transformation events (Kanzler et al., 1996).

The Immunophenotypic expression analysis of surface antigens of RS cells was identical to the one of the H, indicating that the multinuclear cells originate from the mononuclear cells (Drexler et al., 1989).

The first hypothesis suggested for the potential mechanism of RS cell generation was based on H cells fusion (Drexler et al., 1989). However, molecular analysis of primary H and RS cells, led to the exclusion of such hypothesis, and the acytokinetic mitosis, which is defined as mitosis with nuclear

division without cellular division, was postulated as the most favorable hypothesis of mechanism (Küppers et al., 2001; Re et al., 2001b; Rengstl et al., 2014). However, acytokinetic mitotic events were not observed during time-lapsed microscopy studies, and while events where the two daughter cells were still connected by the midbody (incomplete cytokinesis) followed by re-fusion of the two cells was the mechanism which led to multinuclearity (Rengstl et al., 2014). Further studies showed how this endomitotic multinucleation process was strongly correlated with the presence of an aberrant number of mitotic spindles, aberrant 3D telomere organization, and telomere loss, which lead to the incapacity of sustain a proper chromosome segregation (Knecht et al., 2009).

H and RS cells are also characterized by a lack of expression of a functional B cell Receptor (BCR). One of the main reason why these tumor cells do not express functional BCR is the presence of the somatic hypermutation in the IgV genes, but also other mechanisms can lead to the same fate, like the downregulation of transcription factors such as BOB.1 and OCT-2 induced by the disruption of different pathways including the one regulated by EBF1, PAX5 and TCF3, which results into the loss of B-cell identity (Jundt et al., 2002; Re et al., 2001a).

An additional molecule which contributes to the downregulation of transcription factors normally expressed in B cells is Notch (Jundt et al., 2002). Activation of the Notch pathway following its binding to Jagged1, ligand expressed in H and RS surface, leads to degradation of TCF3, while increasing expression of the TCF3 inhibitor ABF1 (Jundt et al., 2008). Two main factors play a role in the activation of the Notch pathway: in EBV+ cHL, the latent membrane protein 2 (LMP2) produced by the virus can induce Notch expression (Portis et al., 2003), while in EBV- cHL, lack of expression of Deltex1, a Notch1 inhibitor, and overexpression of Mastermind-like-2, a Notch co-activator, are responsible for the activation of Notch (Jundt et al., 2008).

When the BCR is not functional in normal GC B cells, these cells quickly undergo apoptosis. However, H and RS cells are able to evade apoptosis through the deregulation of different pathways. One of the pathways is the NF-κB signaling pathway, which in cHL is constitutively activated (Bargou et al., 1996). Stimulation of TNF receptors like CD30, CD40, TACI, BCMA and RANK (Carbone et al., 1995; Chiu et al., 2007; Fiumara et al., 2001; Horie et al., 2002) and crosstalk between the Notch pathway and the NF-κB pathway (Schwarzer et al., 2012) can all lead to activation of NF-κB. Activation of the receptors leads to the activation of the IKK complex (composed of IKKα, IKKβ and NEMO), which phosphorylates and degrades the NF-κB inhibitors IκBα and IκBε. In EBV+ cHL, LMP1 can activate the NF-κB pathways functioning as a constitutively active homologue of CD40 (Lam and Sugden, 2003).


Genomic Instability in cHL

H and RS cells from cHL are characterized by chromosomal aberrations, including aneuploidy and chromosomal structural abnormalities as shown after fluorescence immunophenotyping and interphase cytogenetics analysis (FICTION) (Weber-Matthiesen et al., 1995). Aberrations from the normal positioning of chromosomes in H cells were detected, and the nuclear chromosome positions were reflected by chromosomal rearrangements as demonstrated by chromosome painting experiments followed up for all chromosomes using SKY. In particular, as H cells transition to RS cells, some nuclei show unequal chromosome distribution and others become 'ghost' nuclei, devoid of the normal DNA content (Guffei et al., 2010).

Fluorescence in situ hybridization studies revealed the presence of chromosomal translocations in the Ig loci, with the *IGH* loci being the most common, with partner genes like *BCL6*, *MYC*, *BCL3*, and *REL*, all commonly expressed in cHL. As result of these translocations, aberrant expression of BCL6, MYC and BCL3 transcription factors is observed and errors in VDJ, CSR, or somatic hypermutation processes (Martín-Subero et al., 2006). These translocations involved partners like (Martín-Subero et al., 2006).

As mentioned before, the transition from H to RS cells is correlated with aberrant number of mitotic spindles, aberrant 3D telomere organization, and telomere loss (Knecht et al., 2009). RS cells are also characterized by an increased number of mitotic spindles and multiple pairs of centrosomes which don't correlate with the number of nuclei (Knecht et al., 2009). Telomeres length and organization play a role in the H cells outcome: when the aberration of the telomeric 3D structure is not advanced, the endomitosis can still progress to generate additional nuclei leading to the formation of bi-nuclear RS cells, which can then become tri-, tetra- and multi-nuclear RS cells. However, when the number of TAs increases and the telomere are critically short, the endomitosis becomes impossible and the cells cannot perform further nuclear division, resulting in multinucleated end-stage RS cells characterized by a telomere-poor 'ghost' nucleus (Knecht et al., 2009). The presence of critically short telomeres in RS cells ("t-stumps") has been demonstrated to be completely independent from the EBV status of the cells, since both EBV+ and EBV- RS cells were characterized by high number of very short telomeres, a loss of total telomere mass and a significant increase of aggregates when compared with mononuclear H cells (Knecht et al., 2010). EBV protein LMP-1, however effects the expression levels of the shelterin proteins TRF1, TRF2, and POT1 (Lajoie et al., 2015). In particular, LMP-1 downregulates TRF2 and affects its localization within the nucleus, affecting the 3D nuclear telomere organization resulting in the formation of multi-nuclear RS cells (Lajoie et al., 2015). Downregulation of TRF2 shelterin proteins leads to disruption of the physiological 3D telomere–TRF2 interaction, with consequent telomere deprotection and genomic instability (Knecht et al., 2017).

Super resolution microscopy (3D-structured illumination microscopy, 3D-SIM) investigation showed that the nuclear DNA structure is significantly changed in H and RS cells when compared to normal primary lymphocytes, with a significant increase in the amount of DNA-free or DNA-poor nuclear spaces defined by the absence of 4',6-diamidino-2-phenylindole (DAPI)-staining (Righolt et al., 2014, 2016). The number of DAPI-free spaces is increased in cancer cells during the transition from H to RS cells (Righolt et al., 2014).


**MULTIPLE MYELOMA**


Pathogenesis of Multiple Myeloma

Multiple myeloma is a plasma cell disorders are characterized by the proliferation of neoplastic plasma cells of B-cell lineage that produce monoclonal immunoglobulin (Dimopoulos and Terpos, 2010; Rajkumar et al., 2006). These plasma cells accumulate in bone marrow and overexpress a monoclonal protein. The monoclonal protein is an abnormal immunoglobulin (Ig) (IgG, IgM, or IgA, or, rarely, IgE or IgD) or a light chain protein (kappa or lambda). Plasma cell malignancies include a spectrum of diseases, from monoclonal gammopathy of undetermined significance (MGUS) to smoldering multiple myeloma (SMM), clinical multiple myeloma (MM) and plasma cell leukemia. The disease process is insidious, with end-organ damage occurring over years. While the MGUS and SMM can be asymptomatic, they are considered to be pre-existing condition needed for the development of MM (Dimopoulos and Terpos, 2010; Landgren et al., 2009; Rajkumar et al., 2006). Patients with MGUS present significantly increased fracture risk compared to the healthy population, and the prevalence of MGUS is increased in patients with osteoporosis (Drake, 2014). In the absence of clinical symptoms, MGUS is diagnosed based on the percentage of plasma cell population in the bloodstream and bone marrow (BM), specifically when the plasma cell population is <10% in the BM. When the plasma cell content exceeds 10%, the disease state transitions into either SMM or MM (Berenson et al., 2010). During the MGUS phase, analysis of the M-protein level can be used to stratify patients, as values of M-protein below ≤1.5g/dL (mostly IgG subtype) are considered low risk for MM development (Go and Rajkumar, 2018). In the first five years, the risk of MGUS progression to MM is around 1% per year (Kyle et al., 2007).

SMM is an intermediate clinical stage between MGUS and MM. It is characterized by high serum or urinary monoclonal protein as well as clonal BM plasma cells in the range of 10–60%, without the presence of MM features like hypercalcemia, renal insufficiency, anemia, or bone lesions (Rajkumar et al., 2014). The SMM risk of progression to MM in the first five years after diagnosis is different when compared to MGUS since it is around 10% per year (Kyle et al., 2007).

In MM the "CRAB" criteria are present: calcium (hypercalcemia), renal impairment, anemia and bone involvement. Invasive bone lesions can cause pathologic fractures, bone pain, osteoporosis, and hypercalcemia. Bone marrow invasion leads to anemia, and immunologic changes cause recurrent infections (Bianchi and Anderson, 2014; Michels and Petersen, 2017; Moreau et al., 2017; Nau and Lewis, 2008; Rajkumar, 2016; Rajkumar et al., 2014; Röllig et al., 2015).

Around 1–2% of patients diagnosed with MGUS will progresses to MM (Barlogie et al., 2004; Jemal et al., 2009; Pawlyn et al., 2015; Röllig et al., 2015), while around 10% of patients with SMM will progress to MM (Greipp, 2007).

MM in an incurable disease. The treatments face numerous difficulties due to the heterogeneity of the disease, disease progression, and development of drug resistance (San-Miguel and Mateos, 2011), but patient risk stratification is gaining importance to ensure optimal treatment according to risk group, as the identification of a critical mutations to target in the patient could translate into better treatment (Chng et al., 2014).

Genomic Instability in Multiple Myeloma

Different studies have demonstrated that MGUS, SMM and MM cell genome is complex, and the disease is characterized by high heterogeneity (Chng et al., 2005; de Mel et al., 2014). Genomic instability and the resulting ongoing clonal evolution is a key driving mechanism of the heterogeneity in MM, as CIN, MSI, and base-pair mutations are commonly found (Cagnetta et al., 2015).

Two different types of CIN have been observed in MM, hyperdiploid and the non-hyperdiploid. The hyperdiploid MM (H-MM) is characterized by a number of chromosomes within the range of 47 to 75, where unique pattern of trisomies affecting chromosomes 3, 5, 7, 9, 11, 15, 19, and 21 are commonly found (Fonseca et al., 2004). The non-hyperdiploid MM (NH-MM) is divided into three subgroups: the hypodiploid MM, where the number of chromosome is less than 45, the pseudodiploid MM, where the number of chromosome is within the range of 45 to 46, and the near tetraploid MM, where the number of chromosome is greater than 75 (Van Wier et al., 2013). The non-hyperdiploid is characterized by different chromosomal translocations affecting the IgV and associated with poorer overall survival (Munshi et al., 2011).

Chromosomal gains and deletions are common in MM, including gain of chromosome 1q21 and deletion of chromosome 13, chromosome 17p13 and chromosome 1p (de Mel et al., 2014). Chromosome 13 deletion is an early event present in the majority of MGUS, and includes regions contain *RB1* and *NBEA* genes (O'Neal et al., 2009), while deletion of chromosome 17p13, which is associated with disease progression, affects the region containing the *TP53* gene (Boyd et al., 2011; Neri and Bahlis, 2013).

A number of recurrent translocations have been identified in since the MGUS pre-lesion, which are responsible for the deregulation of FGFR3, Cyclin D (Cyclin D1 and Cyclin D3), and MAFs (Fonseca et al., 2009). A secondary translocation event which may be important for disease progression is the one observed in *MYCC* rearrangement. Translocation of *MYCC* can be detected in about 15% of newly diagnosed patients (Avet-Loiseau et al., 2001). It has been shown that the MYCC pathway is activated in majority of myeloma patients and may be an important transforming event from MGUS to MM (Chng et al., 2011)

Mutations have also been described in MM. *RAS* was one of the commonly mutated genes in MM and it was detected in 20–45% of newly diagnosed MM patients (Fonseca et al., 2004), while *TP53* gene was found to be mutated in around 9% of cases (Lohr et al., 2014).

Studies on the 3D nuclear architecture showed increased telomere attrition during disease progression MGUS to MM with shorter telomeres in MM when compared to the precancerous lesion, with presence of larger TAs, very short t-stumps, and an increase in nuclear volume (Klewes et al., 2013). 3D distribution of centromeres has also been found to be different between MM and MGUS, as the centromeres in MGUS were more distributed toward the nuclear periphery than the nuclear center in when compared to centromeres in MM. Also, unlike the centromeres in MGUS, the centromeres in MM patient samples were found to form clusters, suggesting position alteration, breakage, rearrangement or fusion of the chromosomes (Yu et al., 2019).

## LAMIN A/C

Lamin proteins: from genes to protein

In eukaryotic cells, the nuclear genome is enclosed by a highly organized double membrane known as nuclear envelope. The nuclear envelope is characterized by two membranes: i) the outer nuclear membrane, which is continuous with the endoplasmic reticulum (ER) and is covered with ribosomes; ii) the inner nuclear membrane. These two individual lipid bilayers are separated by a luminal space of 30–50 nm in human cells, named the lumen or perinuclear space. For the transport of macromolecules in and out of the nucleus, both membranes connect to form pore membranes where the nuclear pore complexes (NPCs) responsible for transport regulation are inserted (Alvarado-Kristensson and Rosselló, 2019). Underneath the nucleoplasmic side of the nuclear envelope, there is the nuclear lamina, a filamentous network of lamin proteins and lamin-binding proteins that are embedded in the inner nuclear membrane (Gruenbaum et al., 2003).

Lamin proteins are type V intermediate filament proteins characterized by the presence of a short N-terminal domain and a long C-terminal domain, both of which are highly conserved. Lamin proteins

are divided into two groups based on their biochemical structure and their role during the process of mitosis: B-type lamins and A-type lamins.

B-type lamins are encoded by the *LMNB1* gene (for lamin B1) (Lin and Worman, 1995) and the *LMNB2* gene (for lamin B2) (Höger et al., 1990). B-type lamins are essential for cell survival and they are constantly expressed during the development. Lamins B1 and B2 are expressed in most cells, although lamin B2 is more ubiquitous than lamin B1 (Harborth et al., 2001). Three different A-type lamins are encoded by the *LMNA* gene following alternative splicing: lamin A, lamin A10 and lamin C (Fisher et al., 1986). A-type lamins, however, are normally only expressed in differentiated cells (Willis et al., 2008).

Correct lamin organization is necessary to allow proper DNA replication, but their specific role still remain unclear. In particular it is not known if lamin proteins have a direct interaction with replication elongation complexes during DNA synthesis, or if the presence of the lamin network is necessary for the attachment and assembly of replication foci (Goldman et al., 2002; Gruenbaum et al., 2003).

Numerous is the amount of protein/protein interactions which *in vitro* have been found to involve lamin proteins (Maraldi and Lattanzi, 2005). Such interactions include transmembrane proteins associated to the inner nuclear membrane (INM proteins), chromatin-associated proteins and transcription factors/transcriptional regulators. The INM proteins known to interact with lamin proteins include nesprin, emerin, lamina-associated proteins 1 and 2 (LAP1 and LAP2), the lamin B receptor (LBR) and MAN1. Nesprins and SUN proteins are important for mediating the interactions of lamin proteins with cytoskeletal proteins (Mislow et al., 2002; Padmakumar et al., 2005). More specifically, the nesprins mediate lamin A-actin interactions (Padmakumar et al., 2005), suggesting that A-type lamins are involved in the formation of protein complex at the nuclear envelope which are necessary for linking the actin cytoskeleton to the nuclear lamina (Fridkin et al., 2009). Lamin proteins also bind to chromatin-associated proteins, including H2A and H2B histone dimers, H3–H4 histone tetramers, non-histone proteins Ha95, BAF (Bengtsson and Wilson, 2004) and the HP1 (Lattanzi et al., 2007). The interaction between lamin proteins and chromatin-associated proteins is important for chromatin remodeling and regulation of gene silencing through heterochromatin organization (Maraldi and Lattanzi, 2005).

Lamin proteins are also involved in the regulation of the transcriptional process, since the disruption of the their normal organization leads to inhibition of the RNA polymerase II activity, but does not affect the activity of RNA polymerase I and III (Spann et al., 2002). Lamin proteins are also responsible for the regulation of different transcription factors, like OCT-1 and pRb. OCT-1 is a collagenase repressor which co-localize with lamin B1 and whose disassociation with the protein lead to digestion of the collagen (Imai et al., 1997). pRb, in its active form, is found to bind lamin A/C

associated protein LAP2 (Markiewicz et al., 2002), allowing the silencing of the E2F–DP complex and the progression of the cell cycle to the S phase.

Lamin proteins also interact with the chromatin. Lamin proteins are necessary for the initial positioning and assembly of the mitotic spindles, and they associate with centromeres and telomeres (Franklin and Cande, 1999). More specifically, while lamin B1 interacts specifically with the TRF-1 telomere shelterin protein, lamin A/C interacts specifically with TRF2 (Bronshtein et al., 2015; Wood et al., 2014).

Laminopathies and lamin A/C role in cancer

The laminopathies are diseases characterized by mutations at the level of the *LMNA* gene. These mutations are commonly found in disorders of cardiac and/or skeletal muscles (Vigouroux and Bonne, 2002).

The very first laminopathy to ever been described was the autosomal dominant Emery-Dreifuss muscular dystrophy (EDMD), a disease similar to the Duchenne muscular dystrophy (DMD) caused by a mutation at the level of the emerin gene, which is characterized by contractures of elbows and Achilles tendons, progressive muscle wasting and weakness, which lead to a lethal cardiomyopathy with conduction blocks (Bonne et al., 1999). Other laminopathies of the striated muscles are the autosomal recessive Emery-Dreifuss Muscular Dystrophy, Autosomal Dominant Cardiomyopathy Dilated 1A and the Autosomal Dominant Limb Girdle Muscular Dystrophy Type 1B (Worman and Bonne, 2007).

Laminopathies can be also associated with peripheral neuropathies (like the Charcot Marie Tooth Disease type 2B1 or CMT2B), lipodystrophies and premature aging syndromes such as Atypical Werner Syndrome (AWS), characterized by *LMNA* R133L mutation (Chen et al., 2003), and Hutchinson Gilford Progeria Syndrome (HGPS).

It is known that lamin A and lamin C originate from alternative splicing of the *LMNA* gene, and the two resulting protein are identical up to residue 574. Lamin A is synthesized as a 664-residue prelamin A precursor that after post-translational modifications will become mature lamin A with 646 residues (Gonzalo et al., 2017). The Hutchinson Gilford Progeria Syndrome is characterized by the mutation at the position C.1824C>T which lead to the in-frame deletion of 50 amino acids near the C-terminal domain of prelamin A. The aberrant generated lamin A, named "progerin", induces various nuclear abnormalities which result in cellular and organismal decline (Gonzalo et al., 2017). The amount of progerin produced is proportional to the severity of the disease (Moulson et al., 2007; Reunert et al., 2012). HGPS is characterized by growth retardation, loss of subcutaneous fat, atherosclerosis, bone

deformations, delayed dentition, hair loss, sclerodermatous skin and cardiovascular disease (Gruenbaum et al., 2005).

Aberrant lamin proteins expression and interactions with other proteins, are often present in tumor cells. Due to lamin proteins interaction with transcription factors like emerin and pRb, and due to their involvement in different signaling pathways, including p53, Wnt, TGF-β, Notch and NF-kβ, the aberrant lamin proteins expression could affect tumor progression (Sakthivel and Sehgal, 2016).

Lamin A/C has been identified as a substrate for phosphorylation by PKB/Akt1 in Emery–Dreifuss muscular dystrophy and this modification was involved in the regulation of lamin A/C expression levels (Cenni et al., 2008). In cancer cells, Akt is important for transducing extracellular (growth factor and insulin) and intracellular (receptor tyrosine kinases, Ras, and Src) oncogenic signals (Cheng et al., 2005). In around 20% of prostate cancers, the alteration of PI3K/Akt pathway due to loss or mutation of the tumor suppressor gene *PTEN*, is correlated with aberrant regulation of cell proliferation, transformation, tumor growth and angiogenesis (Fang et al., 2007; Paez and Sellers, 2003; Sun et al., 2009; Uzoh et al., 2009). Downregulation of lamin A/C diminishes protein levels of activated Akt protein, revealing the existence of a lamin A/C-PI3K feedback loop and its involvement in the tumorigenic process (Kong et al., 2012). Ligand engagement to receptor tyrosine kinase binding PI3K, interrupts the inhibitory action of the PI3K regulatory subunit p85 on the PI3K catalytic subunit p110. PIP3 formed by the activated PI3K stimulates then the phosphorylation and activation of Akt/PKB, transmitting the signal to downstream targets, thus orchestrating a variety of key cellular functions, including growth, proliferation and survival. Downregulation of lamin A/C trough lamin A/C shRNA treatment led to decreased PI3K activity and diminished protein levels of activated Akt protein, revealing that lamin A/C is involved in cell proliferation, migration and invasion (Kong et al., 2012).

Even if it has been demonstrated that the overexpression of lamin A/C plays a role in tumor progression, the levels of lamin expressions among different tumors are very inconsistent, since both cancers with overexpression of lamin A/C or cancers with lack of expression of lamin A/C can be found, and the role of lamin A/C as tumor biomarker remains a point of debate (Sakthivel and Sehgal, 2016).

In Nodal diffuse large B-cell lymphoma the hypermethylation of the CpG island of the *LMNA* gene promoter leads to loss of lamin A/C expression has been correlated with a decrease in overall survival and poor prognosis (Agrelo et al., 2005). In gastric carcinoma, patient with down-regulated lamin A/C expression have poorer prognosis compared with those expressing lamin A/C (Wu et al., 2009). However, colorectal cancer patients with high expression of lamin A/C presents worse prognosis when compared with patients with tumors showing negative expression (Willis et al., 2008).

# RATIONALE, HYPOTHESIS AND AIMS

## RATIONALE

Lamin A/C binding to telomeres is mediated, at least partly, by the shelterin protein TRF2. The association between lamin A/C and TRF2 is found to be important both for the maintenance of the t-loops structures at the level of the telomeres, and also for stabilizing the formation of interstitial t-loops (ITLs) at the level of the interstitial telomeric sequences (ITSs), tandem telomeric repeats localized at the intrachromosomal level (Wood et al., 2014). Aberrant lamin A/C structure and expression lead to fewer ITLs and profound telomere loss, since overexpression of mutant and wild-type lamin A in human fibroblasts results in accelerated telomere shortening and replicative senescence (Huang et al., 2008). Lamin proteins organization plays also an important role for gene localization, since it depends on interactions between genomic loci and the nuclear lamina through formation of lamina-associated domains (LADs). (Bronshtein et al., 2015; Guelen et al., 2008; Ottaviani et al., 2009). LADs are thought to regulate the interaction of chromatin with the nuclear lamina, generally leading to a repressive transcriptional effect (Guelen et al., 2008).

The 3D nuclear organization of the genome is altered in tumor cells from different hematological tumors, like cHL and MM. In cHL, the order of the genome is characterized by telomere dysfunction (Knecht et al., 2009), alterations in chromosome territories (Guffei et al., 2010), a new order of DNA packaging in the nucleus (Righolt et al., 2014, 2016), and the failure of TRF2 to cap all telomeres (Lajoie et al., 2015). MM is characterized by short telomeres, with large TAs, very short t-stumps, and an increased in nuclear volume when compared to normal lymphocytes (Klewes et al., 2013; Yu et al., 2019).

Since lamin A/C spatial organization plays an important role in the telomere homeostasis and deregulation of lamin A/C has been correlated with tumorigenesis, we set out to investigate the 3D nuclear organization of lamin A/C in two different cancer models, cHL and MM. As previously mentioned, the transition from H to RS cells is correlated with aberrant 3D telomere organization, telomere loss and increased number of DNA-poor spaces (Knecht et al., 2009; Righolt et al., 2014), and for this reason we explored whether the deregulation of lamin A/C plays a role in the transition from H to RS cells. Finally, since TRF2 fails to cap the short telomeres in cHL (Lajoie et al., 2015), and since telomere uncapping and mobility set the stage for a dynamic and self-propagating process of genomic instability via telomere fusions and illegitimate recombination, we investigated if the localized absence of TRF2 was causal to the genome remodeling.

**HYPOTHESIS**

We hypothesize that the deregulation of lamin A/C expression and spatial distribution affects telomere stability in cHL and MM, and that lamin A/C plays a role in the transition from H to RS cells. Also, we hypothesize that the localized unbinding of TRF2- telomere-lamin A/C is key to the organizational aberrations of the genome previously described in cHL.

**AIM #1. To investigate the 3D nuclear organization of lamin A/C in two different cancer models, cHL and MM**

By using three different cHL-derived cell lines (HDLM-2, L-428 and L-1236), one MM-derived cell line (MM1R CRL-2975), resting and LPS-treated isolated peripheral blood lymphocytes from healthy donors, we will investigate the 3D spatial distribution of lamin A/C using 3D fluorescent microscopy. To validate the results found in the cell lines, we will use twelve primary paraffin-embedded pre-treatment lymph node samples from patients diagnosed with cHL and ten pre-treatment blood samples from treatment-naïve patients who were newly diagnosed with MM.

**AIM #2. To investigate if the deregulation of lamin A/C plays a role in the transition from H to RS cells**

By silencing lamin A/C mRNA transcription in cHL-derived cell line HDLM-2, we want to understand if deregulation of lamin A/C would affect telomere 3D spatial distribution and nuclear organization using both conventional 3D fluorescent microscopy and super resolution imaging (SIM).

**AIM #3. To investigate if the localized absence of TRF2 is causal to the genome remodeling in cHL**

To investigate if the localized absence of TRF2 is causal to the genome remodeling in Hodgkin's lymphoma, we will perform co-localization analysis for telomeres-TRF2-lamin A/C in the three different cHL-derived cell lines HDLM-2, L-428 and L-1236 and using immortalized fibroblasts BJ5-ta cell line and LPS-treated peripheral blood lymphocytes as control.

# MATERIALS AND METHODS

**Cell Lines**

- cHL-derived cell lines HDLM-2, L-428 and L-1236

Three different EBV-negative cHL-derived cell lines were used for this project: Nodular Sclerosis cHL-derived cell lines HDLM-2 and L-428, and Mixed Cellularity cHL-derived cell line L-1236 (DSMZ, Braunschweig, Germany). The HDLM-2 and L-428 cell lines were grown in RPMI-1640 medium, supplemented with 20% fetal bovine serum (FBS), 1% L-glutamine, 1% sodium pyruvate, and 1% penicillin–streptomycin (reagents from Invitrogen/Gibco, Burlington, ON, Canada). The L-1236 cell line was grown in RPMI-1640 medium, supplemented with 10% FBS, 1% L-glutamine, 1% sodium pyruvate, and 1% penicillin–streptomycin. The cells were cultured in Nunc™ EasYFlask™ 75cm$^2$ (Thermo Scientific, Roskilde, Denmark), split every 48-72h with a dilution of 1:4, and incubated at 37°C with 5% $CO_2$ in a humidified atmosphere. Fresh slides were prepared before every experiment spreading the cells onto poly-L-lysine (SIGMA, p8920, St. Louis, MO, USA) coated slides.

- MM-derived cell line MM.1R CRL-2975

MM-derived cell line MM.1R CRL-2975 were grown in RPMI-1640 medium, supplemented with 10% FBS, 1% L-glutamine, 1% sodium pyruvate, and 1% penicillin–streptomycin. The cells were cultured in Nunclon™ Delta Surface, split every 48h with a dilution of 1:3, and incubated at 37°C with 5% $CO_2$ in a humidified atmosphere. Slides were prepared before every experiment: Cells were placed onto spreading the cells onto poly-L-lysine coated slides.

- Immortalized fibroblast cell line BJ-5ta

BJ-5ta cells were grown in a 4:1 mixture of Dulbecco's medium and Medium 199, supplemented with 10% FBS, 1% L-glutamine, 1% sodium pyruvate, and 1% penicillin–streptomycin. The cells were cultured in Nunclon™ Delta Surface, split every 72h with a dilution of 1:3, and incubated at 37°C with 5% $CO_2$ in a humidified atmosphere. 24h prior to the experiments, an aliquot of cell suspension was settled on sterile slides and incubated overnight to allow cell adhesion to the slide surface.

**cHL patient samples and Reactive Tonsils samples**

For this project we analyzed 12 primary Hodgkin's lymphoma paraffin embedded pre-treatment lymph node samples from patients diagnosed with cHL were analyzed. The patients were consented to participate into this research, which was approved by the research ethics board at the Jewish General Hospital in Montreal (protocol 16-016). Clinical information from these patients are

summarized in the following table (Table 1). Five reactive tonsils biopsy tissue sections from patients were used as control.

Table 1. Clinical data of patients diagnosed with cHL. Abbreviations: ABVD—doxorubicin, bleomycin, vinblastine, dacarbazine; CHLVPP—chlorambucil, vinblastine, procarbazine, prednisone; EBV—Epstein Barr Virus.

| Case | Gender | Age | Stage | Type of Chemotherapy | Relapse | EBV Status |
|------|--------|-----|-------|----------------------|---------|------------|
| 1 | Male | 24 | IV | ABVD | N | − |
| 2 | Female | 55 | III | ABVD | Y | − |
| 3 | Female | 25 | I | ABVD | N | + |
| 4 | Male | 55 | III | ABVD | Y | − |
| 5 | Male | 47 | I | ABVD | N | + |
| 6 | Female | 75 | IV | ABVD | N | − |
| 7 | Male | 22 | II | ABVD | N | − |
| 8 | Male | 19 | II A | ABVD | N | − |
| 9 | Male | 50 | III A | ABVD | N | − |
| 10 | Male | 37 | I A | ABVD | N | + |
| 11 | Male | 85 | III | CHLVPP | Y | − |
| 12 | Male | 28 | IA | ABVD | N | − |

**MM patient samples**

Ten pre-treatment blood samples were collected from CancerCare Manitoba (Winnipeg, Manitoba, Canada) from treatment-naïve patients who were newly diagnosed with MM. All the samples were obtained and processed within the same day. Clinical information is shown in table 2 (Table 2). This thesis project was approved by the Research Ethics Review Board on Human Studies of the University of Manitoba (Ethics Reference No. H2010:170).

Table 2. Clinical data of patients diagnosed with MM. Abbreviations: LC—Light Chain, SFLC—Serum Free Light Chain

| Case | Age | BMCP% | IgG | IgA | IgM | LC Kappa | LC Lambda | SFLC Kappa | SFLC Lambda | SFLC Ratio | M band g/l |
|------|-----|-------|-------|------|------|----------|-----------|------------|-------------|------------|------------|
| 1 | 68 | 16.2 | 20.80 | 0.80 | 0.62 | IgG | | 487.50 | 11.20 | 43.53 | 14 |
| 2 | 75 | 9.6 | 22.20 | 1.04 | 0.77 | IgG | | / | / | / | 3.7/8.0 |
| 3 | 70 | 26.8 | 32.22 | 1.08 | 1.42 | IgG | | 890.00 | 9.09 | 97.91 | 29 |

| 4 | 61 | 11.4 | 27.60 | 3.13 | 0.35 | IgG | | 29.30 | 21.10 | 1.39 | 16 |
|---|----|------|-------|------|------|-----|-----|--------|-------|-------|----|
| 5 | 73 | 16.4 | 4.42 | 11.60 | 0.30 | | IgA | / | / | / | / |
| 6 | 70 | 37.4 | 2.32 | 32.60 | 0.06 | IgA | | / | / | / | 19 |
| 7 | 66 | 29.8 | 4.28 | 16.60 | 0.19 | IgA | | 21.58 | 1.63 | 13.24 | 12 |
| 8 | 65 | 1.6 | 18.00 | 1.74 | 0.06 | IgG | | 143.04 | 4.43 | 32.29 | 10 |
| 9 | 76 | 68 | 2.96 | 0.08 | <0.04 | | IgD | / | / | / | / |
| 10 | 56 | 8.2 | 29.50 | 0.25 | 0.76 | | IgG | <2.70 | 11.70 | 0.23 | 25 |

## Identification of MM cells in MM patient samples

A previous study confirmed CD138+ myeloma nuclei corresponded to the larger and darker nuclei (Klewes et al., 2013). CD138 staining confirms them as terminally differentiated plasma cells, while CD56 staining targets adhesion molecules which distinguish myeloma cells from non-malignant plasma cells. Double positive staining for CD138 and CD56 was used to recognize MM cells from normal white blood cells. Immuno-staining for CD138 was performed using Alexa Fluor 594 anti-human CD138 antibody (ab) (Cedarlane, Burlington, ON, Canada) while immuno-staining for CD56 was performed using Alexa Fluor 488 labelled Mouse anti-human CD56 ab (BD Bioscience, San Jose, CA, USA).

## Peripheral blood lymphocytes isolation

Peripheral blood lymphocytes (PBLs) were isolated from peripheral blood from healthy donors through Ficoll-gradient centrifugation (Ficoll-PaqueTM Plus, GE Healthcare, Little Chalfont, UK). The blood was diluted with PBS (7:2) and layered with a ratio of 3:2 on Ficoll. The obtained buffy coat was collected and washed twice in 1XPBS. This isolation method, however, retains all monocytes. For this reason, the CD 20 marker was used to identify B cells (CD20 conjugated with FITC (1:50 dilution), sc-393894, Santa Cruz Biotechnology, Dallas, Texas, EUA), since CD20 is a B cell differentiation antigen widely expressed in B cell development from early pre-B until mature B cell stage (Ernst et al., 2005).

## LPS-stimulation of PBLs

Lipopolysaccharide (LPS)-stimulated B cells have been used as control in this project. Stimulation of B-lymphocytes was achieved culturing PBLs with $50 \mu M$ of LPS ($1 \mu g/ml$) (SIGMA, L2630, St. Louis, MO, USA) Isolated resting and LPS-treated PBLs were then placed onto poly-l-lysine (SIGMA, p8920, St. Louis, MO, USA) coated slides. For this procedure, ninety activated B cells were analyzed per healthy donor (10 healthy donors in total). Two LPS stocks from two different lots have been tested on PBLs without success before finding the good lot (Lot#096M4092V).

**Cell fixation and permeabilization**

- Cell lines

Glass slides were stored in a solution of 70% EtOH/$H_2O$. Before the experiments, the slides were removed from the solution, air dried and coated with poly-l-lysine. The cell lines were spotted on the glass slide and fixed in 3.7% formaldehyde/1× PBS, to maintain the 3D structure and followed by two 1X PBS washes. Permeabilization of the cells was performed with 0.1% Triton-X 100. Three 1× PBS washes were performed to wash the solution off.

- cHL patient samples and reactive tonsil samples

Formalin-fixed, paraffin-embedded tissue slides (5μm thickness) were de-paraffinized at room temperature in xylene until the paraffin was completely dissolved (2 incubations of 15 minutes each). De-paraffinized slides were subsequently rehydrated in a descending gradient of ethanol-water solutions, from 100% EtOH to 50% EtOH/$H_2O$, and transferred to PBS before fixation in 3.7% formaldehyde/1× PBS. Two 1X PBS washes were performed to wash the extra formaldehyde solution. Permeabilization of the cells was performed with 0.1% Triton-X 100. Three 1× PBS washes were performed to wash the solution off.

- MM patient samples

PBLs isolated from peripheral blood through Ficoll-gradient centrifugation have been placed onto poly-L-lysine coated slides and fixed in 3.7% formaldehyde solution for 10 minutes. Dehydration from 70% EtOH/$H_2O$ to 100% EtOH was performed after fixation to store the samples in the -20° freezer.

Before the start of the experiments, the slides were rehydrated in decreasing EtOH concentrations from 100% EtOH to 50% EtOH/$H_2O$ to maintain the cell 3D structure. No permeabilization step was performed for these sample due to the need of maintaining surface markers for cell identification proposes.

- Resting and LPS-stimulated PBLs

Resting and LPS-stimulated PBLs have been placed onto poly-L-lysine coated slides and fixed in 3.7% formaldehyde solution for 10 minutes. Dehydration from 70% EtOH/$H_2O$ to 100% EtOH was performed after fixation to store the samples in the -20°C freezer.

Before the start of the experiments, the slides were rehydrated in decreasing EtOH concentrations from 100% EtOH to 50% EtOH/$H_2O$ to maintain the cell 3D structure. No permeabilization step was performed for these sample due to the need of maintaining surface markers for cell identification proposes.

**Immuno-staining for lamin A/C and lamin B1**

Before immuno-staining, the slides were blocked in 4% BSA/4×SSC blocking solution for 5 minutes at 37℃, in humidified atmosphere.

The immuno-staining experiments were performed using: i) Primary Anti-Lamin A ab (rabbit polyclonal, ab26300, Abcam Ltd., Cambridge, UK); ii) Primary Anti-Lamin B1 ab (rabbit polyclonal, ab16048, Abcam Ltd. UK); iii) Alexa Fluor® 488anti-CD20 ab (mouse monoclonal IgM, sc-393894, Santa Cruz Biotechnology, Dallas, Texas, USA); iv) secondary goat anti-rabbit ab conjugated with the Alexa 488 fluorophore (Molecular Probes, Waltham, MA, USA); secondary goat anti-rabbit ab conjugated with the Cy3 fluorophore (Sigma Chemical, St. Louis, MO, USA).

A dilution of 1:200 and 1:500 in 4%BSA/4×SSC blocking solution have been used for the primary and the secondary ab respectively.

Slides were incubated with primary ab for 45 min at 37℃ in humidified atmosphere, and washed three times in 1xPBS washes (5 min each). Incubation with secondary ab was performed for 30 min at 37℃ in humidified atmosphere, and washed three times in 1xPBS washes (5 min each). DNA of the nuclei was counterstained with DAPI. Glycerol-based mounting medium Vectashield (Vector Laboratories Inc, Burlingame, CA, USA) was used as to prevent photobleaching of the sample and maintain the 3D structure of the cell.

Since the paraffin embedded HL lymphoma samples and Reactive tonsils samples were characterized by a very high auto-fluorescence, an additional incubation of the slides in the Target Retrieval Solution (DAKO, S1700, Santa Clara, CA, USA) for 20 min at 90°C, and then 20 min at room temperature (RT) was performed before the incubation with the blocking solution.

**Quantitative analysis of lamin A/C patterns**

2D images of the cells representing the identified pattern were selected and used for the quantitative analysis of lamin A/C on ZEN Blue Version 2.3 Software (Carl Zeiss, Jena, Germany). Based on the 3D lamin A/C pattern, a single z-stack (representative of the specific pattern) was selected from each cell. The "draw spline contour" tool was used to define two areas in the selected z-stack, the external area and the internal area. The external area included the part of the image characterized by the presence of lamin A/C structures. The internal area included the part of the image characterized by the absence of lamin A/C structures. The external lamin A/C intensity ($I_e$) was calculated using the total signal intensity within the external area, while the internal total lamin A/C intensity ($I_i$) was calculated using the total signal intensity within the internal area. Example of the two areas is in Figure 1 (Figure 1). An intensity ratio ($I_e/I_i$) was calculated dividing $I_e$ by $I_i$ to normalize the intensity values for the cell area.
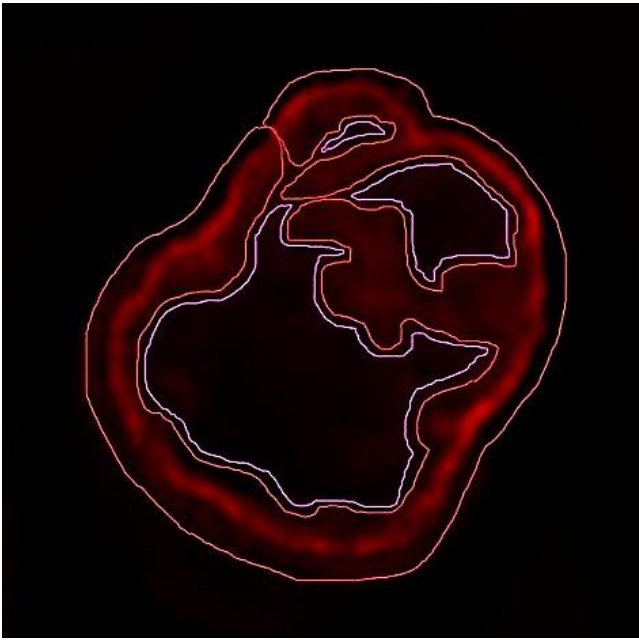
Figure 1. Example of quantitative analysis performed in lamin A/C patterns. The external total lamin A/C intensity (Ie) was calculated within the areas bordered in Red. The internal total lamin A/C intensity (Ii) was calculated within the areas bordered in Violet. The final ratio was calculated between the Ie resulting from the red area, dived by Ii, resulting from the sum of the total intensities within the three violet areas.

**Western Blot Analysis**

For the protein extraction, cells from the three cHL-derived cell lines, resting and LPS-treated lymphocytes were collected in separate tubes and centrifuged at 800rpm for 10 minutes. The supernatant was removed and the cells have been washed twice with cold 1XPBS and transferred in Eppendorf tubes. 1mL of cold RIPA Buffer (25mM Tris-HCl pH 7.6, 150mM NaCl, 1% NP-40, 1% sodium deoxycholate, 0.1% SDS) was added to the cells after the removing the 1XPBS. The tubes were kept on ice for 30 minutes. The tubes underwent sonication and then they were centrifuged at 4°C for 1 minute. The supernatant containing the proteins was transferred into a new tube and the pellet was discarded.

For the Western Blot (WB), the protein content was quantified using the Micro BCA protein assay kit, and 20 µg of total protein were loaded into a 4–20% Mini-PROTEAN® TGX Stain-Free™ Protein Gels, 10 well, 50 µl (4568094, Biorad, Hercules, California, USA). The run was performed at 140 Volts for 65 minutes.

Proteins from the gel were transferred to Immun-Blot® PVDF membranes (Biorad, Hercules, California, USA). The membrane was then blocked in a 5% milk/TBST solution for 1h at 4°C. Anti-

Lamin A ab (rabbit polyclonal, ab26300, Abcam Ltd., Cambridge, UK) and anti-Cyclophilin B ab (rabbit polyclonal, ab16045, Abcam Ltd., Cambridge, UK) were diluted at 1:1000 and 1:3000 respectively in 5% milk/TBST solution. The membranes were incubated with the primary ab overnight at 4°C. Four TBST washes were performed to remove the unbounded ab. The membranes were then incubated in the presence of the secondary ab (Goat Anti-Rabbit IgG H&L (HRP), ab6721, Abcam Ltd., Cambridge, UK), diluted at 1:20.000 in 5% milk/TBST for 2h at 4°C, and then rinsed four times in TBST to remove the ab excess.

The protein imunobloting was visualized using a SuperSignal West Dura kit according to the manufacturers' instructions (Thermo Fisher scientific, Waltham, Massachusetts, USA) and the MyECL Imager (ThermoFisher Scientific, Mississauga, Canada). The immunoblot analyses was performed using the pixel densitometry of target bands under respective constitutive bands obtained using software ImageJ (NIH, ImageJ 1.49v, Madison, WI, USA). The protein of interest was normalized to the respective loading control (Cyclophilin B). All WB assays were done in triplicate.

**Real Time Quantitative PCR (qRT-PCR)**

Total RNA from cell lines was extracted using Total RNA purification Kit (Norgen Biotek Corp, Ontario, Canada), according to the manufacturers' instructions. RNA concentration and purity were analyzed by 260/280 nm spectrophotometer using NanoDrop 1000 (Thermo Scientific, Waltham, MA, USA). We used 1μg RNA to synthesize complementary DNA (cDNA) with High-Capacity RNA-to-cDNA™ Kit (Thermo Scientific, Waltham, MA, USA).

For real-time quantitative PCR (qRT-PCR), the following Taqman probes from Applied Biosystems were utilized: LMNA (Lamin A gene) (Assay ID: Hs00153462_m1), and GAPDH (Assay ID: Hs02758991_g1) as an endogenous reference.

The $2^{-\Delta\Delta C_T}$ method (Livak and Schmittgen, 2001) was used to quantify the expression levels in different controls (resting lymphocytes, LPS-activated lymphocytes) and cHL-derived cell lines samples (HDLM-2, L-428 and L-1236), using a QuantStudio™ 5 Real-Time PCR Instrument (Applied Biosystems, MA, USA). The $C_T$ values for lamin A/C (gene of interest) and GAPDH (house-keeping gene) provided from real-time PCR instrument were imported into Microsoft Excel and averaged for each control and sample. The $\Delta C_T$ values were calculated as: $\Delta C_T$ = averaged lamin A/C $C_T$ – averaged GAPDH $C_T$. The $\Delta C_T$ values were calculated for each control and sample. The average for the $\Delta C_T$ control was calculated (Control Average $\Delta C_T$) was calculated. The $\Delta\Delta C_T$ values were calculated as: $\Delta\Delta C_T = \Delta C_T$ – Control Average $\Delta C_T$. The $\Delta\Delta C_T$ values were calculated for all the controls (resting lymphocytes and LPS-treated lymphocytes) and the cHL-derived cell lines

(HDLM-2, L-428 and L-1236). With the obtained $\Delta\Delta C_T$ values, the $2^{-\Delta\Delta CT}$ values were calculated and compared.

All PCR assays were done in triplicate.

**siRNA silencing of lamin A/C**

Transient silencing of lamin A/C was performed using siRNA lamin A/C (Target Sequence: GGUGGUGACGAUCUGGGCU), while scrambled siRNA (Target Sequence: UAGCGACUAAACACAUCAA) was used as a negative control for the silencing. Different concentrations of siRNA were used in this project to achieve the lamin A/C mRNA silencing: 12.5 nM, 25 nM and 50 nM. The silencing was monitored for 24 h, 48 h, 72 h and 96 h. siRNA lamin A/C transfection with 50 nM was also performed on two additional time points, 120 h and 144 h, to investigate the complete kinetics of siRNA-mediated lamin A/C silencing. After siRNA treatment, lamin A/C protein expression was monitored using WB as previously described.

he fold-decrease for the siRNA is relative to the negative control (Scrambled siRNA for each concentration) and the scrambled siRNA is relative to control without transfection (Control). These experiments were performed in triplicate using cells from different passages.

**Co-immuno-Staining for Lamin A/C and TRF2/Telo-Q-FISH**

The co-immuno-staining for lamin A/C and TRF2 combined with telomere Q-FISH for the co-localization study in BJ-5ta, LPS-treated lymphocytes and cHL-derived cell lines, has been performed by modifying the protocol previously described by Knecht and Mai in 2017 (Knecht and Mai, 2017). Following fixation and permeabilization of the samples, the Q-FISH was performed using 8µl of Cy3-labeled PNA-telomere probe (Dako, Glostrup, Denmark). A single cycle of denaturation for 3 min at 80°C followed by hybridization for 2 h at 30°C was performed using the Hybrite™ (Vysis/Abbott, Abbott Laboratories. Abbott Park, Illinois, USA). The slides were then placed in 70% formamide/10 mM and washed in 0.1× SSC at 55°C. An additional wash in 2× SSC/0.05% Tween 20 was performed. After an incubation in 4%BSA/4×SSC blocking solution for 5 minutes at 37°C, the slides were then incubated with primary rabbit polyclonal anti-lamin A ab (Abcam Ltd., Cambridge, UK) (diluted 1:200 in 4%BSA/4×SSC) overnight at 37°C in humidified atmosphere. The following day, three 1× PBS washes were performed to wash away the extra primary ab. Incubation with secondary donkey anti-rabbit ab conjugated with the Cy5 fluorophore (ThermoFisher, Eugene, OR, USA) (diluted 1:500 in 4%BSA/4×SSC) was performed for 1 hour at 37°C in humidified atmosphere. Three 1× PBS washes were performed to wash away the extra ab. After an additional incubation in 4%BSA/4×SSC blocking solution for 5 minutes at 37°C, an incubation with rabbit anti-donkey ab conjugated with

Alexa 650 (ThermoFisher, Eugene, OR, USA) (diluted 1:200 in 4%BSA/4×SSC) was performed for 1 hour to enhance the signal. Three 1× PBS washes were performed to wash away the extra ab. Following the washes, the slides have been incubated for 30 minutes at 37°C in humidified atmosphere in 10%BSA/4×SSC blocking solution.

The TRF2 immuno-staining was performed with the primary anti-TRF2 rabbit polyclonal ab (Novus Biologicals, Centennial, CO, USA). A general problem in immuno-fluorescence experiments is the fact that when primary abs are raised in the same host species, the secondary species specific ab can cross-react with each of the primary antibodies (Buchwalow et al., 2018). For this reason, since both the anti-lamin A ab and the anti-TRF2 ab were raised in rabbit, we manually conjugated the anti-TRF2 ab with the Alexa 488 fluorophore using the Alexa Fluor 488 Ab Labeling Kit (ThermoFisher, Eugene, OR, USA) and diluted it 1:25 in 10%BSA/4×SSC. Incubation with TRF2 ab was performed for 1 hour at 37°C in humidified atmosphere. Three 1× PBS washes were performed to wash away the extra ab. DNA of the nuclei was counterstained with DAPI. Glycerol-based mounting medium Vectashield (Vector Laboratories Inc, Burlingame, CA, USA) was used as to prevent photobleaching of the sample and maintain the 3D structure of the cell.

**3D Image Acquisition**

The manual 3D image acquisition was performed on 30 H, 30 RS, 30 Lymphocytes, 30 Centrocytes and 30 MM cells per experiment. The 3D conventional imaging of was performed using ZEISS Axio Imager.Z2 (Carl Zeiss, Toronto, ON, Canada) with a cooled AxioCam HR B&W, FITC, Cy3 and DAPI filters in combination with a Planapo 63x/1.4 oil objective lens (Carl Zeiss, Toronto, ON, Canada). 80 z-stacks at 200nm step-size were imaged for every fluorophore of every cell. Images were obtained using AxioVision 4.8 (Carl Zeiss, Toronto, ON, Canada), deconvolved using the constrained iterative restoration algorithm with Theoretical PSF and Clip Normalization. The resolution of the images was 102nm in the x, y directions and 200nm in the z-direction.

To observe the 3D reconstruction of the cells the Maximum Intensity Projection rendering mode and the Surface Reconstruction rendering mode of the Axiovision software were used. Maximum Intensity Projection shows a 3D view of data by displaying pixels of the highest intensity along the projection axis. The Surface Reconstruction the grey values in the images are computed as solid surfaces (a.k.a. iso surfaces).

The automated image acquisition of interphase nuclei was performed using the ScanView system [Applied Spectral Imaging (ASI), Carlsbad, CA, USA], using a Zeiss Imager Z2 microscope with a Basler CCD camera (Basler AG, Ahrensburg, Germany) and equipped with a motorized nine-slide stage (Märzhäuser, Wetzlar, Germany). The 3D-images were acquired with dry 40× objective and a

0.6× c-mount (Olympus, Tokyo, Japan) taking 9 z-stacks at 300nm step-size per field of view. Exposure times were constant at 1ms (DAPI) and 100ms (FITC) throughout the experiments. The tissue sample mode with cell circularity setting of 1.4 was used to enable segmentation of touching cells and cell detection. Cells touching the border of the field of view were excluded. Approximately 1000 cells per experiment were scanned and analyzed for the cHL-derived cell line, and 1000 cells per experiment for the MM-derived cell lines. For data acquisition and analysis, the software modules GenASIs (ASI, Carlsbad, CA, USA) and SpotScan (ASI, Carlsbad, CA, USA) were used.

3D SIM imaging was performed using Zeiss PS.1 ELYRA microscopy system equipped with 63x 1.4 NA objective lens and IXon 885 EMCCD Camera (Andor, Oxford, UK). Images were acquired using 1.518 refractive index (RI) immersion oil. 405 nm laser was used for excitation of the DAPI channel. A SIM grating period of 28μm was used. The z-step ($\Delta z$) was set at 91nm. The number of z-stacks used to image the cells was not maintained fixed but was adjusted based on the size of every cell. Once the images were acquired, the reconstruction was performed with ZEN 2012 black edition software (Carl Zeiss, Jena, Germany) with Noise filter set to −3.0 and deactivation of the Baseline Cut option. The resolution of the reconstructed images was 40nm in the x, y directions and 91nm in the z-direction.

**Image Analysis**

- _3D analysis of lamin A/C-TRF2-telomeres co-localization_

For 3D co-localization of lamin A/C-TRF2-telomeres, following deconvolution of the images, a minimum of 30 H and 30 RS cells from three independent experiments with the HDLM-2, L-428, L-1236 cell line were used. 30 BJ-5ta and 30 LPS-treated lymphocytes from three different experiments were used as controls. Image processing of the acquired immuno-stained cells was performed using NIH Image J Software (version 1.52e) and Tools for Analysis of Nuclear Genome Organization (TANGO) software (version 0.97) (Ollion 2013, Natarajan 2016).

The set of 30 cells per cell type were loaded in the software. A total number of four "channel images" was set for the analysis: DAPI (for the DNA), Cy3 (for the telomeres), FITC (for the TRF2) and Cy5 (for the lamin A/C). A total number of four "structures" was set for the analysis: DNA, telomeres, TRF2 and lamin A/C. Every structure was associated to the respective channel image.

All structures were segmented using the "stock segmentation" tool, and the background was subtracted for each channel. Signal quantification and simple geometric measurement were performed for every channel. The overlapping percentage of the Cy3 signals of the telomeres, the FITC signal of the TRF2 and the Cy5 signal of the lamin A/C was examined by putting the generated data through a binary logic gate: a value of 0 was assigned by the software when no overlap was

detected between a telomere signal, a TRF2 signal and lamin A/C; a value of 1 was assigned when overlap was detected. Co-localization was determined through the overlap between FITC signal of TRF2, Cy3 signal of the telomeres and Cy5 signals of the lamin A/C.

- Telomere analysis

For telomeres' analysis of siRNA treated cells and controls, deconvolved images were converted into TIFF files and exported for 3D analysis using the TeloView software program (version 2.0, Telo Genomics, Toronto, ON, Canada) (Chuang 2004). TeloView has been used for the analysis of the following parameters: (i) total number of telomeres' signals; (ii) total number of telomere aggregates; (iii) *a/c* ratio, defining the nuclear space occupied by telomeres, which can be represented by three axes of length *a*, *b*, and *c*. The ratio between the a and c axes, the *a/c* ratio, is dynamic, and changes at different stages of the cell cycle (G0/G1, S, G2); (iv) nuclear volume; (v) average telomere signal intensity; (vi) total telomeres' signal intensity.

- Granulometry analysis

The granulometry analysis of the super resolved DNA structure, DNA-free space and all computations were performed using the DIPimage toolbox for Matlab (version R2012a, MathWorks, Natick, MA, USA) as described by Righolt et al. in 2014 (Righolt et al., 2014).


**Statistical Analysis**

- Lamin A/C patterns analysis

Chi-square ($\chi$2) test (McHugh, 2013) was used to assess the differences among the frequencies observed for the different patterns in all the cell lines, cHL patient samples and MM patient samples. This test was also used to assess the differences between $I_e/I_i$ ratios obtained for each lamin A/C pattern. Significance levels were set at $p \leq 0.05$.

- Telomere analysis, WB, qRT-PCR and lamin A/C-TRF2-telomeres co-localization

Statistical analysis of data was conducted using the GraphPad Prism 5.0 (GraphPad Software, San Diego, USA). The two-way ANOVA with Bonferroni posttest analysis was used to analyze: i) WB; ii) qRT-PCR; iii) telomeric parameters in the lamin A/C siRNA treated VS scrambled RNA H and RS cells (McHugh, 2011).

Multiple comparisons using the least-square means tests (Vaillant and Olliaro, 2007) followed in which interaction effects between two factors were found to be significant. Significance levels were set at $p \leq 0.05$.

- Granulometry analysis

Two-sided, two-sample Kolmogorov–Smirnov test (Berger and Zhou, 2014) was used to determine statistical significance of the differences measured in the granulometry analysis. Significance levels were set at p ≤ 0.05.

# RESULTS

**Lamin proteins in normal B-cells regularly surround the cell nucleus**

Since H cells originates from germinal center B cells carrying crippling mutations at the level of the BCR (Kanzler et al., 1996), to assess lamin proteins spatial distribution in healthy control, GC lymphocytes (precursors of the H cells) from five reactive tonsils biopsy tissue sections were immuno-stained for lamin A/C , using lamin B1 as nuclear envelope marker. While previous studies demonstrated GC lymphocytes positivity for lamin B1 (Jansen et al., 1997), immunohistochemical analysis of the GC revealed weak-to-no positivity for lamin A/C (Figure 2A–C). Analysis of the centrocytes within the dark zone (DZ) of the GC confirmed the absence of lamin A/C staining (Figure 2D–G).

Although previous studies have reported the absence of lamin A/C in unstimulated human and mouse T lymphocytes (Guilly et al., 1987; Röber et al., 1990), lamin A/C positivity has been reported in activated human peripheral blood lymphocytes, CD4+ T lymphocytes and in CD30+ lymphoid cell (Jansen et al., 1997; Stadelmann et al., 1990; Wheeler et al., 2011). However, while data were previously published for lamin A/C expression in T-lymphocytes, no published records were found on lamin A/C expression in B-lymphocytes. For this reason, immuno-staining for lamin A/C (Figure 3A-F) and lamin B1(Figure 4A-D) was performed on both resting- and LPS-treated CD20+ lymphocytes, used to induce specific activation of the B cells (Parekh et al., 2003).

Lamin A/C staining showed that resting B-lymphocytes were characterized by little to no detectable lamin A/C expression (Figure 3E). However, upon LPS treatment, B-cells presented with an increased lamin A/C expression (Figure 3F). The investigation of the lamin A/C 3D spatial distribution in LPS-treated B-cells revealed a regular spherical expression pattern where lamin A/C surrounds the nucleus (Figure 3F). Lamin B1 staining showed that both resting and LPS-treated B cells are positive for lamin B1 (Figure 4A–C). Investigation of lamin B1 3D spatial distribution revealed a very similar pattern to the one of lamin A/C (Figure 4D).
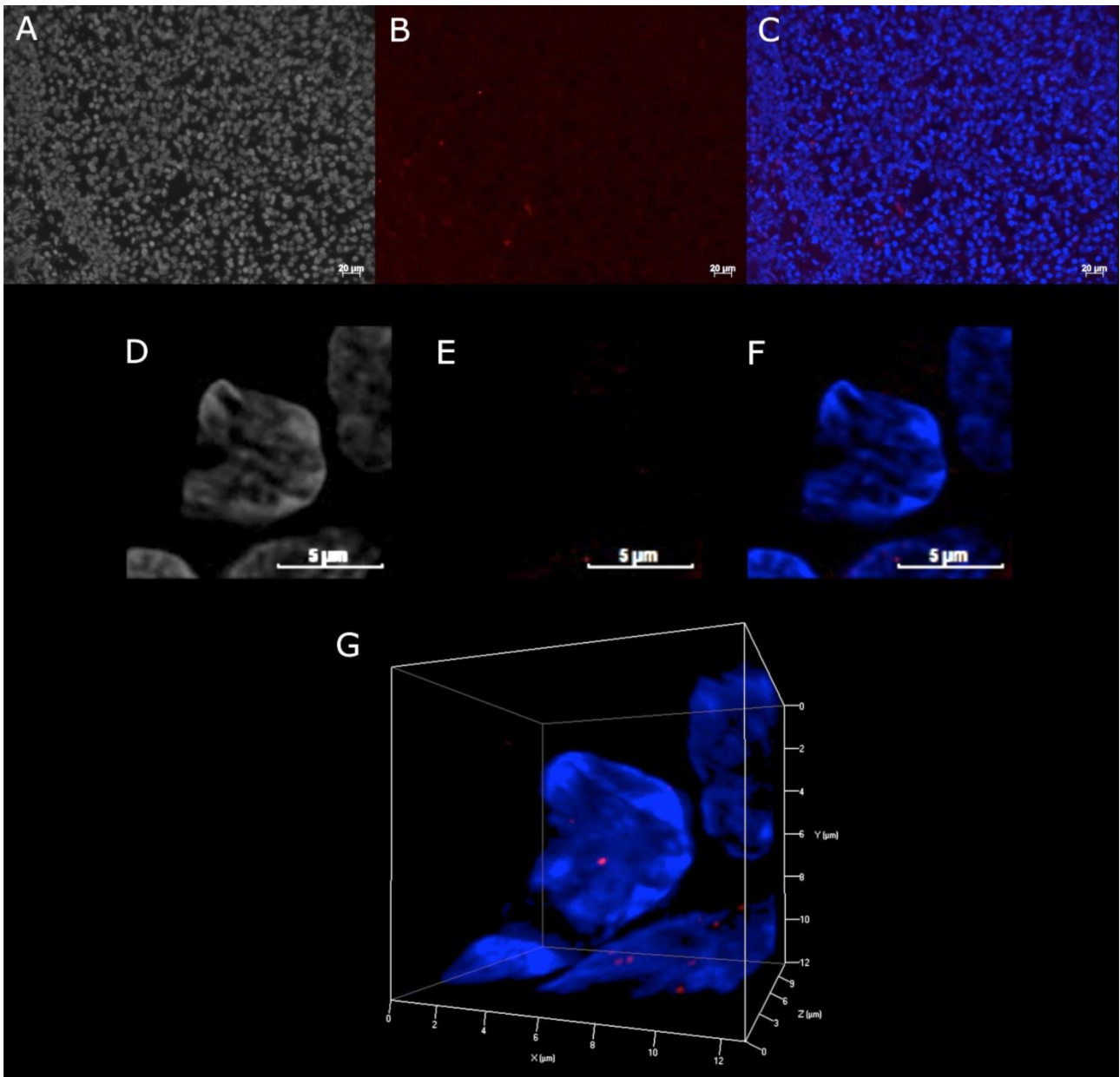
Figure 2. Lamin A/C expression in primary Germinal Centre (GC) centrocytes from paraffin embedded reactive tonsil tissue from healthy controls. (A) 2D image of GC cells stained with DAPI (gray scale) (20X magnification); (B) 2D image of anti-lamin A/C ab immunostaining (red) and (C) 2D merged image showing weak to no lamin AC staining among the germinal center cells. (D) 2D image of centrocyte nucleus stained with DAPI (gray scale); (E) 2D image of anti-lamin A/C ab immunostaining (red); (F) 2D merged image. (G) 3D reconstruction of centrocyte presenting low level of detected lamin A/C staining.
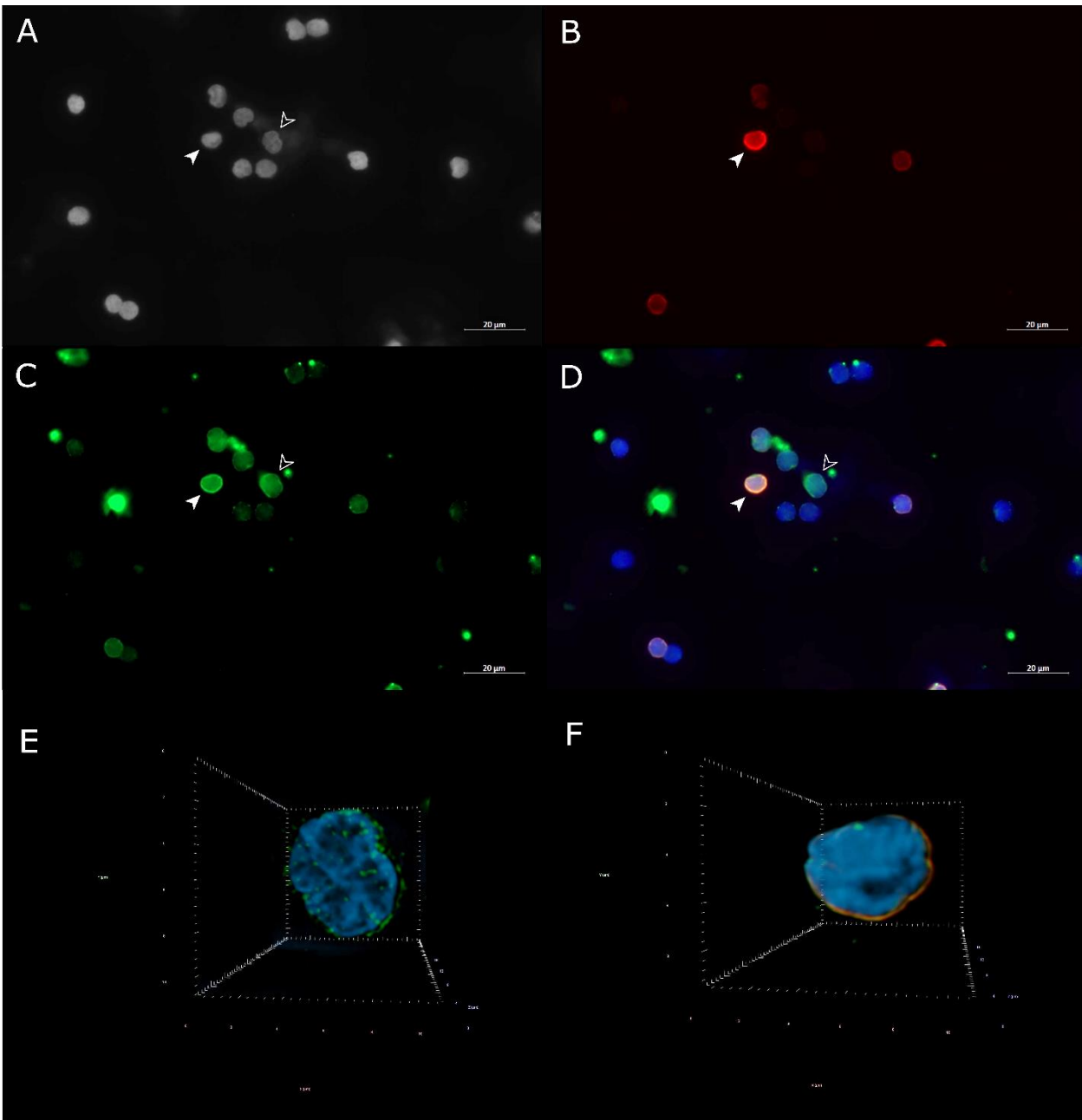
Figure 3. Immunostaining of LPS-treated lymphocytes from healthy donor using lamin A/C and CD20. (A) 2D image of nuclei stained with DAPI (gray scale); (B) 2D image of lamin A/C ab immunostaining (red); (C) 2D image of CD20 ab immunostaining (green); (D) 2D merged image showing a lamin A/C+/CD20+ LPS-treated lymphocyte (solid arrow) and a lamin A/C-/CD20+ resting lymphocyte (empty arrow). Complete 3D reconstitution of resting (E) and LPS-treated lymphocyte (F).
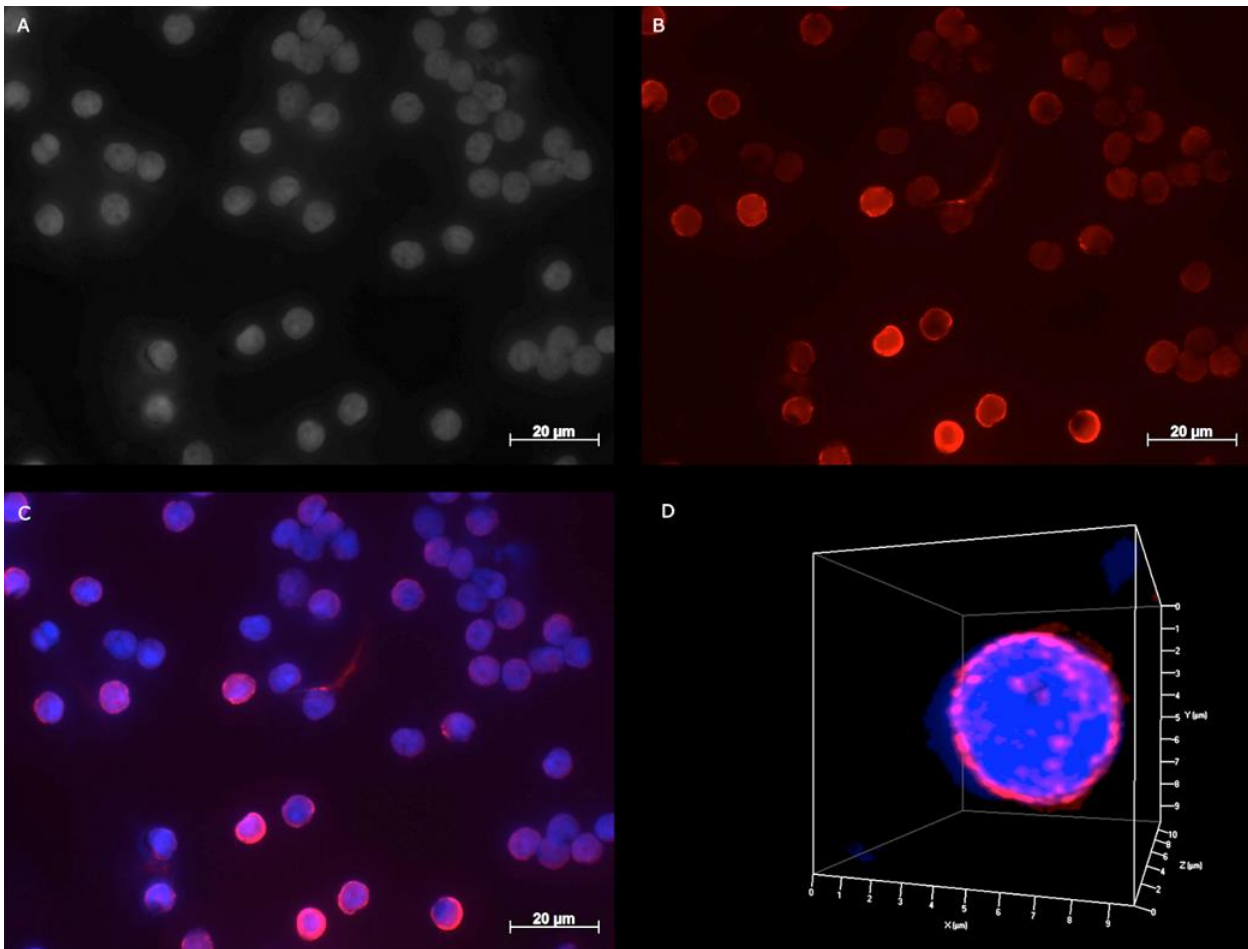
Figure 4. Lamin B1 immunostaining of lymphocytes from PB of a healthy donor. (A) 2D image of nuclei stained with DAPI (gray scale); (**B**) 2D image of anti-lamin B1 ab immunostaining (red); (**C**) 2D merged image showing lymphocytes with expressing lamin B1. Complete 3D reconstitution of a lymphocyte expressing lamin B1 (**D**).

**cHL-derived cell lines are characterized by an aberrant lamin 3D spatial distribution and the presence of internal lamin structures**

To first examine lamin A/C positivity in H and RS cells, we performed immunostaining for lamin A/C in three cHL-derived cell lines. Immunohistochemical analysis revealed that both H and RS cells from all the cHL-derived cell lines stained positive for lamin A/C as expected (Figure 5A–C). The lamin A/C 3D spatial distribution analysis, however, revealed that the regular spherical expression pattern observed in the LPS-treated B-lymphocytes was replaced in H and RS cells by a more irregular one, characterized by the presence of internal lamin A/C structures, dividing the 3D structure into multiple compartments not seen in the normal lymphocytes (Figure 6A-H).

Interestingly, our data revealed 3D different spatial organization patterns for lamin A/C in H and RS cell. We categorized these patterns into five different types of lamin A/C patterns for H cells (0, A, B, C and D), and four for the RS cells (bi-nuclear, tri-nuclear, tetra-nuclear and multi-nuclear) (Table

3; Table 4). Quantitative analysis of the identified patterns for both H and RS cells was performed investigating the ratio of the external total lamin A/C intensity ($I_e$) on the internal total lamin A/C intensity ($I_i$) (Table 3).

The five different lamin A/C patterns of the H cells and the four different lamin A/C patterns of the RS cells were observed in all three cHL-derived cell lines analyzed in this study. H cells were divided into groups based on how the lamin A/C 3D internal structures divided the nucleus (Figure 6A–E). Pattern 0 had similar architecture to that found in LPS-activated normal B cells (Figure 6A). Pattern A was characterized by the presence of small internal structures and by the irregular 3D profile of lamin A/C (Figure 6B). In Pattern B, C, and D, the aberrant lamin A/C staining divided the 3D structure of mono-nuclear H cells into two, three and four different compartments, defined by internal lamin structures (Figure 6C–E). Mononuclear cells expressing pattern B constituted a majority (42.16%), followed by patterns A (29.15%), 0 (15.48%), C (11.63%) and D (1.59%). The pattern classification for H cells described increasing complexity of the internal lamin A/C structure and the quantitative analysis reflected this change as the Ie/Ii ratio increased ($p < 0.05$).

RS cells were divided into different groups according to the numbers of total nuclei. Every nucleus of the RS cells was covered by a spherical lamin surface, and characterized by a more irregular pattern when compared to the mononuclear H cells. Anomalous lamin A/C features observed in H cells were also present (Figure 6F-H). Bi-nuclear RS cells were found to be the most frequent (57.66%) in the RS cell population analyzed, followed by tri- (22.27%), tetra- (10.29%) and multi-nuclear (9.79%) RS cells. In RS cells as the pattern classification complexity of the lamin A/C structures increased from bi- to multi-nuclear, the quantitative analysis reflected this change with an increasing $I_e/I_i$ ratio ($p < 0.05$).

In order to understand if the entire nuclear lamina was characterized by aberrant 3D spatial distribution, we also performed immuno-staining for lamin B1. Investigation of lamin B1 3D spatial distribution revealed the presence of the same types of patterns identified for lamin A/C in all the three cHL-derived cell lines (Figure 7A-E).
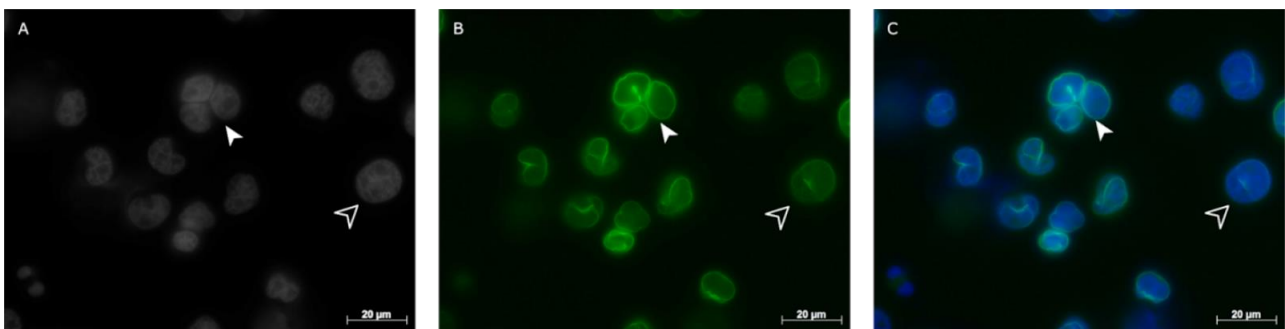
Figure 5. Example of lamin A/C protein staining in cells from Hodgkin's lymphoma (HDLM-2). (A) Two-dimensional (2D) image of nuclei stained with 4′,6-diamidino-2-phenylindole (DAPI)-(gray scale); (B) 2D image of anti-lamin A/C ab immunostaining (green); (C) 2D merged image showing both mono-nuclear H (empty arrowhead) and bi- to multi-nuclear RS cells (solid arrowhead) expressing lamin A/C.
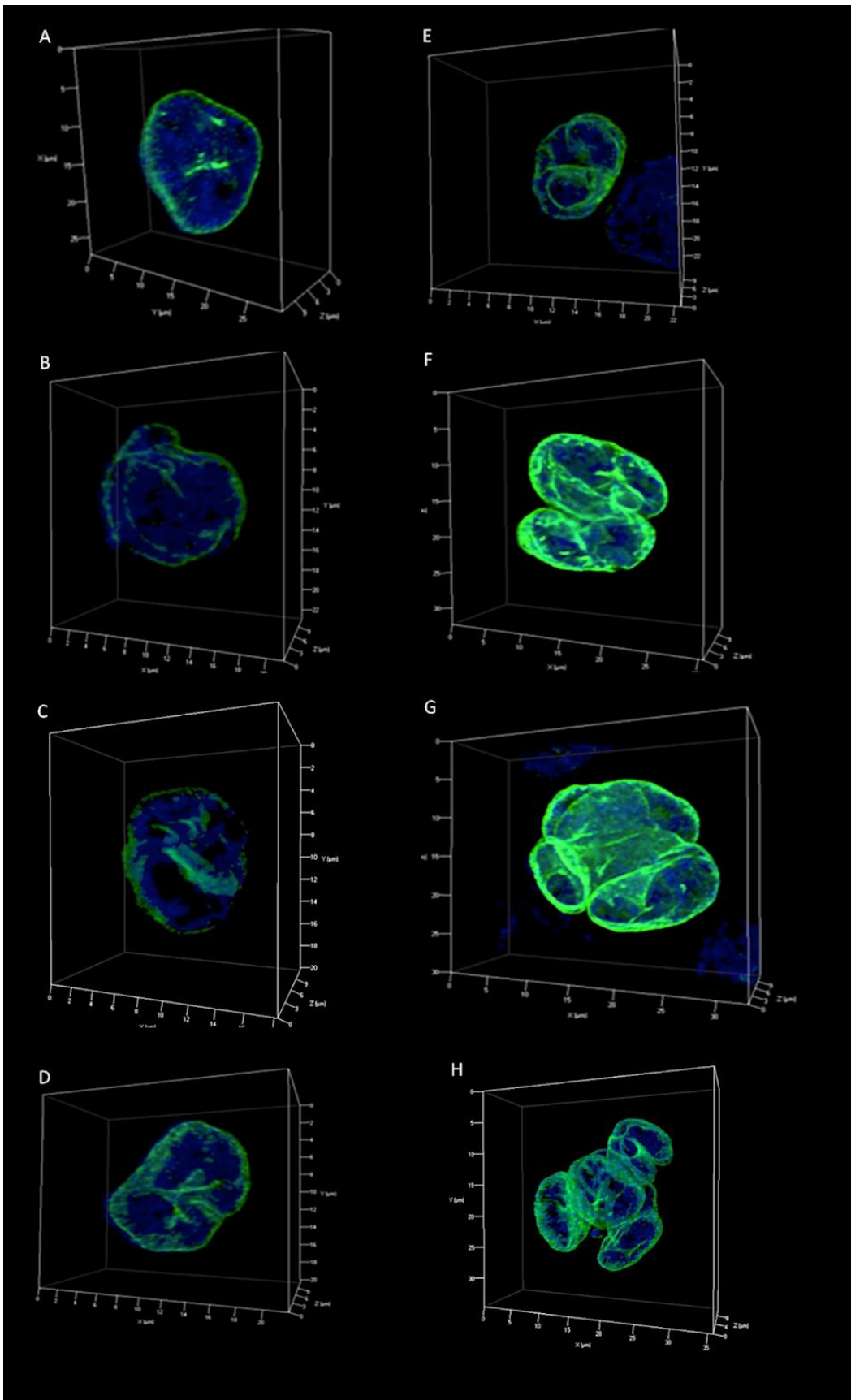
Figure 6. Lamin A/C patterns in 3D reconstructions of H and RS nuclei from HDLM-2. (A-E) H cells patterns according to how the internal lamin structures divide the 3D structure of lamin A/C: (A) pattern 0, characterized by a 3D pattern similar to the regular pattern of the LPS-activated

lymphocytes, showing, however, localized accumulation of the lamin A/C; (B) pattern A, characterized by the irregular lamin A/C 3D distribution and the presence of invaginations due to short internal lamin structures; (C) pattern B, characterized by a single long internal lamin A/C 3D structure, which divides the nucleus into 2 different compartments; (D) pattern C, characterized by 3D multiple internal lamin structures which divide the nucleus into 3 different compartments; (E) pattern D, characterized by 3D division of the nucleus into 4 different compartments. (F–H) RS cells patterns according to the number of nuclei: (F), bi-nuclear RS cell; (G) tetra-nuclear RS cell; (H) multi-nuclear RS cell.
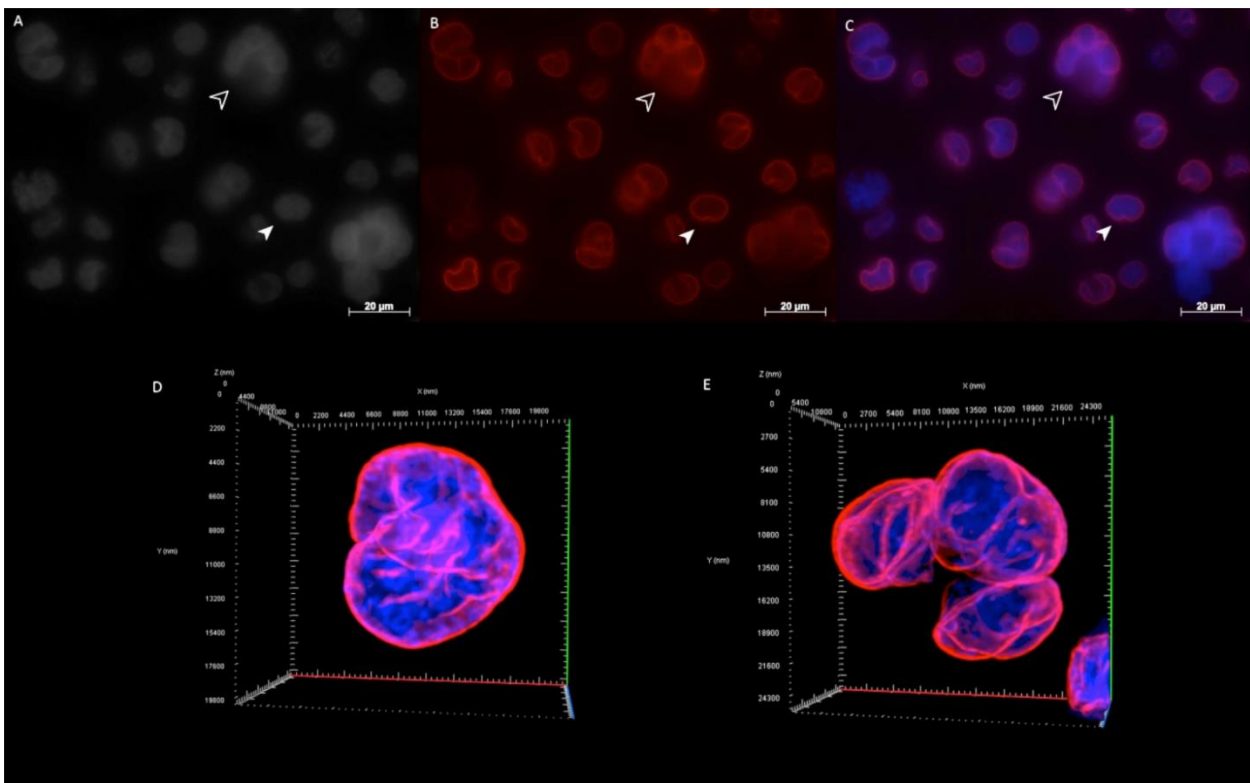


Figure 7. Example of lamin B1 protein staining in cells from Hodgkin's Lymphoma (HDLM-2). (**A**) 2D image of nuclei stained with DAPI (gray scale); (**B**) 2D image of anti-lamin B1 ab immunostaining (Cy3); (**C**) 2D merged image showing both mono-nuclear H (empty arrowhead) and bi- to multi-nuclear RS cells (solid arrowhead) expressing lamin B1. Complete 3D reconstitution of a H cell (**D**) and a RS cell (**E**).

Table 3. Quantitative analysis of lamin A/C patterns in H and RS cells. 30 H and 30 RS cells of the cHL-derived cell line HDLM-2 from three independent experiments were analyzed. Total external lamin A/C signal intensity ($I_e$) was divided by the total internal lamin A/C signal intensity ($I_i$) to obtain a ratio. Resulting ratios, S.D. and frequencies observed for each pattern are shown.

| Lamin A/C Pattern | $I_e/I_i$ | S.D. | Frequencies |
|---|---|---|---|
| LPS-treated Lymphocytes | 1.10 | 0.02 | 100% |
| Hodgkin Cell Pattern 0 | 1.88 | 1.17 | 15.48% |
| Hodgkin Cell Pattern A | 2.65 | 1.15 | 29.15% |
| Hodgkin Cell Pattern B | 3.65 | 2.12 | 42.16% |
| Hodgkin Cell Pattern C | 4.02 | 2.66 | 11.63% |
| Hodgkin Cell Pattern D | 5.43 | 0.04 | 1.59% |
| Bi-nuclear Reed-Sternberg | 2.96 | 1.07 | 57.66% |
| Tri-nuclear Reed-Sternberg | 3.57 | 1.26 | 22.27% |
| Tetra-nuclear Reed-Sternberg | 4.50 | 3.37 | 10.29% |
| Multi-nuclear Reed-Sternberg | 4.55 | 2.95 | 9.79% |

Table 4. Means of total area, total lamin A/C signal intensity and frequencies of the lamin A/C 3D patterns observed in cHL-derived cell line HDLM-2. 1000 cells were automatically scanned and manually divided according to the lamin A/C 3D pattern shown.

*Area: Region of pixels recognized by the software as a cell; **Total intensity: Sum of pixels' intensity in the area.

| Lamin A/C Pattern | *Area (Mean) | **Total Intensity (Mean) | Percentage |
|---|---|---|---|
| Hodgkin Cell Pattern 0 | 2068.30 | 3599853,26 | 15.31% |
| Hodgkin Cell Pattern A | 1682.52 | 3339595,81 | 53.74% |
| Hodgkin Cell Pattern B | 1772.61 | 3455334,77 | 25.29% |
| Hodgkin Cell Pattern C | 1730.18 | 3384059,04 | 5.03% |
| Hodgkin Cell Pattern D | 1646.67 | 3501005,55 | 0.63% |
| Bi-nuclear Reed-Sternberg | 2084.06 | 4286375,45 | 82.48% |
| Tri-nuclear Reed-Sternberg | 2515.25 | 5438447,75 | 13.87% |
| Tetra-nuclear Reed-Sternberg | 2879.00 | 6864649,50 | 1.46% |
| Multi-nuclear Reed-Sternberg | 3141.50 | 7670371,33 | 2.19% |

**Investigation of H and RS cells from patient samples confirms the presence of aberrant 3D lamin A/C spatial distribution**

To determine whether the aberrant lamin A/C 3D spatial distribution found in H and RS cells from cHL-derived cell lines was also observed in H and RS from patient samples, twelve primary diagnostic classical Hodgkin's lymphoma pre-treatment lymph node biopsy tissue sections were

immunostained for lamin A/C. CD30 positivity was used to recognize H and RS (Figure 8A–C). Immunohistochemical analysis revealed that the majority of the non-neoplastic lymphocytes in the lymph node were lamin A/C negative, while all H and RS cells stained positively for lamin A/C. However, the lamin A/C fluorescent signal was not consistent throughout the patients' samples, as some patient samples where characterized by stronger lamin A/C signals when compared to others. In the patient samples with strong lamin A/C staining, H and RS cells presented an irregular 3D lamin A/C staining pattern characterized by internal lamin structures (Figure 9). The aberrant lamin A/C patterns previously observed in the H and RS cells from cHL-derived cell lines were also identified in the H and RS cells of patient samples (Figure 9D-E). The majority of H cells expressed pattern 0 (45.71%) or pattern A (34.29%). Patterns B (14.29%) and C (5.71%) were not observed. Quantitative analysis of the identified patterns for the H was performed investigating the ratio of the $I_e$ on the $I_i$ as shown in Table 5.
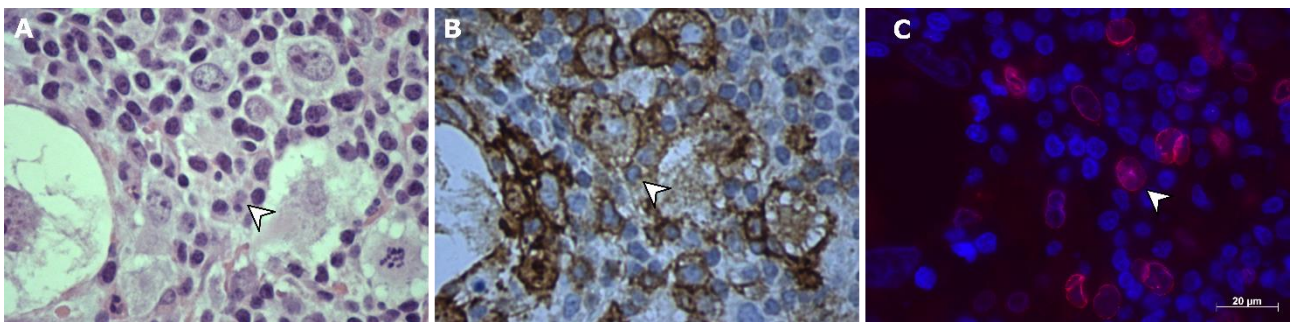


Figure 8. H&E, CD30 and lamin A/C staining of the same region in primary Hodgkin's Lymphoma paraffin embedded pre-treatment lymph node tissues from patients diagnosed with cHL. (A) Hematoxylin and Eosin (H&E) staining of primary HL paraffin embedded sample (B) Immunohistochemistry (IHC) for CD30 shows CD30 expression in H and RS cells from cHL patient sample. Images were acquired with a magnification of 40X. (C) Immunofluorescence (IF) staining of the same field of view revealed lamin A/C positive (red) staining in CD30+ cells. Nuclei were counterstained with DAPI (blue). Immunofluorescence image was acquired with a magnification of 63XOil. Full arrowheads indicate the same H cell in the different staining.
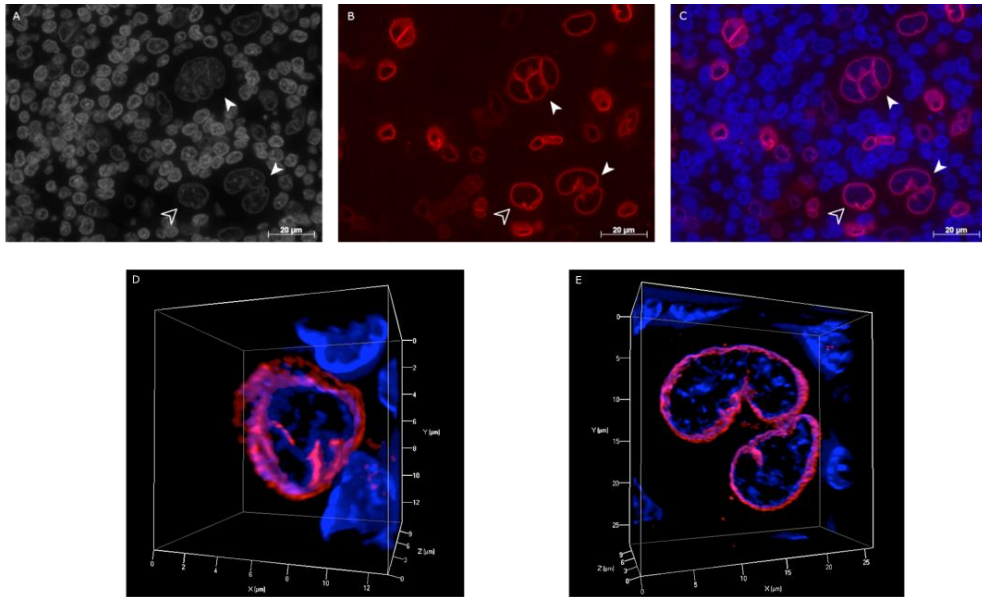
Figure 9. Example of lamin A/C expression in primary Hodgkin's lymphoma paraffin-embedded pre-treatment lymph node tissues from patients diagnosed with cHL. (A) 2D image of nuclei stained with DAPI (gray scale); (B) 2D image of anti-lamin A/C ab immunostaining (red); (C) 2D merged image showing H (empty arrowhead) and RS (solid arrowhead) cells positively stained for lamin A/C. 3D reconstruction of patient-derived mono-nuclear H cell (D), and bi-nuclear RS cells (E), presenting the sam patterns of irregular lamin A/C 3D structure characterized by internal lamin structures and points of protein accumulation, similar to those seen in the cHL-derived cell lines.

Table 5. Quantitative analysis of lamin A/C patterns in H cells. 30 H cells from 12 cHL patient samples were analyzed. Total external lamin A/C signal intensity ($I_e$) was divided by the total internal lamin A/C signal intensity ($I_i$) to obtain a ratio. Resulting ratios and S.D. are together with the frequencies observed for each pattern.

| Lamin A/C Pattern | $I_e/I_i$ | S.D. | Frequencies |
|---|---|---|---|
| Hodgkin Cell Pattern 0 | 2.97 | 0.08 | 45.71% |
| Hodgkin Cell Pattern A | 3.25 | 0.02 | 34.29% |
| Hodgkin Cell Pattern B | 4.1 | 0.32 | 14.29% |
| Hodgkin Cell Pattern C | 4.9 | 0.41 | 5.71% |
| Hodgkin Cell Pattern D | | | 0% |

**MM-derived cell line is characterized by aberrant 3D spatial distribution**

Immuno-staining of the MM-derived cell line MM.1R CRL-2975 showed that all cells express lamin A/C, but the lamin A/C intensity levels vary among cells. The investigation of lamin A/C's 3D spatial

distribution revealed the presence of irregular patterns characterized by the presence of a variable number of internal lamin A/C structures compartmentalizing the nuclear 3D structure into sub-compartments. Four different 3D spatial patterns (pattern 0, A, B and C) were identified based on the presence of lamin A/C internal structures (Figure 10A-D). Lamin internal structures were similar to the one previously observed in H cells from cHL. Quantitative analysis of the average $I_e/I_i$ ratio and the standard deviation for the different patterns was performed (Table 6; Table 7). As the irregularity and number of the internal lamin A/C structures in the pattern increases, so does the $I_e/I_i$ ratio, reflecting the observed change ($p<0.05$). By investigating the pattern frequencies, we found that the majority of the cells were associated with the pattern 0 (52.6%), followed by pattern A (23.2%), pattern B (16%) and C (7.4%).

Investigation of lamin B1 3D spatial distribution revealed the presence of the same types of patterns identified for lamin A/C.
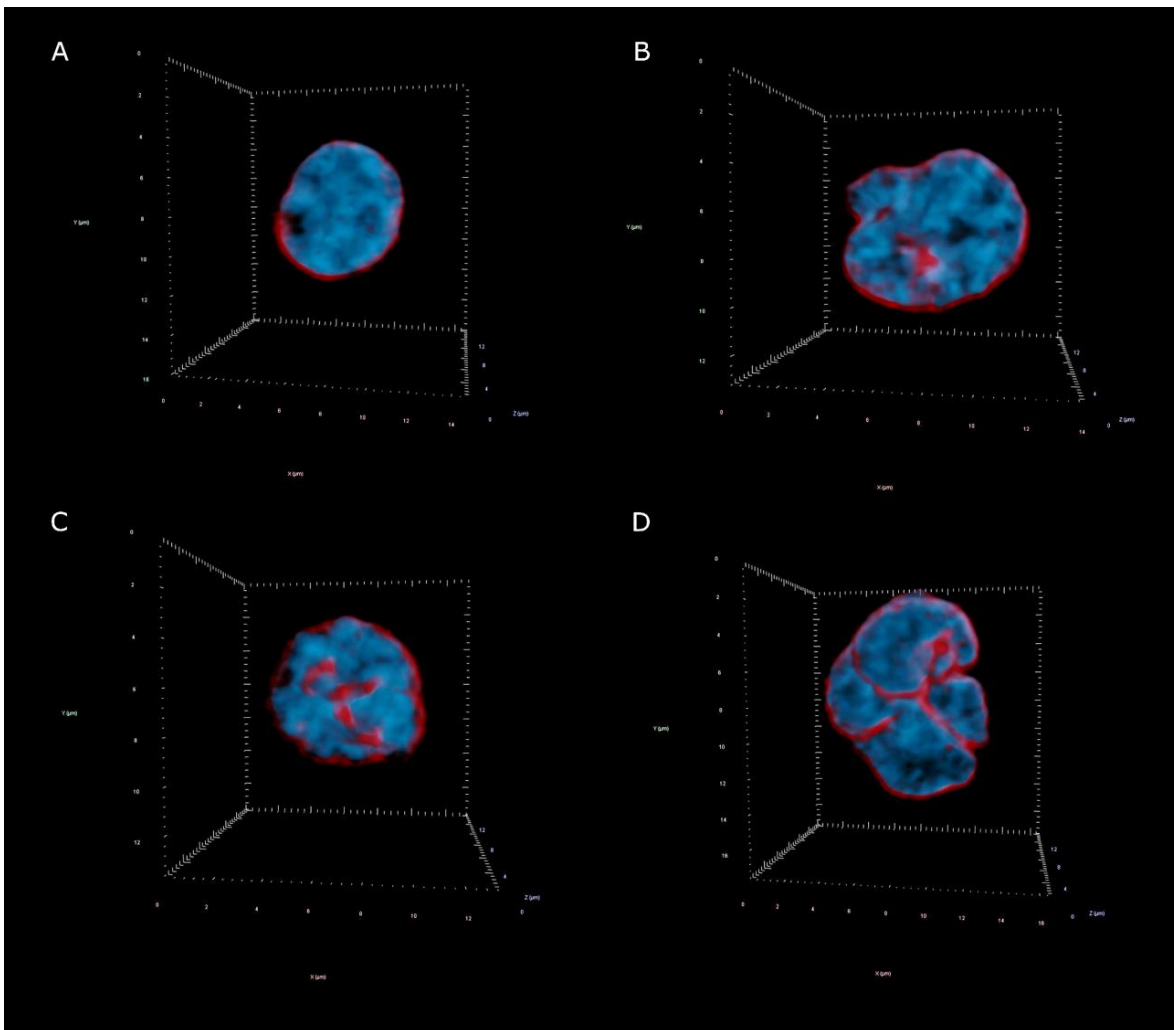


Figure 10. Lamin A/C patterns in 3D reconstructed nuclei from the MM.1R CRL-2975 cell line. (A–D) Cell patterns according to how the internal lamin structures (red) divide the 3D structure of lamin A/C: (A) pattern 0, characterized by a regular 3D pattern similar one observed in LPS-treated

lymphocytes; (B) pattern A, characterized by the irregular lamin A/C 3D distribution and the presence of invaginations due to short internal lamin structures; (C) pattern B, characterized by a single long internal lamin A/C 3D structure, which divides the nucleus into 2 different compartments; (D) pattern C, characterized by 3D multiple internal lamin structures which divide the nucleus into multiple compartments.

Table 6. Quantitative analysis and frequency of lamin A/C patterns in MM.1R CRL-2975 cell line, using ZEN Blue 2.6 (Zeiss) computer software.

| Lamin A/C Pattern | $I_e/I_i$ | S.D. | Frequencies |
|---|---|---|---|
| CRL-2975 Cell Pattern 0 | 1.81 | 0.15 | 53.62% |
| CRL-2975 Cell Pattern A | 2.02 | 0.26 | 23.19% |
| CRL-2975 Cell Pattern B | 2.29 | 0.30 | 15.94% |
| CRL-2975 Cell Pattern C | 2.62 | 0.16 | 7.25% |

Table 7. Means of total area, total lamin A/C signal intensity and frequencies of the lamin A/C 3D patterns observed in MM.1R CRL-2975 cell line. 1000 cells were automatically scanned and manually divided according to the lamin A/C 3D pattern shown.

*Area: Region of pixels recognized by the software as a cell; **Total intensity: Sum of pixels' intensity in the area.

| Lamin A/C Pattern | *Area (Mean) | **Total Intensity (Mean) | Percentage |
|---|---|---|---|
| CRL-2975 Cell Pattern 0 | 2068.30 | 3599853,26 | 15.31% |
| CRL-2975 Cell Pattern A | 1682.52 | 3339595,81 | 53.74% |
| CRL-2975 Cell Pattern B | 1772.61 | 3455334,77 | 25.29% |
| CRL-2975 Cell Pattern C | 1730.18 | 3384059,04 | 5.03% |

**MM cells from patient samples present similar aberrant lamin A/C structures found in MM-derived cell line**

To investigate the presence of the aberrant lamin A/C 3D spatial distribution in MM cells from the MM.1R CRL-2975, immuno-staining for lamin A/C was performed on ten pre-treatment blood samples from treatment-naïve patients newly diagnosed with MM (Figure 11A-E). Identification of the MM cells was performed through co-immuno-staining for CD138 and CD56, as CD138+ plus CD56+ cells were identified as MM cells (Figure 11C-D). Immuno-staining for lamin A/C revealed that all MM cells express lamin A/C. MM cells from patient samples presented similar lamin A/C 3D

patterns as observed in the MM.1R cell line, as they were characterized by aberrant 3D profiles and presence of lamin A/C internal structures (Figure 12A-D).

Quantitative analysis of the patterns was performed to investigate the $I_e/I_i$ ratio as shown in Table 8. Investigation of the frequencies revealed a slight predominance of pattern A (37%), followed by pattern C (31%), pattern B (19%), and pattern 0 (13%).
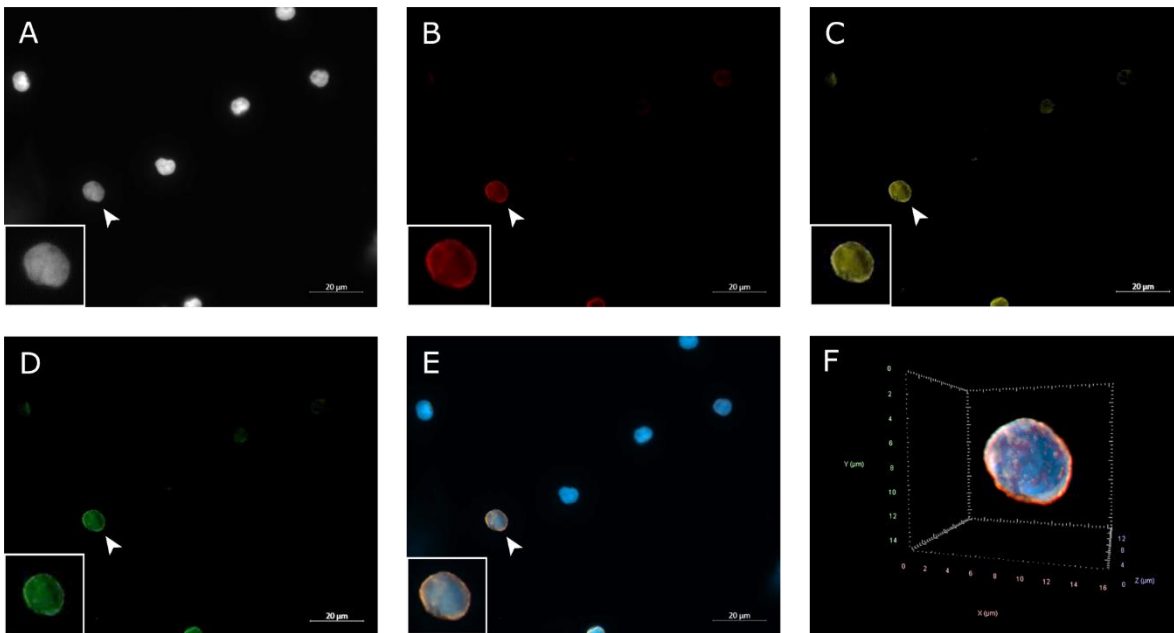


Figure 11. Immunostaining for lamin A/C, CD138 and CD56 of a representative patient sample from a patient diagnosed with MM. (A) 2D image of nuclei stained with DAPI (gray scale); (B) 2D image of anti-lamin A/C ab immunostaining (red); (C) 2D image of anti-CD138 ab immunostaining (olive); (D) 2D image of anti-CD56 ab immunostaining (green); (E) 2D merged image showing a lamin A/C+ CD138+ and CD56+ MM cell (arrowhead). Zoomed in image of MM cell is included in the white box of each image; (F) Complete 3D reconstruction of MM cell.
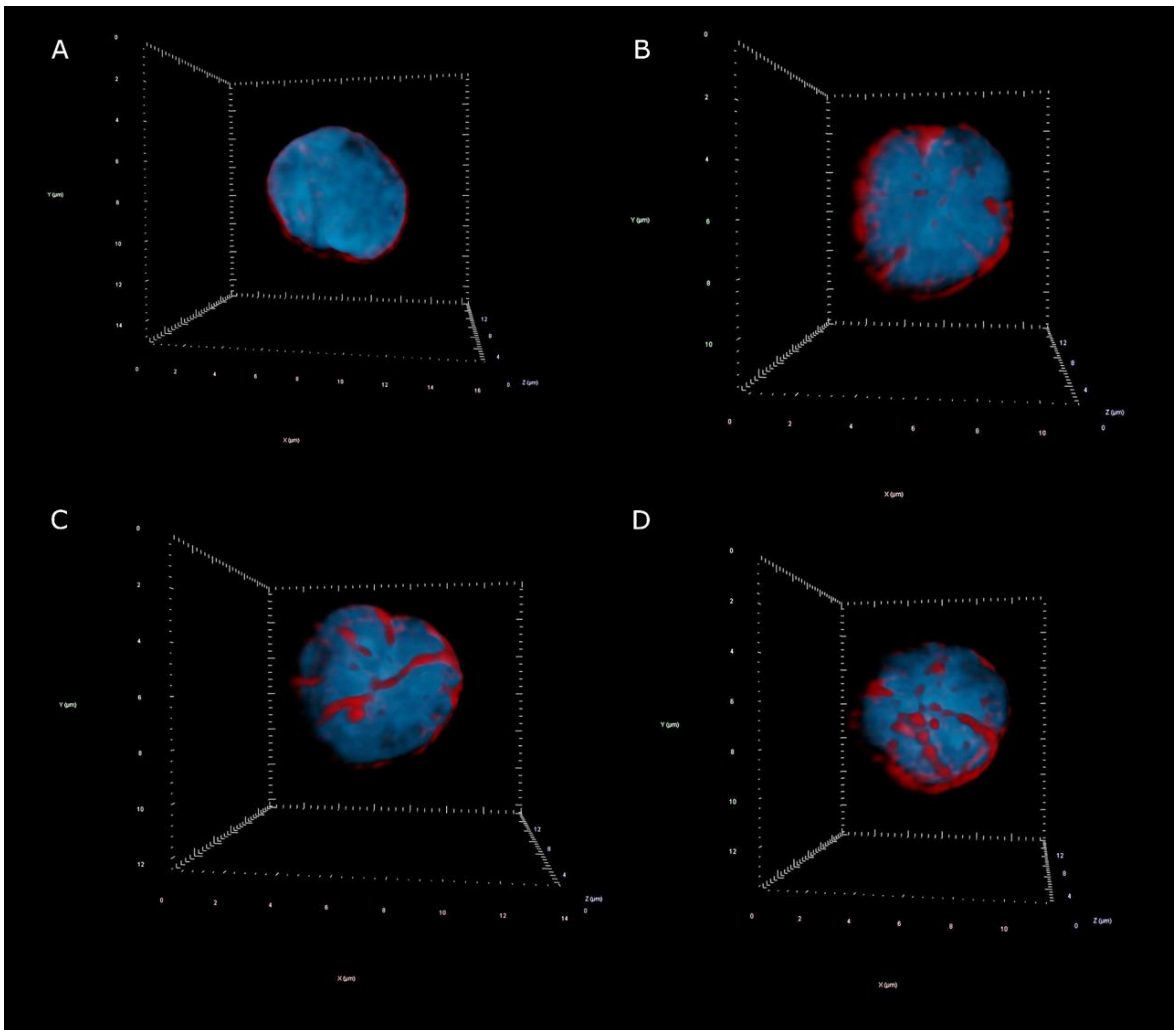
Figure 12. Lamin A/C patterns in 3D reconstructed nuclei from patients diagnosed with MM. (A–D) Cell patterns according to how the internal lamin structures (red) divide the 3D structure of lamin A/C: (A) pattern 0, characterized by a spherical 3D pattern; (B) pattern A, characterized by the irregular lamin A/C 3D distribution and the presence of invaginations due to short internal lamin structures; (C) pattern B, characterized by a single long internal lamin A/C 3D structure, which divides the nucleus into 2 different compartments; (D) pattern C, characterized by 3D multiple internal lamin structures which divide the nucleus into multiple compartments.

Table 8. Quantitative analysis and frequency of lamin A/C patterns in patients diagnosed with MM: Comparison between healthy donors and the MM.1R CRL-2975 using ZEN Blue 2.6 (Zeiss) computer software

| Lamin A/C Pattern | $I_e/I_i$ | S.D. | Frequencies |
|---|---|---|---|
| CRL-2975 Cell Pattern 0 | 2.87 | 0.01 | 12.87% |
| CRL-2975 Cell Pattern A | 3.05 | 0.28 | 37.11% |

CRL-2975 Cell Pattern B   3.31   0.40   19.02%

CRL-2975 Cell Pattern C   4.03   0.57   4.54%

**Lamin A/C protein transcription and expression are upregulated in H and RS cell when compared to normal B-lymphocytes**

After the investigation of the lamin A/C 3D spatial distribution, we wanted to determine if H and RS were characterized by lamin A/C protein upregulation when compared to the B-lymphocytes, or if they were only defined by an alternative, aberrant remodeling of the lamin A/C protein.

In order to assess the lamin A/C transcription and expression levels, we performed Western Blot (Figures 13,14) and qRT-PCR (Figure 15) analysis in the cHL-derived cell lines HDLM-2, L-428 and L-1236 and compared the results with resting and LPS-treated lymphocytes. The two-way ANOVA with Bonferroni posttest analysis was used to determine statistical significance for the Western Blots and qRT-PCR results. A value of $p < 0.05$ was considered statistically significant. All quantification experiments were done in triplicate. Relative protein expression compared to unstimulated lymphocytes was at a 2.7-fold increase in LPS-treated lymphocytes, at a 19.9-fold increase in L-428, at a 21.7-fold increase in L-1236, and at a 24.8-fold increase in H & RS cells of HDLM2 ($p<0.0001$ for all H-cell lines compared to resting and activated lymphocytes). Lamin A/C mRNA expression in unstimulated lymphocytes was set at 1. Relative mRNA expression in activated lymphocytes showed a 1.67-fold increase, in L-428 and L-1236 H & RS cells a 2.67- and 3.34-fold increase, respectively, and peaked a at 5.5-fold increase in HDLM2 H & RS cells ($p<0.0001$ for all H-cell lines compared to resting and activated lymphocytes).
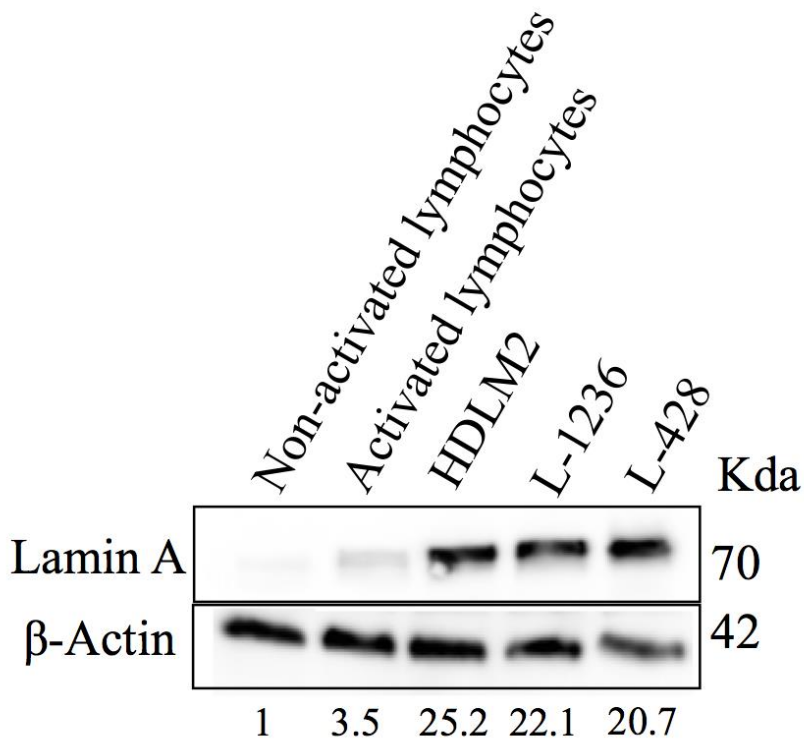
Figure 13. Lamin A/C protein expression in lymphocytes compared to cHL-derived cell lines. Example of lamin A/C protein expression measurement performed Western Blot in resting and LPS-treated lymphocytes (control) and compared to the three cHL-derived cell lines HDLM-2, L-1236 and L-428. β-actin was used as a loading control.
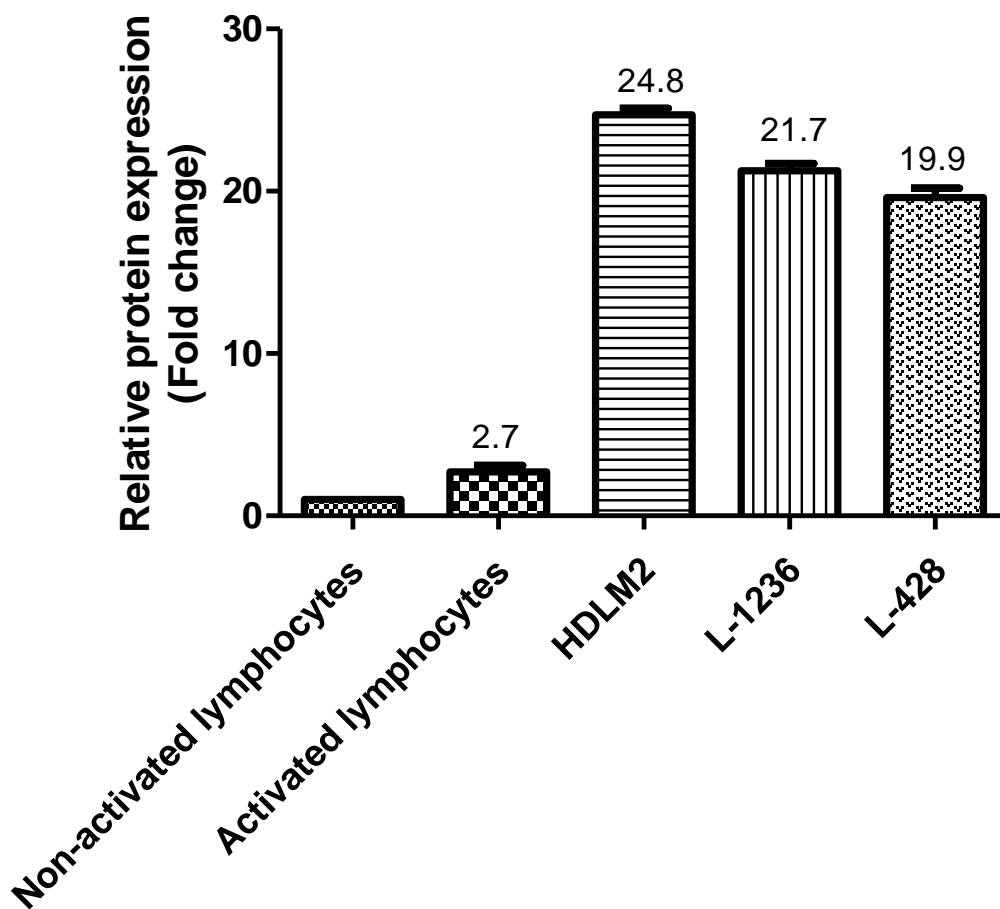
Figure 14. Relative protein expression in cHL-derived cell lines compared to resting and activated lymphocytes. Compared to resting lymphocytes, activated lymphocyte presented a 2.7-fold increase in lamin A/C expression ($p < 0.001$), HDLM-2 presented a 24.8-fold increase ($p < 0.001$), L-1236 presented a 21.7-fold increase ($p < 0.001$), and L-428 presented a 19.9-fold increase ($p < 0.001$). Single comparisons of the different combinations were all statistically significant ($p < 0.05$), with the exception of the L-1236 *vs* L-428 comparison (p=0.05).
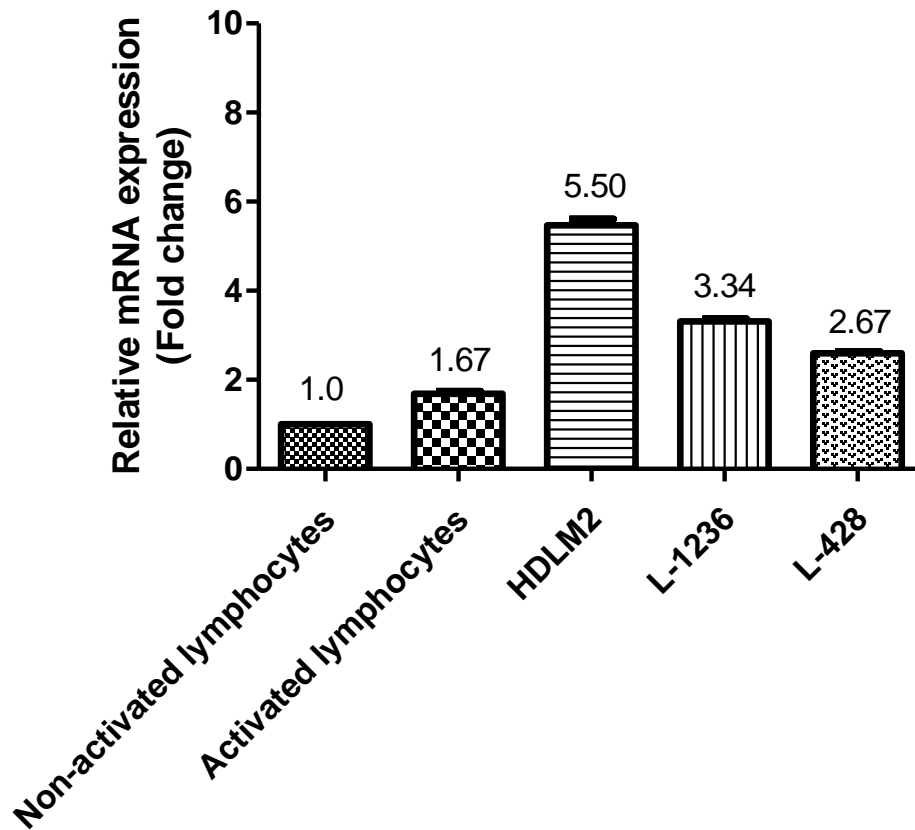
Figure 15. Relative mRNA expression in cHL-derived cell lines compared to resting and activated lymphocytes. Compared to resting lymphocytes, activated lymphocyte presented a 1.67-fold increase in lamin A/C transcription ($p < 0.001$), HDLM-2 presented a 5.50-fold increase ($p < 0.001$), L-1236 presented a 3.34-fold increase ($p < 0.001$), and L-428 presented a 2.67-fold increase ($p < 0.001$). Single comparisons of the different combinations were all statistically significant ($p < 0.05$).

**Deregulation of lamin A/C interferes with the transition from H to RS cells and induce aberrant 3D nuclear organization of telomeres and formation of telomere aggregates**

In order to explore how the lamin A/C silencing in the HDLM-2 cells affects the multinucleation process and the genomic instability, we transfected the HDLM-2 cells with siRNA lamin A/C and non-targeting siRNA (scrambled sequence) using four different concentrations for 24 h, 48 h, 72 h and 96h. Lamin A/C silencing was evaluated by WB (Figure 16) which revealed a decrease in lamin A/C expression after 24 h with an even greater decrease after 96 h compared to control cells. After 96 h, the expression of lamin A/C was down-regulated by about 70% (Figure 16), and the number of RS cells decreased from 48.37 to 25% in the HDLM2 siRNA lamin A/C when compared to the scrambled siRNA.

To investigate how lamin A/C silencing would affect the 3D nuclear organization of telomeres and to understand the complete kinetics of siRNA-mediated lamin A/C silencing, subsequent time points

of 96h, 120 h and 144 h were investigated. After 96 h, the silencing effect of lamin A/C siRNA started to decrease as shown in Figure 17 (Figure 17). We analyzed the lamin A/C silencing effects on the 3D telomere nuclear organization by combining the immuno-staining for lamin A/C with telomere Q-FISH.

Nuclei of 30 H and 30 RS cells transfected with siRNA lamin A/C were used for the telomere analysis. Scrambled siRNA treated H and RS cells were used as controls. siRNA treated H cells, after 96 h, were characterized by a decrease in the average telomere signal intensity (p = 0.0119), and by changes in the overall telomere spatial organization, as demonstrated by an increased *a/c* ratio, when compared to the control (p = 0.0079). The increased *a/c* ratio was also observed after 120 h (p = 0.0038) and 144 h (p = 0.0015). siRNA treated RS cells, after 96 h, were characterized by an increase in the total number of telomeres (p = 0.0013), an increase in number of telomere aggregates (p = 0.0073), an increase in nuclear volume (p < 0.0001), and a decrease in average telomere signal intensity (p = 0.0006) when compared to the scrambled siRNA treated control. The nuclear volume was still increased after 120 h (p < 0.0001) and 144 h (p = 0.0057) when compared to the scrambled siRNA treated control.

Moreover, the comparison among the 96 h, 120 h and 144 h time points revealed other telomere related abnormalities. In siRNA treated H cells, while both the total number of signals (p = 0.0308) and the total number of aggregates (p = 0.0473) increased from 96 h to 144 h. At the same time, the average telomere intensity (p = 0.0081), the total telomere signal intensity (p = 0.0311), the *a/c* ratio (p<0.0001) and the nuclear volume (p < 0.0001) decreased from 96 h to 144 h. The total number of telomere signals (p = 0.0280) and the total number of telomere aggregates (p = 0.0208) were found to be increased also in siRNA treated RS cells after 144 h when compared to 96 h, and the average telomere intensity (p = 0.0002), the total telomere signal intensity (p = 0.0318) and the nuclear volume (p = 0.0027) decreased as observed in the H cells. Prolonged downregulation of lamin A/C induced genomic instability in both H and RS cells, suggesting a prominent role of lamin A/C in the maintenance of telomere 3D spatial organization.
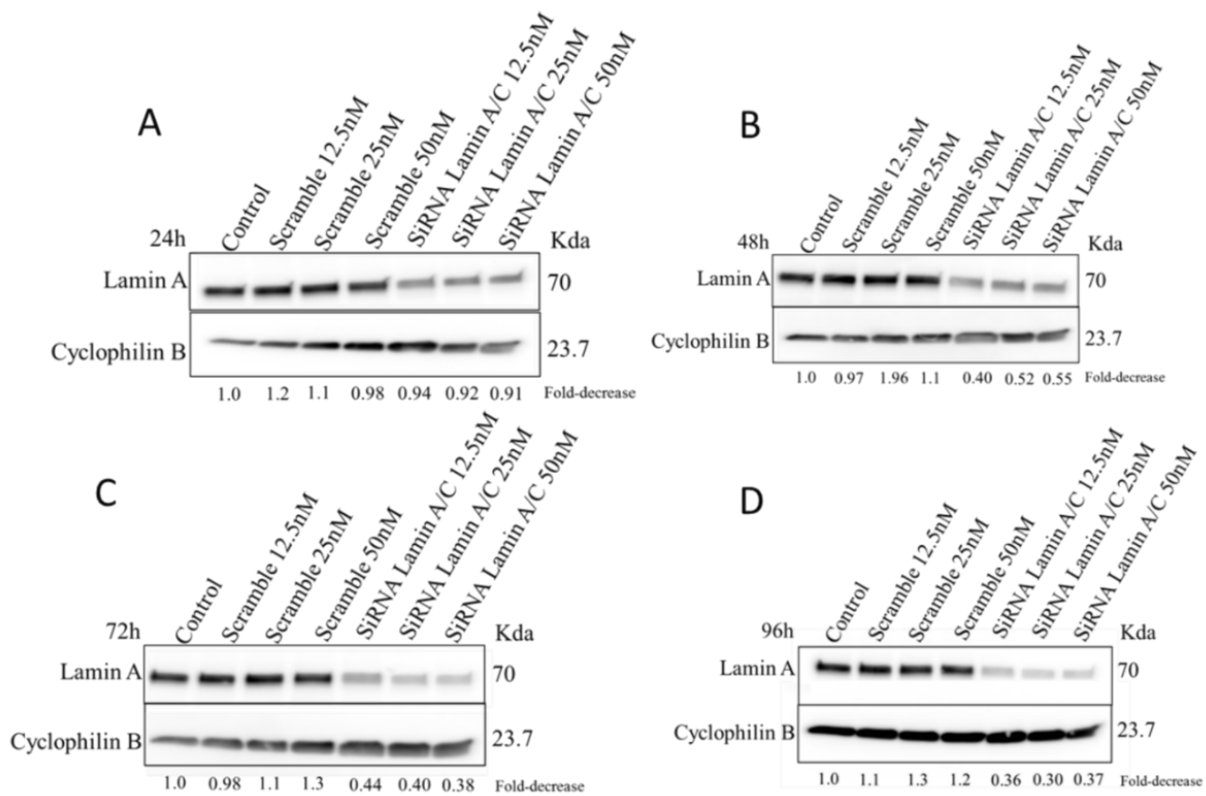
Figure 16. siRNA silencing of lamin A/C in HDLM-2. Lamin A/C expression was monitored by Western Blot after siRNA lamin A/C transfection in different concentration (12.5 nM, 25 nM and 50 nM) for 24 h (A), 48 h (B), 72 h (C) and 96 h (D). Scrambled siRNA was used as a negative control and Cyclophilin B was used as a loading control. The fold-decrease for the siRNA is relative to the negative control (Scrambled siRNA for each concentration) and the scrambled siRNA is relative to control without transfection (Control). These experiments were performed in triplicate using cells from consecutive passages.
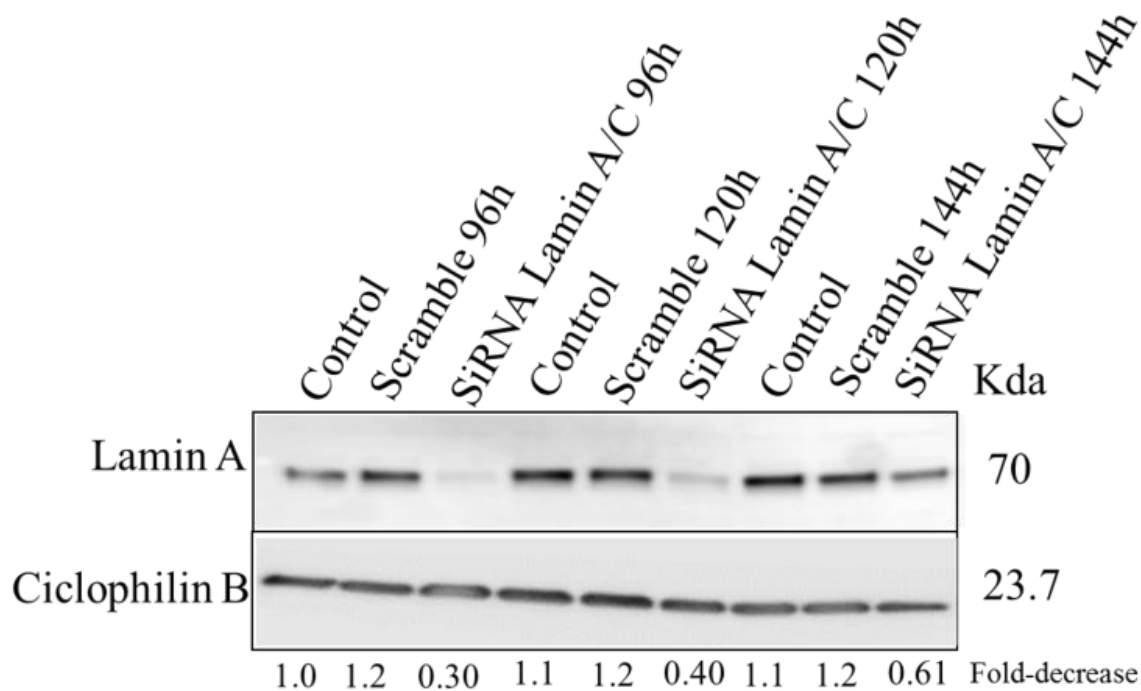
Figure 17. Investigation of siRNA silencing of lamin A/C in HDLM-2 for additional time points. Lamin A/C expression was monitored by Western Blot after siRNA lamin A/C transfection for 96 h, 120 h and 144 h (50 nM). Scrambled siRNA was used as a negative control and Cyclophilin B was used as a loading control. The fold-decrease for the siRNA is relative to the negative control (Scrambled siRNA for each concentration) and the scrambled siRNA is relative to control without transfection (Control). These experiments were performed in triplicate using cells in consecutive passages.

**Lamin A/C is involved in the maintenance of the nuclear architecture**

To further investigate the effects of lamin A/C deregulation on the genomic stability, 3D structured super resolution microscopy (3D-SIM) of 30 H and 30 RS cells from three independent siRNA lamin A/C samples (50 ng, 96 h) (Figure 18B,E respectively) and scrambled siRNA controls (Figure 18A,D respectively) was used to compare the 3D structural organization of the nuclear DNA of the two experimental arms. Granulometry was used to quantify both the DNA structure and the structure of DNA-free/poor spaces inside interphase nuclei, by measuring the cumulative size distribution (Figure 18C,F). The difference in the sub-micron size range was caused by differences in the DNA structure size (Righolt et al., 2014).

Two-sided, two-sample Kolmogorov–Smirnov test showed that the size distribution of both the DNA structure ($p = 0.26$) and DNA-free/poor spaces ($p = 0.37$) were not significantly different between

siRNA transfected H cells and scrambled siRNA H cells. However, the comparison between siRNA transfected RS cells and scrambled siRNA RS cells showed a difference, as both the DNA structure ($p < 0.001$) and structure of the DNA-free/poor spaces ($p <0.001$) contained finer structure in siRNA lamin A/C cells, suggesting a prominent role of lamin A/C in the nuclear architecture maintenance.
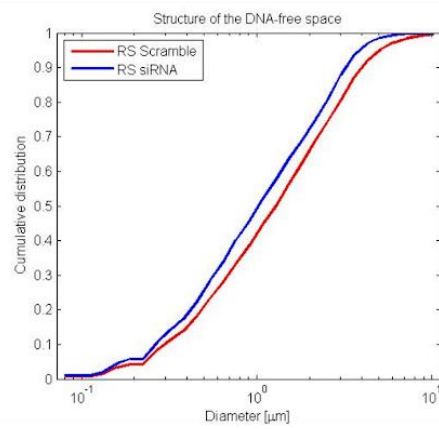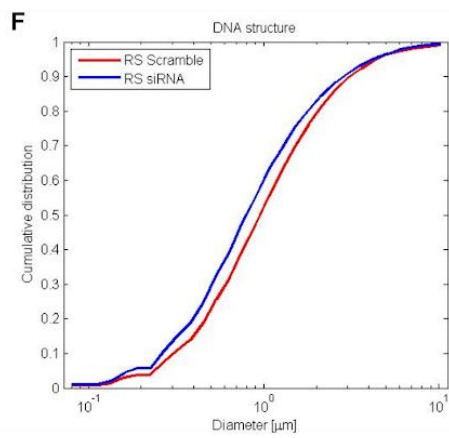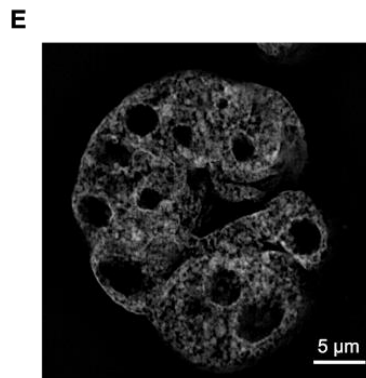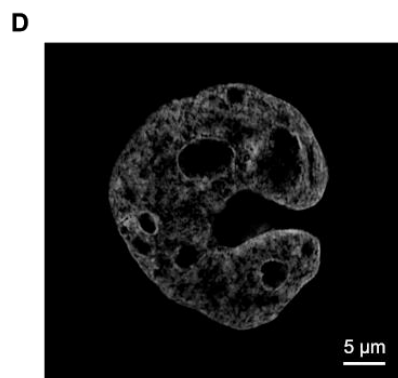
A

B

C

DNA structure

Structure of the DNA-free space
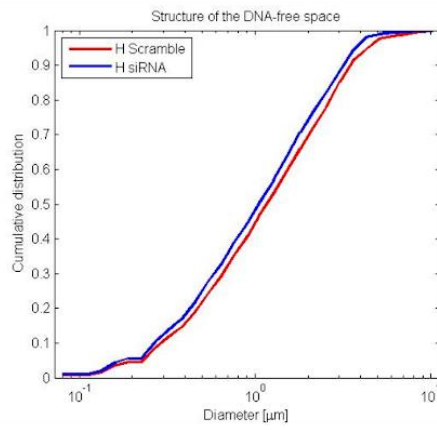
D

E

F

DNA structure
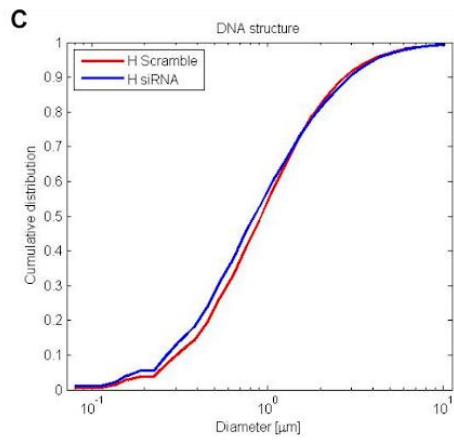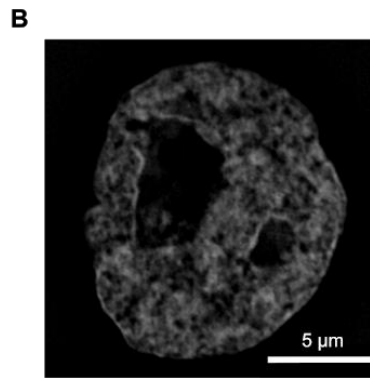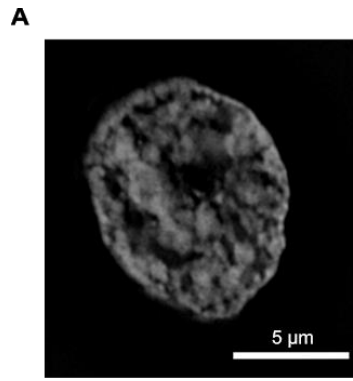
Structure of the DNA-free space

Figure 18. Granulometry analysis of siRNA lamin A/C cells and scrambled siRNA cells: (A) SIM image of scrambled siRNA H cell; (B) SIM image of lamin A/C siRNA H cell; (C) Measurements of the size distribution of DNA structure and structure of the DNA-free/poor spaces in SIM images of Hoechst (33258) stained nuclei of 30 H cells from three independent experiments; (D) SIM image of scrambled siRNA RS cell; (E) SIM image of lamin A/C siRNA RS cell; (F) Measurements of the size distribution of DNA structure (H: p = 0.26; RS: p<0.001) and structure of the DNA-free/poor spaces (H: p = 0.37; RS: p < 0.001) in SIM images of Hoechst (33258) stained nuclei of 30 RS cells from three independent experiments.

**Lack of co-localization of telomeres-TRF2-lamin A/C is observed in H and RS cells**

To investigate the interaction of lamin A/C, TRF2 and telomeres in cHL-derived cell lines, we combined the co-immuno-staining for lamin A/C and TRF2 with telomere quantitative fluorescent *in-situ* hybridization (Q-FISH) (Figure 19). Since the interaction between lamin A/C and TRF2 was previously described in normal human primary lung fibroblasts (Wood et al., 2014), the normal human fibroblast cell line BJ-5ta was used as an experimental control (Bodnar et al., 1998). LPS-treated lymphocytes were used as healthy controls. Preliminary data for the co-localization values for telomeres-TRF2-lamin A/C are shown in Table 9. While in the BJ-5ta control cells, co-localization of telomeres-TRF2-lamin A/C was commonly observed (68.08%), direct lamin A/C-TRF2-telomere interaction could not be observed in LPS-activated lymphocytes (17.07%), H and RS cells from cHL-derived cell lines (respectively: 14.84% in HDLM-2 H cells; 6.36% in HDLM-2 RS cells; 16.90% in L-428 H cells; 11.04% in L-428 RS cells; 10.89% in L-1236 H cells; 7.09% in L-1236 RS cells). Most of the co-localized telomere-TRF2-lamin A/C signals have been observed in the periphery of the cell for the activated lymphocytes and for the cHL-derived cell lines. Preliminary quantitative analysis of the co-localization of telomeres-TRF2-lamin A/C showed a profound decrease in the co-localization of LPS-activated lymphocytes, H and RS from cHL-derived cell lines when compared to the BJ-5ta control. When compared to LPS-treated lymphocytes, H cells from the HDLM-2 and L-1236 cell lines and RS from all three cHL-derived cell lines showed a decrease in the co-localization of telomeres-TRF2-lamin A/C. Comparison between H and RS cells in cHL-derived cell lines showed that RS cells are characterized by a decrease in the co-localization of telomere-TRF-2-lamin A/C. Comparison of the cHL-derived cell lines revealed that the L-1236 presents the least co-localization, followed by the HDLM-2 and the L-428. These results, however, are still a work in progress, as additional experiments will be needed to further investigate the co-localization of lamin A/C, TRF2 and telomeres.
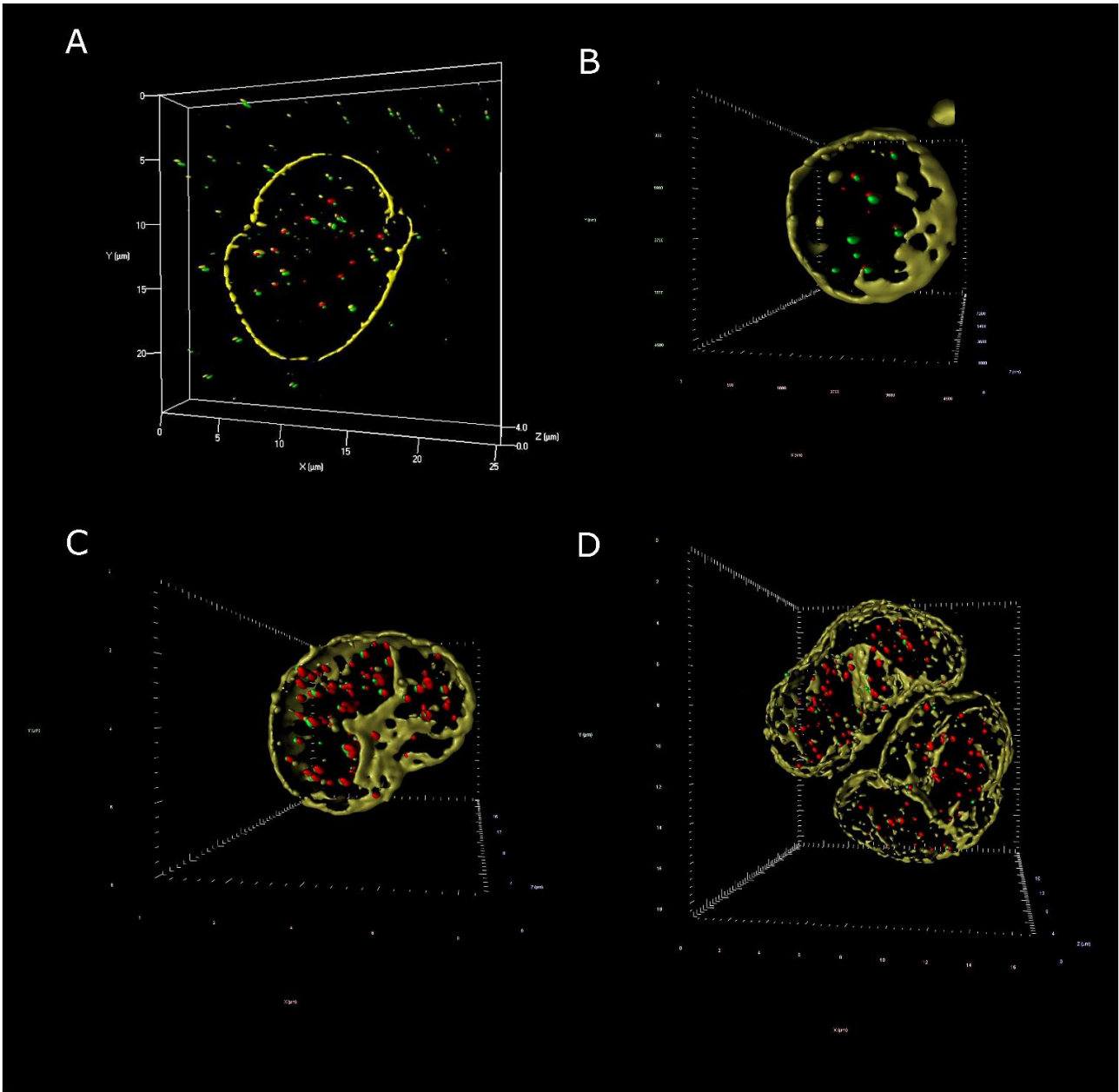
Figure 19. Co-localization of telomeres-TRF2-lamin A/C in BJ-5ta, LPS-activated lymphocytes and cHL-derived cell line HDLM-2. 3D reconstruction of a (A) BJ-5ta cell, (B) activated lymphocyte, (C) H and (D) RS cell from the HDLM-2 cell line stained for TRF2 (green), telomeres (red) and lamin A/C (olive).

Table 9: Preliminary data on co-localization of telomeres, TRF2 and lamin A/C in BJ-5ta cell line, LPS-activated lymphocytes and H and RS from cHL-derived cell lines HDLM-2, L-428 and L-1236.

| Cell Types | % of Co-localization ± S.D. |
|---|---|
| BJ-5ta cells | 68.08±10.40% |
| LPS-activated lymphocytes | 17.07±2.96% |

| | |
|---|---|
| HDLM-2 H cells | 14.84±1.32% |
| HDLM-2 RS cells | 6.36±0.28% |
| L-428 H cells | 16.90±1.64% |
| L-428 RS cells | 11.04±1.93% |
| L-1236 H cells | 10.89±0.99% |
| L-1236 RS cells | 7.09±0.88% |

# DISCUSSION

**Irregular lamin A/C 3D spatial distribution: impact on cell nuclear organization and aberrant gene expression in cHL and MM?**

My project was focused on investigating lamin A/C expression and its 3D spatial distribution in two different blood tumors, Hodgkin's Lymphoma and Multiple Myeloma, and studying its possible role in genomic instability.

Changes in lamin shape have been described in premature aging diseases such as Hutchinson–Gilford Progeria Syndrome and atypical Werner syndrome (Lammerding et al., 2004), but data on lamin morphologic profiles in cancer cells are scarce.

The analysis of lamin A/C in H cells, RS cells and MM cells revealed an irregular lamin 3D distribution pattern compared to the regular and continuous spherical lamin A/C matrix found in LPS-activated lymphocytes. More specifically, these cancer cells were characterized by the presence of prominent lamin A/C internal structures, which subdivided the nuclei into multiple compartments.

Aberrant 3D spatial distribution of lamin A/C can potentially interfere with cellular functions. It has indeed been demonstrated that in fibroblasts derived from patients with different laminopathies, as well as in lamin A/C-negative mouse fibroblasts, an altered nuclear lamina led to abnormally shaped nuclei, affecting mechanical properties of the cells and increasing the nuclear fragility (Lammerding et al., 2004; Mattout et al., 2006; Smith et al., 2018b).

An altered nuclear lamina can affect gene expression leading to a deregulation of different tissue-specific genes, either directly or at the epigenetic level (indirectly) (Lammerding et al., 2004). As previously described, lamin A/C and its binding partners can interact with DNA, histones, transcription factors and chromatin through lamin associated domains (LADs) (Guelen et al., 2008; Prokocimer et al., 2009). One of the regulation mechanism of gene expression is bringing the chromatin in contact with compartments of the nucleus that either upregulate or downregulate transcription. For example, during adipogenesis, the internalization of the nuclear position of several genes correlates with the upregulation of gene expression (Szczerbal et al., 2009). Although the interaction of the gene with the nuclear lamina has been generally associated with gene repression, DNA interaction with the nuclear lamina at the level of the nuclear pore complex has been correlated with activation of gene transcription (Brickner and Walter, 2004; Taddei, 2007). The nuclear position of a gene depends on the position of the chromosome within the nucleus. Each chromosome maintains its individuality during the cell cycle and occupies a spatially limited volume, known as a chromosome territory (Cremer and Cremer, 2001; Meaburn et al., 2007). cHL cells showed increasing

disruption of their nuclear architecture starting with H cells and dynamically progressing to RS cells. RS cell nuclei showed disrupted chromosomal territories, chromosomal rearrangements, aneuploidy and genetic diversity (Guffei et al., 2010). For this reason, we hypothesize that the irregular lamin A/C 3D spatial distribution may be cause of the aberrant positioning of chromosome territories in cHL leading to dysregulated gene expression. In order to investigate this hypothesis, further studies on co-localization of chromosome-territories and lamin A/C in cHL must be performed to determine if localized unbinding of lamin A/C from the chromatin is responsible for the disruption of regular positions of chromosome territories. Also, a larger cohort of patients for both cHL and MM will be required to confirm the distribution of lamin A/C patterns among the tumor cells in patient samples.

**Lamin A/C may be involved in the transition from H to RS cells**

Subdivision of the nucleus into multiple sub-compartments could anticipate the transition of a mono-nuclear H cell to a bi- to multi-nuclear RS cell, making the investigation of lamin A/C a potential tool to predict the future behavior of the H cell. Silencing experiments of the lamin A/C mRNA through siRNA transfection were performed, and a decrease in the number of total RS cells, telomere loss and aggregation, and progressive disruption of nuclear DNA organization were observed in treated cells compared to the control.

Deregulation of lamin A/C can affect DNA transcription, replication and repair, inducing genomic instability, a common feature of cancer progression (Gonzalez-Suarez et al., 2009; Gonzalo, 2014; Huang et al., 2008). Lamin A/C regulates both mitotic spindle assembly and positioning (Qi et al., 2015) and telomere length and positioning, thus playing an important role in the mitotic process (Allsopp et al., 1992; Gonzalez-Suarez et al., 2009; Kudlow et al., 2008; Raz et al., 2006, 2008).

Previous studies showed that cells displaying deregulation of lamin A/C were characterized by a high frequency of lagging chromosomes during mitosis, which increased proportionally with the level of lamin A/C deregulation, causing a marked increase of the number of bi-nuclear cells and giant nuclei in HGPS cells (Cao et al., 2007; Eisch et al., 2016).

ChIP–qPCR analysis revealed an enrichment of lamin A/C at the level of the TRF2 telomere-binding protein of the shelterin complex, and reduction in lamin A/C led to a significant decrease in the binding of TRF2 to the telomeres, suggesting that interaction between these two protein is crucial for telomeres stabilization and protection (Wood et al., 2014).

Depletion and overexpression of lamin proteins have also been associated with aberrant nuclear shapes, since it has been demonstrated that cells characterized by either lamin-A knockdown or overexpression of lamin A presented aberrant nuclear morphology, DNA damage, and micronuclei formation (Cui et al., 2007; Wang et al., 2019).

RS cells from cHL present an aberrant number and assembly of mitotic spindles, and a disrupted 3D telomeric structure characterized by critically short telomeres and a significant increase of telomere aggregates when compared with mononuclear H cells (Knecht et al., 2009, 2010). Extreme disruption of the 3D telomeric structure prevents further division (Knecht et al., 2009). We hypothesize that deregulation of lamin A/C is involved in the multinucleation process from H to RS cells, affecting the positioning of the mitotic spindles, telomere 3D spatial organization and the nuclear structure. However, live cell imaging of lamin-GFP-transfected cells is necessary to confirm lamin A/C's role in the multinucleation process during the transition from H to RS cell.

**Deregulation of the Akt/Pi3K pathway may be responsible for lamin A/C overexpression in cHL**

H and RS cells from cHL-derived cell lines showed high lamin A/C protein expression levels and mRNA levels when compared to LPS-treated lymphocytes and resting lymphocyte.

In normal cells, regulation of *LMNA* gene expression is regulated through the PI3K/Akt/mTOR pathway. The PI3K/Akt/mTOR pathway is involved in pre-lamin A transcription during interphase, through the regulation of the transcription factors FoxO1, Sp1/Sp3, AP1 and CREB (Bauer and Baier, 2002; Bertacchini et al., 2013; Kong et al., 2012).

In T cells, the PI3K protein is a downstream target of the CD28 protein, a cell surface receptor which can enhance cell signaling following T Cell Receptor stimulation upon cell activation (Smith-Garvin et al., 2009), which leads to upregulation of lamin A/C protein expression .(Rocha-Perugini and González-Granado, 2014).

In B cells, the PI3K/Akt/mTOR pathway activation is initiated when the antigen is recognized by the BCR and enhanced by CD19. The activation of this pathway regulates the activity of the transcription factor FoxO1 by exporting it from the nucleus to the cytoplasm, resulting in the transcription of different transcription factors, including PAX5 and Notch. leading to B cell development, activation and differentiation into antibody-secreting plasma cells (Abdelrasoul et al., 2018; Limon and Fruman, 2012).

Lamin A/C is not only a target of the PI3K/AKT/PTEN pathway, but it can also modulate the pathway itself. The existence of a lamin A/C-PI3K feedback loop, in fact, has been described in prostate cancer cells and leads to tumorigenesis (Kong et al., 2012). The PI3K/Akt/mTOR pathway is activated in a number of human neoplasms that are then characterized by lower overall and disease free survival (Ferté et al., 2010). This pathway plays a key role in the regulation of tumor cell survival, cell proliferation, cell transformation, metabolic activities and angiogenesis (Fang et al., 2007; Laplante and Sabatini, 2012; Paez and Sellers, 2003; Sun et al., 2009; Uzoh et al., 2009). Its anti-apoptotic

activity in particular prevents the release of cytochrome c from mitochondria and inactivates forkhead transcription factors known to induce expression of pro-apoptotic factors such as Fas ligand. Akt/PKB phosphorylates and inactivates the pro-apoptotic factors BAD and pro-caspase-9. Moreover, Akt/PKB leads to activation of IκB kinase, a positive regulator of NF-κB, which results in transcription of anti-apoptotic genes (Testa and Bellacosa, 2001).

cHL is characterized by the aberrant activation of the PI3K/Akt/mTOR pathway (Márk et al., 2013), and aberrant activation of the transcription factor PAX5 and Notch is commonly (Jundt et al., 2002, 2008)

We propose that a deregulation of the PI3K/Akt/mTOR may contribute to lamin A/C overexpression and tumor development in cHL and MM. However, the reason for neoplastic regulation of lamin proteins in cancer and their contribution to cancer progression are still unclear, so further investigation is needed. The transient silencing of Akt/PKB through siRNA in cHL and MM cell lines, and the overexpression of the PI3K/Akt/mTOR pathway in normal lymphocytes, may be useful to understand the downstream effects of the PI3K/Akt/mTOR pathway in lamin A/C expression in cHL and MM.


**Lamin A/C's potential role in cHL and MM cell migration**

Besides its important role in the regulation of gene expression, one of the main functions of lamin A/C is determining the rigidity and viscosity of the nucleus. Lamin A/C downregulation is commonly found in cells with high migratory capacity like bone marrow-derived mesenchymal stem cells (BMSCs), and is associated with metastasis in breast cancer cells (Chiotaki et al., 2014; de Leeuw et al., 2018; Liu et al., 2017).

As commonly known, metastasis is responsible for more than 90% of cancer patient mortality (Seyfried and Huysentruyt, 2013). The metastatic process is characterized by two critical steps: the intravasation of tumor cells into the blood vessels and the extravasation from blood vessels at target organs (Chiang et al., 2016). The extravasation of tumor cells to target tissue varies depending on the permeability of the capillaries. While some organs are easier to reach due to more permeable sinusoids, others present a relatively impermeable network of capillaries. The size and stiffness of the nucleus constitutes a limitation for cell migration, since cell nuclei are drastically pushed, pulled and deformed in order to progress through tight spaces (Davidson et al., 2014; Wolf et al., 2013). Current investigations address how the stiffness of the nuclear envelope affects cell extravasation in different parenchyma. Leukocytes characterized by stiff nuclear lamina were found to successfully cross inflamed endothelial monolayers, albeit with a small delay in nuclear squeezing into their sub-endothelial pseudopodia. However, crossing of tighter barriers was dramatically delayed by lamin A

overexpression, negatively affecting cell migration during the cell migration process (Yadav et al., 2018).

Lamin A/C has been found to be upregulated in prostate, skin, and ovarian cancer (Ho and Lammerding, 2012; Isermann and Lammerding, 2013; de Las Heras et al., 2013).

On the other hand, lamin A/C is downregulated in human acute lymphoblastic leukemia, non-Hodgkin's lymphoma, small cell lung cancer, lung adenocarcinoma, breast cancer and colorectal cancer (Capo-chichi et al., 2011; Denais and Lammerding, 2014; Foster et al., 2010; Kaspi et al., 2017; Stadelmann et al., 1990), with reduced levels of lamin A/C negatively correlating with disease-free survival in breast cancer (Wazir et al., 2013). The reduced levels of lamin A/C and the associated increased nuclear deformability facilitate migration of metastatic cancer cells through dense extracellular matrix and tight interstitial spaces as shown for human lung carcinoma cell line, mesenchymal stem cells and glioblastoma multiforme cell line (Davidson et al., 2014; Harada et al., 2014).

cHL lymphoma typically arises within the mediastinum, hematogenous (extranodal) metastases occur in approximately 10-15% of cases (Gharbaran et al., 2014), where cancer cells most commonly spread to local lymph nodes, thymus, spleen and distant lymph nodes via lymphatic system. More rarely, cHL can spread to the liver, lung parenchyma, hearth, chest wall, stomach, small intestine, bone marrow and bone (Toma et al., 2007). MM is a common malignant bone marrow lesion where MM cells migrate from one region of the bone marrow to another. (Park et al., 2018).

The presence of circulating tumor cells (CTCs) have been described in both cHL and MM (Gharbaran et al., 2014; Paiva et al., 2013). The CTCs in these diseases rarely migrate to organs characterized by the presence of dense parenchyma rich in collagen type I and III, like in the liver or in the lung (van Kuppevelt et al., 1995; Voss et al., 1980).

To better understand how lamin A/C affects cell migration, we will evaluate cell migration of tumor cells overexpressing lamin A/C through the Boyden Chamber assay. To understand lamin A/C regulation in CTCs, we will investigate lamin A/C expression and spatial distribution in CTCs and compare them to the one of the corresponding primary tumor cells.


**cHL is characterized by localized absence of telomeres-TRF2-lamin A/C**

Lamin A/C is involved in telomere stability and homeostasis (Allsopp et al., 1992; Decker et al., 2009; Gonzalez-Suarez et al., 2009; Kudlow et al., 2008; Wood et al., 2014), telomere mobility (De Vos et al., 2010) and sub-nuclear positioning (Ottaviani et al., 2009). In particular, the functional interaction between lamin A/C and TRF2 is responsible for the stabilization of the telomeres through

a higher order structure, stabilizing chromosome ends and protecting them from degradation (Smith et al., 2018a; Wood et al., 2014). Co-localization of telomeres-TRF2-lamin A/C in fibroblasts confirmed the previous observation that only part of the TRF2 co-localized with lamin A/C (Wood et al., 2014).

Our preliminary data showed that the BJ-5ta fibroblasts were characterized by co-localization of telomere-TRF2-lamin A/C. When compared to the fibroblasts, the co-localization in LPS-treated lymphocyte, and H and RS cells from the three cHL-derived cell lines, was decreased. The co-localization data obtained for the LPS-treated lymphocytes in particular, were not in line with the literature, as normal cells are normally characterized by the interaction of lamin A/C, TRF2 and telomeres (Wood et al., 2014). Super resolution imaging of immuno-stained lamin proteins in mouse embryo fibroblast (MEFs) revealed that instead of a network of fibrous structures, lamin proteins were initially found in a spotty staining pattern (Shimi et al., 2015). The explanation provided by the authors on why, in the MEFs, the lamin organization was not in line with the literature, was the lack of antibody accessibility or an inability of some lamin proteins to form connected networks. The expression of mEmerald-tagged lamin proteins showed that all lamin proteins form continuous networks, demonstrating that the spotty staining patterns were caused by issues with antibody accessibility (Shimi et al., 2015). For this reason, low co-localization of lamin A/C-TRF2-telomeres in activated lymphocytes may be explained by the impossibility of the anti-lamin A/C ab to correctly reach the target ab. Further studies involving high resolution microscopy will be necessary to better clarify the interaction between lamin A/C, TRF2 and telomeres.

# CONCLUSION AND FUTURE DIRECTIONS

**Conclusion**

cHL and MM are characterized by aberrant lamin A/C 3D spatial distribution characterized by the presence of internal lamin A/C structures not observed in the normal cells. In cHL in particular, the investigation of the 3D spatial organization aided to gain a better understanding of the transition from mononuclear H- to bi- and multi-nucleated RS-cells. The telomere analysis and the analysis of the nuclear architecture upon lamin A/C silencing suggested the involvement of lamin A/C in the multinucleation process. We conclude that the technology of 3D analysis holds the potential for becoming an invaluable predictive tool in the clinical management of this complex disease.

**Future Directions**

- <u>Investigation of lamin A/C aberrant 3D spatial distribution role in the multinucleation process</u>: Live cell imaging of lamin A/C-GFP transfected cells would be necessary for the visualization of the internal lamin A/C structures formation process, and to confirm their impact in the multinucleation process during the transition from H to RS cell.

- <u>Investigation of telomere-TRF2-lamin A/C co-localization</u>: Co-localization analysis showed lack of interaction among telomeres-TRF2 and lamin A/C in cancer cells, suggesting that lack of this interaction could be cause of genomic instability and nuclear remodeling in H and RS cells. However, ChIP–qPCR analysis for lamin A/C and TRF2 on H and RS cells will be needed to confirm the presence of the interaction of these two proteins. Transfection of a cDNA fragment encoding lamin A/C and inserted into mEmerald-C1 may be used to induce the expression of lamin A/C combined with 3D-SIM imaging would be necessary to confirm the presence of co-localization LPS-treated lymphoctres. Also, co-localization analysis should be performed on pre-treatment lymph node biopsy tissue sections from cHL patient to confirm the existence of such lack of interaction in patient samples, and to determine whether the TRF2-telomere-lamin A/C binding is different in patients with recurrent vs. non-recurrent disease.

  The examination of the impact of localized unbinding of TRF2 from lamin A/C and its impact on nuclear organization by using 3D telomere FISH and by using combinations of chromosome paints, will enable us to further understand nuclear remodeling in interphase nuclei.

- <u>Investigate Akt/PKB potential involvement in lamin A/C upregulation</u>: The identified deregulation of lamin A/C mRNA transcription and protein expression could potentially play an important role in cancer progression. Further studies to understand the pathway which leads to such deregulation are required to better understand the dynamics behind lamin A/C overexpression. The transient silencing of the Akt/PKB protein through siRNA in cHL cell lines and MM cell line, and the overexpression of the PI3K/Akt/mTOR pathway in normal lymphocytes, would be helpful to identify the impact of the PI3K/Akt/mTOR pathway on lamin A/C overexpression.

- <u>Investigate if lamin A/C spatial distribution and expression levels throughout the migration process</u>: The impact of the upregulation of lamin A/C on the cancer cell migration capability in cHL and MM is still unknown. To better understand how lamin A/C affects tumor cell migration, we will perform a comparison of the lamin A/C expression and spatial distribution in primary tumors compared to the corresponding CTCs and investigate cell migration capability in tumor cell overexpressing lamin A/C using the Boyden Chamber assay.

# ACKNOWLEDGMENTS

With sincere appreciation, the PhD candidate would like to like to express his gratitude to the different institutions and people who made this project possible. A special thanks goes to the following:

- I acknowledge my two supervisors, Prof. Roberta Vanni and Prof. Sabine Mai, who taught me and guided me through all these years, and helped me become a better student and a better researcher.

- I acknowledge the clinicians, Dr. Hans Knecht and Dr. Rami Kotb, whose knowledge on Hodgkin's Lymphoma and Multiple Myeloma helped me understanding the dynamics of the diseases and whose comments allowed me to move forward with the project.

- I acknowledge Dr. Aline Rangel-Pozzo, who helped me with some experiments, becoming an invaluable contributor to the project

# REFERENCES

- Abdelrasoul, H., Werner, M., Setz, C.S., Okkenhaug, K., and Jumaa, H. (2018). PI3K induces B-cell development and regulates B cell identity. Sci. Rep. *8*, 1327.

- Agrelo, R., Setien, F., Espada, J., Artiga, M.J., Rodriguez, M., Pérez-Rosado, A., Sanchez-Aguilera, A., Fraga, M.F., Piris, M.A., and Esteller, M. (2005). Inactivation of the lamin A/C gene by CpG island promoter hypermethylation in hematologic malignancies, and its association with poor survival in nodal diffuse large B-cell lymphoma. J. Clin. Oncol. Off. J. Am. Soc. Clin. Oncol. *23*, 3940–3947.

- Akıncılar, S.C., Khattar, E., Boon, P.L.S., Unal, B., Fullwood, M.J., and Tergaonkar, V. (2016). Long-Range Chromatin Interactions Drive Mutant TERT Promoter Activation. Cancer Discov. *6*, 1276–1291.

- Allsopp, R.C., Vaziri, H., Patterson, C., Goldstein, S., Younglai, E.V., Futcher, A.B., Greider, C.W., and Harley, C.B. (1992). Telomere length predicts replicative capacity of human fibroblasts. Proc. Natl. Acad. Sci. *89*, 10114–10118.

- Alvarado-Kristensson, M., and Rosselló, C.A. (2019). The Biology of the Nuclear Envelope and Its Implications in Cancer Biology. Int. J. Mol. Sci. *20*, 2586.

- Anderson, M.W., Reynolds, S.H., You, M., and Maronpot, R.M. (1992). Role of proto-oncogene activation in carcinogenesis. Environ. Health Perspect. *98*, 13–24.

- Avet-Loiseau, H., Gerson, F., Magrangeas, F., Minvielle, S., Harousseau, J.L., Bataille, R., and Intergroupe Francophone du Myélome (2001). Rearrangements of the c-myc oncogene are present in 15% of primary human multiple myeloma tumors. Blood *98*, 3082–3086.

- Azzalin, C.M., Reichenbach, P., Khoriauli, L., Giulotto, E., and Lingner, J. (2007). Telomeric repeat containing RNA and RNA surveillance factors at mammalian chromosome ends. Science *318*, 798–801.

- Bailey, S.M., and Murnane, J.P. (2006). Telomeres, chromosome instability and cancer. Nucleic Acids Res. *34*, 2408–2417.

- Bailey, M.H., Tokheim, C., Porta-Pardo, E., Sengupta, S., Bertrand, D., Weerasinghe, A., Colaprico, A., Wendl, M.C., Kim, J., Reardon, B., et al. (2018). Comprehensive Characterization of Cancer Driver Genes and Mutations. Cell *173*, 371-385.e18.

- Bargou, R.C., Leng, C., Krappmann, D., Emmerich, F., Mapara, M.Y., Bommert, K., Royer, H.D., Scheidereit, C., and Dörken, B. (1996). High-level nuclear NF-kappa B and Oct-2 is a common feature of cultured Hodgkin/Reed-Sternberg cells. Blood *87*, 4340–4347.

- Barlogie, B., Shaughnessy, J., Tricot, G., Jacobson, J., Zangari, M., Anaissie, E., Walker, R., and Crowley, J. (2004). Treatment of multiple myeloma. Blood *103*, 20–32.

- Bartkova, J., Horejsí, Z., Koed, K., Krämer, A., Tort, F., Zieger, K., Guldberg, P., Sehested, M., Nesland, J.M., Lukas, C., et al. (2005). DNA damage response as a candidate anti-cancer barrier in early human tumorigenesis. Nature *434*, 864–870.

- Bartkova, J., Rajpert-De Meyts, E., Skakkebaek, N.E., Lukas, J., and Bartek, J. (2007). DNA damage response in human testes and testicular germ cell tumours: biology and implications for therapy. Int. J. Androl. *30*, 282–291; discussion 291.

- Bauer, B., and Baier, G. (2002). Protein kinase C and AKT/protein kinase B in CD4+ T-lymphocytes: new partners in TCR/CD28 signal integration. Mol. Immunol. *38*, 1087–1099.

- Bayani, J., Selvarajah, S., Maire, G., Vukovic, B., Al-Romaih, K., Zielenska, M., and Squire, J.A. (2007). Genomic mechanisms and measurement of structural and numerical instability in cancer cells. Semin. Cancer Biol. *17*, 5–18.

- Bengtsson, L., and Wilson, K.L. (2004). Multiple and surprising new functions for emerin, a nuclear membrane protein. Curr. Opin. Cell Biol. *16*, 73–79.

- Berenson, J.R., Anderson, K.C., Audell, R.A., Boccia, R.V., Coleman, M., Dimopoulos, M.A., Drake, M.T., Fonseca, R., Harousseau, J.-L., Joshua, D., et al. (2010). Monoclonal gammopathy of undetermined significance: a consensus statement. Br. J. Haematol. *150*, 28–38.

- Berger, V.W., and Zhou, Y. (2014). Kolmogorov-Smirnov Test: Overview. In Wiley StatsRef: Statistics Reference Online, N. Balakrishnan, T. Colton, B. Everitt, W. Piegorsch, F. Ruggeri, and J.L. Teugels, eds. (Chichester, UK: John Wiley & Sons, Ltd), p. stat06558.

- Bertacchini, J., Beretti, F., Cenni, V., Guida, M., Gibellini, F., Mediani, L., Marin, O., Maraldi, N.M., de Pol, A., Lattanzi, G., et al. (2013). The protein kinase Akt/PKB regulates both prelamin A degradation and Lmna gene expression. FASEB J. Off. Publ. Fed. Am. Soc. Exp. Biol. *27*, 2145–2155.

- Bettin, N., Oss Pegorar, C., and Cusanelli, E. (2019). The Emerging Roles of TERRA in Telomere Maintenance and Genome Stability. Cells *8*, 246.

- Bianchi, G., and Anderson, K.C. (2014). Understanding biology to tackle the disease: Multiple myeloma from bench to bedside, and back. CA. Cancer J. Clin. *64*, 422–444.

- Bianchi, A., Smith, S., Chong, L., Elias, P., and de Lange, T. (1997). TRF1 is a dimer and bends telomeric DNA. EMBO J. *16*, 1785–1794.

- Blasco, M.A. (2005). Telomeres and human disease: ageing, cancer and beyond. Nat. Rev. Genet. *6*, 611–622.

- Bodnar, A.G., Ouellette, M., Frolkis, M., Holt, S.E., Chiu, C.P., Morin, G.B., Harley, C.B., Shay, J.W., Lichtsteiner, S., and Wright, W.E. (1998). Extension of life-span by introduction of telomerase into normal human cells. Science *279*, 349–352.

- Bonne, G., Di Barletta, M.R., Varnous, S., Bécane, H.M., Hammouda, E.H., Merlini, L., Muntoni, F., Greenberg, C.R., Gary, F., Urtizberea, J.A., et al. (1999). Mutations in the gene encoding lamin A/C cause autosomal dominant Emery-Dreifuss muscular dystrophy. Nat. Genet. *21*, 285–288.

- Bouck, N., Stellmach, V., and Hsu, S.C. (1996). How tumors become angiogenic. Adv. Cancer Res. *69*, 135–174.

- Boveri, T. (1902). "Uber mehrpolige Mitosen als Mittel zur Analyse des Zellkerns." Veh. Dtsch. Zool. Ges., Wurtzburg.

- Boveri, T. (1914). "Zur Frage der Entstehung maligner Tumoren." Fischer, Jena.)

- Boyd, K.D., Ross, F.M., Tapper, W.J., Chiecchio, L., Dagrada, G., Konn, Z.J., Gonzalez, D., Walker, B.A., Hockley, S.L., Wardell, C.P., et al. (2011). The clinical impact and molecular biology of del(17p) in multiple myeloma treated with conventional or thalidomide-based therapy. Genes. Chromosomes Cancer *50*, 765–774.

- Brickner, J.H., and Walter, P. (2004). Gene recruitment of the activated INO1 locus to the nuclear membrane. PLoS Biol. *2*, e342.
- Bronshtein, I., Kepten, E., Kanter, I., Berezin, S., Lindner, M., Redwood, A.B., Mai, S., Gonzalo, S., Foisner, R., Shav-Tal, Y., et al. (2015). Loss of lamin A function increases chromatin dynamics in the nuclear interior. Nat. Commun. *6*, 8044.
- Bryan, T.M., and Cech, T.R. (1999). Telomerase and the maintenance of chromosome ends. Curr. Opin. Cell Biol. *11*, 318–324.
- Bryan, T.M., Englezou, A., Gupta, J., Bacchetti, S., and Reddel, R.R. (1995). Telomere elongation in immortal human cells without detectable telomerase activity. EMBO J. *14*, 4240–4248.
- Buchwalow, I., Samoilova, V., Boecker, W., and Tiemann, M. (2018). Multiple immunolabeling with antibodies from the same host species in combination with tyramide signal amplification. Acta Histochem. *120*, 405–411.
- Cagnetta, A., Lovera, D., Grasso, R., Colombo, N., Canepa, L., Ballerini, F., Calvio, M., Miglino, M., Gobbi, M., Lemoli, R., et al. (2015). Mechanisms and Clinical Applications of Genome Instability in Multiple Myeloma. BioMed Res. Int. *2015*, 943096.
- Cao, K., Capell, B.C., Erdos, M.R., Djabali, K., and Collins, F.S. (2007). A lamin A protein isoform overexpressed in Hutchinson-Gilford progeria syndrome interferes with mitosis in progeria and normal cells. Proc. Natl. Acad. Sci. U. S. A. *104*, 4949–4954.
- Capo-chichi, C.D., Cai, K.Q., Smedberg, J., Ganjei-Azar, P., Godwin, A.K., and Xu, X.-X. (2011). Loss of A-type lamin expression compromises nuclear envelope integrity in breast cancer. Chin. J. Cancer *30*, 415–425.
- Carbone, A., Gloghini, A., Gruss, H.J., and Pinto, A. (1995). CD40 ligand is constitutively expressed in a subset of T cell lymphomas and on the microenvironmental reactive T cells of follicular lymphomas and Hodgkin's disease. Am. J. Pathol. *147*, 912–922.
- Carbone, A., Gloghini, A., Gaidano, G., Franceschi, S., Capello, D., Drexler, H.G., Falini, B., and Dalla-Favera, R. (1998). Expression Status of BCL-6 and Syndecan-1 Identifies Distinct Histogenetic Subtypes of Hodgkin's Disease. Blood *92*, 2220.
- Cenni, V., Bertacchini, J., Beretti, F., Lattanzi, G., Bavelloni, A., Riccio, M., Ruzzene, M., Marin, O., Arrigoni, G., Parnaik, V., et al. (2008). Lamin A Ser404 is a nuclear target of Akt phosphorylation in C2C12 cells. J. Proteome Res. *7*, 4727–4735.
- Chen, L., Lee, L., Kudlow, B.A., Dos Santos, H.G., Sletvold, O., Shafeghati, Y., Botha, E.G., Garg, A., Hanson, N.B., Martin, G.M., et al. (2003). LMNA mutations in atypical Werner's syndrome. Lancet Lond. Engl. *362*, 440–445.
- Cheng, K.C., and Loeb, L.A. (1993). Genomic instability and tumor progression: mechanistic considerations. Adv. Cancer Res. *60*, 121–156.
- Cheng, J.Q., Lindsley, C.W., Cheng, G.Z., Yang, H., and Nicosia, S.V. (2005). The Akt/PKB pathway: molecular target for cancer drug discovery. Oncogene *24*, 7482–7492.
- Chiang, S.P.H., Cabrera, R.M., and Segall, J.E. (2016). Tumor cell intravasation. Am. J. Physiol. Cell Physiol. *311*, C1–C14.
- Chiba, K., Johnson, J.Z., Vogan, J.M., Wagner, T., Boyle, J.M., and Hockemeyer, D. (2015). Cancer-associated TERT promoter mutations abrogate telomerase silencing. ELife *4*.

- Chiotaki, R., Polioudaki, H., and Theodoropoulos, P.A. (2014). Differential nuclear shape dynamics of invasive andnon-invasive breast cancer cells are associated with actin cytoskeleton organization and stability. Biochem. Cell Biol. *92*, 287–295.
- Chiu, A., Xu, W., He, B., Dillon, S.R., Gross, J.A., Sievers, E., Qiao, X., Santini, P., Hyjek, E., Lee, J., et al. (2007). Hodgkin lymphoma cells express TACI and BCMA receptors and generate survival and proliferation signals in response to BAFF and APRIL. Blood *109*, 729–739.
- Chng, W.J., Van Wier, S.A., Ahmann, G.J., Winkler, J.M., Jalal, S.M., Bergsagel, P.L., Chesi, M., Trendle, M.C., Oken, M.M., Blood, E., et al. (2005). A validated FISH trisomy index demonstrates the hyperdiploid and nonhyperdiploid dichotomy in MGUS. Blood *106*, 2156–2161.
- Chng, W.-J., Huang, G.F., Chung, T.H., Ng, S.B., Gonzalez-Paz, N., Troska-Price, T., Mulligan, G., Chesi, M., Bergsagel, P.L., and Fonseca, R. (2011). Clinical and biological implications of MYC activation: a common difference between MGUS and newly diagnosed multiple myeloma. Leukemia *25*, 1026–1035.
- Chng, W.J., Dispenzieri, A., Chim, C.-S., Fonseca, R., Goldschmidt, H., Lentzsch, S., Munshi, N., Palumbo, A., Miguel, J.S., Sonneveld, P., et al. (2014). IMWG consensus on risk stratification in multiple myeloma. Leukemia *28*, 269–277.
- Christofori, G., and Semb, H. (1999). The role of the cell-adhesion molecule E-cadherin as a tumour-suppressor gene. Trends Biochem. Sci. *24*, 73–76.
- Chuang, T.C.Y., Moshir, S., Garini, Y., Chuang, A.Y.-C., Young, I.T., Vermolen, B., van den Doel, R., Mougey, V., Perrin, M., Braun, M., et al. (2004). The three-dimensional organization of telomeres in the nucleus of mammalian cells. BMC Biol. *2*, 12.
- Cremer, T., and Cremer, C. (2001). Chromosome territories, nuclear architecture and gene regulation in mammalian cells. Nat. Rev. Genet. *2*, 292–301.
- Croll, D., Zala, M., and McDonald, B.A. (2013). Breakage-fusion-bridge cycles and large insertions contribute to the rapid evolution of accessory chromosomes in a fungal pathogen. PLoS Genet. *9*, e1003567.
- Cui, Y., Koop, E.A., van Diest, P.J., Kandel, R.A., and Rohan, T.E. (2007). Nuclear morphometric features in benign breast tissue and risk of subsequent breast cancer. Breast Cancer Res. Treat. *104*, 103–107.
- Curto, M., Cole, B.K., Lallemand, D., Liu, C.-H., and McClatchey, A.I. (2007). Contact-dependent inhibition of EGFR signaling by Nf2/Merlin. J. Cell Biol. *177*, 893–903.
- Danescu, A., Herrero Gonzalez, S., Di Cristofano, A., Mai, S., and Hombach-Klonisch, S. (2013). Three-dimensional nuclear telomere architecture changes during endometrial carcinoma development. Genes. Chromosomes Cancer *52*, 716–732.
- Datto, M.B., Hu, P.P., Kowalik, T.F., Yingling, J., and Wang, X.F. (1997). The viral oncoprotein E1A blocks transforming growth factor beta-mediated induction of p21/WAF1/Cip1 and p15/INK4B. Mol. Cell. Biol. *17*, 2030–2037.
- Davidson, P.M., Denais, C., Bakshi, M.C., and Lammerding, J. (2014). Nuclear deformability constitutes a rate-limiting step during cell migration in 3-D environments. Cell. Mol. Bioeng. *7*, 293–306.
- Davies, M.A., and Samuels, Y. (2010). Analysis of the genome to personalize therapy for melanoma. Oncogene *29*, 5545–5555.

- De Vitis, M., Berardinelli, F., and Sgura, A. (2018). Telomere Length Maintenance in Cancer: At the Crossroad between Telomerase and Alternative Lengthening of Telomeres (ALT). Int. J. Mol. Sci. *19*.

- De Vos, W.H., Houben, F., Hoebe, R.A., Hennekam, R., van Engelen, B., Manders, E.M.M., Ramaekers, F.C.S., Broers, J.L.V., and Van Oostveldt, P. (2010). Increased plasticity of the nuclear envelope and hypermobility of telomeres due to the loss of A–type lamins. Biochim. Biophys. Acta BBA - Gen. Subj. *1800*, 448–458.

- DeBerardinis, R.J., Lum, J.J., Hatzivassiliou, G., and Thompson, C.B. (2008). The biology of cancer: metabolic reprogramming fuels cell growth and proliferation. Cell Metab. *7*, 11–20.

- Decker, M.L., Chavez, E., Vulto, I., and Lansdorp, P.M. (2009). Telomere length in Hutchinson-Gilford Progeria Syndrome. Mech. Ageing Dev. *130*, 377–383.

- Denais, C., and Lammerding, J. (2014). Nuclear mechanics in cancer. Adv. Exp. Med. Biol. *773*, 435–470.

- Denchi, E.L., and de Lange, T. (2007). Protection of telomeres through independent control of ATM and ATR by TRF2 and POT1. Nature *448*, 1068–1071.

- Deng, Y., Chan, S.S., and Chang, S. (2008). Telomere dysfunction and tumour suppression: the senescence connection. Nat. Rev. Cancer *8*, 450–458.

- Deng, Z., Norseen, J., Wiedmer, A., Riethman, H., and Lieberman, P.M. (2009). TERRA RNA binding to TRF2 facilitates heterochromatin formation and ORC recruitment at telomeres. Mol. Cell *35*, 403–413.

- Di Micco, R., Fumagalli, M., Cicalese, A., Piccinin, S., Gasparini, P., Luise, C., Schurra, C., Garre', M., Nuciforo, P.G., Bensimon, A., et al. (2006). Oncogene-induced senescence is a DNA damage response triggered by DNA hyper-replication. Nature *444*, 638–642.

- Dilley, R.L., and Greenberg, R.A. (2015). ALTernative Telomere Maintenance and Cancer. Trends Cancer *1*, 145–156.

- Dimopoulos, M.A., and Terpos, E. (2010). Multiple myeloma. Ann. Oncol. Off. J. Eur. Soc. Med. Oncol. *21 Suppl 7*, vii143-150.

- Doksani, Y., Wu, J.Y., de Lange, T., and Zhuang, X. (2013). Super-resolution fluorescence imaging of telomeres reveals TRF2-dependent T-loop formation. Cell *155*, 345–356.

- Drake, M.T. (2014). unveiling skeletal fragility in patients diagnosed with MGUS: no longer a condition of undetermined significance? J. Bone Miner. Res. Off. J. Am. Soc. Bone Miner. Res. *29*, 2529–2533.

- Drexler, H.G., Gignac, S.M., Hoffbrand, A.V., and Minowada, J. (1989). Formation of multinucleated cells in a Hodgkin's-disease-derived cell line. Int. J. Cancer *43*, 1083–1090.

- Duesberg, P., Rausch, C., Rasnick, D., and Hehlmann, R. (1998). Genetic instability of cancer cells is proportional to their degree of aneuploidy. Proc. Natl. Acad. Sci. U. S. A. *95*, 13692–13697.

- Eisch, V., Lu, X., Gabriel, D., and Djabali, K. (2016). Progerin impairs chromosome maintenance by depleting CENP-F from metaphase kinetochores in Hutchinson-Gilford progeria fibroblasts. Oncotarget *7*, 24700–24718.

- Ernst, J.A., Li, H., Kim, H.S., Nakamura, G.R., Yansura, D.G., and Vandlen, R.L. (2005). Isolation and characterization of the B-cell marker CD20. Biochemistry *44*, 15150–15158.

- d'Adda di Fagagna, F., Reaper, P.M., Clay-Farrace, L., Fiegler, H., Carr, P., Von Zglinicki, T., Saretzki, G., Carter, N.P., and Jackson, S.P. (2003). A DNA damage checkpoint response in telomere-initiated senescence. Nature *426*, 194–198.
- Fang, J., Ding, M., Yang, L., Liu, L.-Z., and Jiang, B.-H. (2007). PI3K/PTEN/AKT signaling regulates prostate tumor angiogenesis. Cell. Signal. *19*, 2487–2497.
- Fedi, P., Tronick, S.R., and Aaronson, S.A. (1997). Growth factors In Cancer Medicine, J.F. Holland, R.C. Bast, D.L. Morton, E. Frei D.W. Kufe, and R.R. Weichselbaum, eds. (Baltimore, MD: Williams and Wilkins), pp. 41–64
- Felsher, D.W., and Bishop, J.M. (1999). Transient excess of MYC activity can elicit genomic instability and tumorigenesis. Proc. Natl. Acad. Sci. U. S. A. *96*, 3940–3944.
- Ferté, C., André, F., and Soria, J.-C. (2010). Molecular circuits of solid tumors: prognostic and predictive tools for bedside use. Nat. Rev. Clin. Oncol. *7*, 367–380.
- Fisher, D.Z., Chaudhary, N., and Blobel, G. (1986). cDNA sequencing of nuclear lamins A and C reveals primary and secondary structural homology to intermediate filament proteins. Proc. Natl. Acad. Sci. U. S. A. *83*, 6450–6454.
- Fiumara, P., Snell, V., Li, Y., Mukhopadhyay, A., Younes, M., Gillenwater, A.M., Cabanillas, F., Aggarwal, B.B., and Younes, A. (2001). Functional expression of receptor activator of nuclear factor kappaB in Hodgkin disease cell lines. Blood *98*, 2784–2790.
- Fonseca, R., Barlogie, B., Bataille, R., Bastard, C., Bergsagel, P.L., Chesi, M., Davies, F.E., Drach, J., Greipp, P.R., Kirsch, I.R., et al. (2004). Genetics and cytogenetics of multiple myeloma: a workshop report. Cancer Res. *64*, 1546–1558.
- Fonseca, R., Bergsagel, P.L., Drach, J., Shaughnessy, J., Gutierrez, N., Stewart, A.K., Morgan, G., Van Ness, B., Chesi, M., Minvielle, S., et al. (2009). International Myeloma Working Group molecular classification of multiple myeloma: spotlight review. Leukemia *23*, 2210–2221.
- Foster, C.R., Przyborski, S.A., Wilson, R.G., and Hutchison, C.J. (2010). Lamins as cancer biomarkers. Biochem. Soc. Trans. *38*, 297–300.
- Franklin, A.E., and Cande, W.Z. (1999). Nuclear organization and chromosome segregation. Plant Cell *11*, 523–534.
- Fridkin, A., Penkner, A., Jantsch, V., and Gruenbaum, Y. (2009). SUN-domain and KASH-domain proteins during development, meiosis and disease. Cell. Mol. Life Sci. CMLS *66*, 1518–1533.
- Gabay, M., Li, Y., and Felsher, D.W. (2014). MYC activation is a hallmark of cancer initiation and maintenance. Cold Spring Harb. Perspect. Med. *4*.
- Gerlinger, M., and Swanton, C. (2010). How Darwinian models inform therapeutic failure initiated by clonal heterogeneity in cancer medicine. Br. J. Cancer *103*, 1139–1143.
- Gharbaran, R., Park, J., Kim, C., Goy, A., and Suh, K.S. (2014). Circulating tumor cells in Hodgkin's lymphoma - a review of the spread of HL tumor cells or their putative precursors by lymphatic and hematogenous means, and their prognostic significance. Crit. Rev. Oncol. Hematol. *89*, 404–417.
- Gilley, D., and Blackburn, E.H. (1994). Lack of telomere shortening during senescence in Paramecium. Proc. Natl. Acad. Sci. U. S. A. *91*, 1955–1958.

- Gisselsson, D., Pettersson, L., Höglund, M., Heidenblad, M., Gorunova, L., Wiegant, J., Mertens, F., Dal Cin, P., Mitelman, F., and Mandahl, N. (2000). Chromosomal breakage-fusion-bridge events cause genetic intratumor heterogeneity. Proc. Natl. Acad. Sci. U. S. A. *97*, 5357–5362.

- Go, R.S., and Rajkumar, S.V. (2018). How I manage monoclonal gammopathy of undetermined significance. Blood *131*, 163–173.

- Goldman, R.D., Gruenbaum, Y., Moir, R.D., Shumaker, D.K., and Spann, T.P. (2002). Nuclear lamins: building blocks of nuclear architecture. Genes Dev. *16*, 533–547.

- Gonzalez-Suarez, I., Redwood, A.B., Perkins, S.M., Vermolen, B., Lichtensztejin, D., Grotsky, D.A., Morgado-Palacin, L., Gapud, E.J., Sleckman, B.P., Sullivan, T., et al. (2009). Novel roles for A-type lamins in telomere biology and the DNA damage response pathway. EMBO J. *28*, 2414–2427.

- Gonzalez-Vasconcellos, I., Schneider, R., Anastasov, N., Alonso-Rodriguez, S., Sanli-Bonazzi, B., Fernández, J.L., and Atkinson, M.J. (2017). The Rb1 tumour suppressor gene modifies telomeric chromatin architecture by regulating TERRA expression. Sci. Rep. *7*, 42056.

- Gonzalo, S. (2014). DNA Damage and Lamins. In Cancer Biology and the Nuclear Envelope, E.C. Schirmer, and J.I. de las Heras, eds. (New York, NY: Springer New York), pp. 377–399.

- Gonzalo, S., Kreienkamp, R., and Askjaer, P. (2017). Hutchinson-Gilford Progeria Syndrome: A premature aging disease caused by LMNA gene mutations. Ageing Res. Rev. *33*, 18–29.

- Gorgoulis, V.G., Vassiliou, L.-V.F., Karakaidos, P., Zacharatos, P., Kotsinas, A., Liloglou, T., Venere, M., Ditullio, R.A., Kastrinakis, N.G., Levy, B., et al. (2005). Activation of the DNA damage checkpoint and genomic instability in human precancerous lesions. Nature *434*, 907–913.

- Greenman, C., Stephens, P., Smith, R., Dalgliesh, G.L., Hunter, C., Bignell, G., Davies, H., Teague, J., Butler, A., Stevens, C., et al. (2007). Patterns of somatic mutation in human cancer genomes. Nature *446*, 153–158.

- Greider, C.W. (1999). Telomeres do D-loop-T-loop. Cell *97*, 419–422.

- Greiner, A., Tobollik, S., Buettner, M., Jungnickel, B., Herrmann, K., Kremmer, E., and Niedobitek, G. (2005). Differential expression of activation-induced cytidine deaminase (AID) in nodular lymphocyte-predominant and classical Hodgkin lymphoma. J. Pathol. *205*, 541–547.

- Greipp, P. (2007). Progression risk for MGUS and SMM. Blood *110*, 2226–2226.

- Gruenbaum, Y., Goldman, R.D., Meyuhas, R., Mills, E., Margalit, A., Fridkin, A., Dayani, Y., Prokocimer, M., and Enosh, A. (2003). The nuclear lamina and its functions in the nucleus. Int. Rev. Cytol. *226*, 1–62.

- Gruenbaum, Y., Margalit, A., Goldman, R.D., Shumaker, D.K., and Wilson, K.L. (2005). The nuclear lamina comes of age. Nat. Rev. Mol. Cell Biol. *6*, 21–31.

- Guelen, L., Pagie, L., Brasset, E., Meuleman, W., Faza, M.B., Talhout, W., Eussen, B.H., de Klein, A., Wessels, L., de Laat, W., et al. (2008). Domain organization of human chromosomes revealed by mapping of nuclear lamina interactions. Nature *453*, 948–951.

- Guffei, A., Sarkar, R., Klewes, L., Righolt, C., Knecht, H., and Mai, S. (2010). Dynamic chromosomal rearrangements in Hodgkin's lymphoma are due to ongoing three-dimensional nuclear remodeling and breakage-bridge-fusion cycles. Haematologica *95*, 2038–2046.
- Guilly, M.N., Bensussan, A., Bourge, J.F., Bornens, M., and Courvalin, J.C. (1987). A human T lymphoblastic cell line lacks lamins A and C. EMBO J. *6*, 3795–3799.
- Hanahan, D., and Folkman, J. (1996). Patterns and emerging mechanisms of the angiogenic switch during tumorigenesis. Cell *86*, 353–364.
- Hanahan, D., and Weinberg, R.A. (2000). The Hallmarks of Cancer. Cell *100*, 57–70.
- Hanahan, D., and Weinberg, R.A. (2011). Hallmarks of cancer: the next generation. Cell *144*, 646–674.
- Hannon, G.J., and Beach, D. (1994). p15INK4B is a potential effector of TGF-beta-induced cell cycle arrest. Nature *371*, 257–261.
- Harada, T., Swift, J., Irianto, J., Shin, J.-W., Spinler, K.R., Athirasala, A., Diegmiller, R., Dingal, P.C.D.P., Ivanovska, I.L., and Discher, D.E. (2014). Nuclear lamin stiffness is a barrier to 3D migration, but softness can limit survival. J. Cell Biol. *204*, 669–682.
- Harborth, J., Elbashir, S.M., Bechert, K., Tuschl, T., and Weber, K. (2001). Identification of essential genes in cultured mammalian cells using small interfering RNAs. J. Cell Sci. *114*, 4557–4565.
- Harper, J.W., and Elledge, S.J. (2007). The DNA damage response: ten years after. Mol. Cell *28*, 739–745.
- Hastie, N.D., Dempster, M., Dunlop, M.G., Thompson, A.M., Green, D.K., and Allshire, R.C. (1990). Telomere reduction in human colorectal carcinoma and with ageing. Nature *346*, 866–868.
- Hayflick, L. (1965). The limited in vitro lifetime of human diploid cell strains. Exp. Cell Res. *37*, 614–636.
- Hayflick, L. (1997). Mortality and immortality at the cellular level. A review. Biochem. Biokhimiia *62*, 1180–1190.
- Hayflick, L., and Moorhead, P.S. (1961). The serial cultivation of human diploid cell strains. Exp. Cell Res. *25*, 585–621.
- He, H., Multani, A.S., Cosme-Blanco, W., Tahara, H., Ma, J., Pathak, S., Deng, Y., and Chang, S. (2006). POT1b protects telomeres from end-to-end chromosomal fusions and aberrant homologous recombination. EMBO J. *25*, 5180–5190.
- Heaphy, C.M., de Wilde, R.F., Jiao, Y., Klein, A.P., Edil, B.H., Shi, C., Bettegowda, C., Rodriguez, F.J., Eberhart, C.G., Hebbar, S., et al. (2011). Altered telomeres in tumors with ATRX and DAXX mutations. Science *333*, 425.
- Henson, J.D., and Reddel, R.R. (2010). Assaying and investigating Alternative Lengthening of Telomeres activity in human cells and cancers. FEBS Lett. *584*, 3800–3811.
- Hertel, C.B., Zhou, X., Hamilton-Dutoit, S.J., and Junker, S. (2002). Loss of B cell identity correlates with loss of B cell-specific transcription factors in Hodgkin/Reed-Sternberg cells of classical Hodgkin lymphoma. Oncogene *21*, 4908–4920.
- Hironaka, K., Factor, V.M., Calvisi, D.F., Conner, E.A., and Thorgeirsson, S.S. (2003). Deregulation of DNA repair pathways in a transforming growth factor alpha/c-myc

transgenic mouse model of accelerated hepatocarcinogenesis. Lab. Investig. J. Tech. Methods Pathol. *83*, 643–654.

- Ho, C.Y., and Lammerding, J. (2012). Lamins at a glance. J. Cell Sci. *125*, 2087–2093.

- Höger, T.H., Zatloukal, K., Waizenegger, I., and Krohne, G. (1990). Characterization of a second highly conserved B-type lamin present in cells previously thought to contain only a single B-type lamin. Chromosoma *99*, 379–390.

- Horie, R., Watanabe, T., Morishita, Y., Ito, K., Ishida, T., Kanegae, Y., Saito, I., Higashihara, M., Mori, S., Kadin, M.E., et al. (2002). Ligand-independent signaling by overexpressed CD30 drives NF-kappaB activation in Hodgkin-Reed-Sternberg cells. Oncogene *21*, 2493–2503.

- Hsieh, P., and Yamane, K. (2008). DNA mismatch repair: molecular mechanism, cancer, and ageing. Mech. Ageing Dev. *129*, 391–407.

- Hsu, P.P., and Sabatini, D.M. (2008). Cancer cell metabolism: Warburg and beyond. Cell *134*, 703–707.

- Huang, S., Risques, R.A., Martin, G.M., Rabinovitch, P.S., and Oshima, J. (2008). Accelerated telomere shortening and replicative senescence in human fibroblasts overexpressing mutant and wild-type lamin A. Exp. Cell Res. *314*, 82–91.

- Imai, S., Nishibayashi, S., Takao, K., Tomifuji, M., Fujino, T., Hasegawa, M., and Takano, T. (1997). Dissociation of Oct-1 from the nuclear peripheral structure induces the cellular aging-associated collagenase gene expression. Mol. Biol. Cell *8*, 2407–2419.

- Isermann, P., and Lammerding, J. (2013). Nuclear mechanics and mechanotransduction in health and disease. Curr. Biol. CB *23*, R1113-1121.

- Jackson, S.P., and Bartek, J. (2009). The DNA-damage response in human biology and disease. Nature *461*, 1071–1078.

- Jansen, M.P., Machiels, B.M., Hopman, A.H., Broers, J.L., Bot, F.J., Arends, J.W., Ramaekers, F.C., and Schouten, H.C. (1997). Comparison of A and B-type lamin expression in reactive lymph nodes and nodular sclerosing Hodgkin's disease. Histopathology *31*, 304–312.

- Jemal, A., Siegel, R., Ward, E., Hao, Y., Xu, J., and Thun, M.J. (2009). Cancer statistics, 2009. CA. Cancer J. Clin. *59*, 225–249.

- Jiang, B.-H., and Liu, L.-Z. (2009). PI3K/PTEN signaling in angiogenesis and tumorigenesis. Adv. Cancer Res. *102*, 19–65.

- Johnson, J.P. (1991). Cell adhesion molecules of the immunoglobulin supergene family and their role in malignant transformation and progression to metastatic disease. Cancer Metastasis Rev. *10*, 11–22.

- Jones, R.G., and Thompson, C.B. (2009). Tumor suppressors and cell metabolism: a recipe for cancer growth. Genes Dev. *23*, 537–548.

- Jundt, F., Anagnostopoulos, I., Förster, R., Mathas, S., Stein, H., and Dörken, B. (2002). Activated Notch1 signaling promotes tumor cell proliferation and survival in Hodgkin and anaplastic large cell lymphoma. Blood *99*, 3398–3403.

- Jundt, F., Acikgöz, O., Kwon, S.-H., Schwarzer, R., Anagnostopoulos, I., Wiesner, B., Mathas, S., Hummel, M., Stein, H., Reichardt, H.M., et al. (2008). Aberrant expression of

Notch1 interferes with the B-lymphoid phenotype of neoplastic B cells in classical Hodgkin lymphoma. Leukemia *22*, 1587–1594.

- Kamijo, T., Zindy, F., Roussel, M.F., Quelle, D.E., Downing, J.R., Ashmun, R.A., Grosveld, G., and Sherr, C.J. (1997). Tumor suppression at the mouse INK4a locus mediated by the alternative reading frame product p19ARF. Cell *91*, 649–659.
- Kanzler, H., Küppers, R., Hansmann, M.L., and Rajewsky, K. (1996). Hodgkin and Reed-Sternberg cells in Hodgkin's disease represent the outgrowth of a dominant tumor clone derived from (crippled) germinal center B cells. J. Exp. Med. *184*, 1495–1505.
- Karlsson, A., Deb-Basu, D., Cherry, A., Turner, S., Ford, J., and Felsher, D.W. (2003). Defective double-strand DNA break repair and chromosomal translocations by MYC overexpression. Proc. Natl. Acad. Sci. U. S. A. *100*, 9974–9979.
- Kaspi, E., Frankel, D., Guinde, J., Perrin, S., Laroumagne, S., Robaglia-Schlupp, A., Ostacolo, K., Harhouri, K., Tazi-Mezalek, R., Micallef, J., et al. (2017). Low lamin A expression in lung adenocarcinoma cells from pleural effusions is a pejorative factor associated with high number of metastatic sites and poor Performance status. PLOS ONE *12*, e0183136.
- Kim, R., Emi, M., and Tanabe, K. (2007). Cancer immunoediting from immune surveillance to immune escape. Immunology *121*, 1–14.
- Kim, R.H., Kim, R., Chen, W., Hu, S., Shin, K.-H., Park, N.-H., and Kang, M.K. (2008). Association of hsp90 to the hTERT promoter is necessary for hTERT expression in human oral cancer cells. Carcinogenesis *29*, 2425–2431.
- Klewes, L., Vallente, R., Dupas, E., Brand, C., Grün, D., Guffei, A., Sathitruangsak, C., Awe, J.A., Kuzyk, A., Lichtensztejn, D., et al. (2013). Three-dimensional Nuclear Telomere Organization in Multiple Myeloma. Transl. Oncol. *6*, 749–756.
- Knecht, H., and Mai, S. (2017). The Use of 3D Telomere FISH for the Characterization of the Nuclear Architecture in EBV-Positive Hodgkin's Lymphoma. Methods Mol. Biol. Clifton NJ *1532*, 93–104.
- Knecht, H., Sawan, B., Lichtensztejn, D., Lemieux, B., Wellinger, R.J., and Mai, S. (2009). The 3D nuclear organization of telomeres marks the transition from Hodgkin to Reed-Sternberg cells. Leukemia *23*, 565–573.
- Knecht, H., Sawan, B., Lichtensztejn, Z., Lichtensztejn, D., and Mai, S. (2010). 3D Telomere FISH defines LMP1-expressing Reed-Sternberg cells as end-stage cells with telomere-poor "ghost" nuclei and very short telomeres. Lab. Investig. J. Tech. Methods Pathol. *90*, 611–619.
- Knecht, H., Johnson, N.A., Haliotis, T., Lichtensztejn, D., and Mai, S. (2017). Disruption of direct 3D telomere–TRF2 interaction through two molecularly disparate mechanisms is a hallmark of primary Hodgkin and Reed–Sternberg cells. Lab. Invest. *97*, 772–781.
- Kong, L., Schäfer, G., Bu, H., Zhang, Y., Zhang, Y., and Klocker, H. (2012). Lamin A/C protein is overexpressed in tissue-invading prostate cancer and promotes prostate cancer cell growth, migration and invasion through the PI3K/AKT/PTEN pathway. Carcinogenesis *33*, 751–759.
- Kops, G.J.P.L., Foltz, D.R., and Cleveland, D.W. (2004). Lethality to human cancer cells through massive chromosome loss by inhibition of the mitotic checkpoint. Proc. Natl. Acad. Sci. U. S. A. *101*, 8699–8704.

- Kops, G.J.P.L., Weaver, B.A.A., and Cleveland, D.W. (2005). On the road to cancer: aneuploidy and the mitotic checkpoint. Nat. Rev. Cancer *5*, 773–785.
- Kudlow, B.A., Stanfel, M.N., Burtner, C.R., Johnston, E.D., and Kennedy, B.K. (2008). Suppression of proliferative defects associated with processing-defective lamin A mutants by hTERT or inactivation of p53. Mol. Biol. Cell *19*, 5238–5248.
- Küppers, R. (2009). The biology of Hodgkin's lymphoma. Nat. Rev. Cancer *9*, 15–27.
- Küppers, R., Fischer, U., Rajewsky, K., and Gause, A. (1992). Immunoglobulin heavy and light chain gene sequences of a human CD5 positive immunocytoma and sequences of four novel VHIII germline genes. Immunol. Lett. *34*, 57–62.
- Küppers, R., Rajewsky, K., Zhao, M., Simons, G., Laumann, R., Fischer, R., and Hansmann, M.L. (1994). Hodgkin disease: Hodgkin and Reed-Sternberg cells picked from histological sections show clonal immunoglobulin gene rearrangements and appear to be derived from B cells at various stages of development. Proc. Natl. Acad. Sci. U. S. A. *91*, 10962–10966.
- Küppers, R., Bräuninger, A., Müschen, M., Distler, V., Hansmann, M.L., and Rajewsky, K. (2001). Evidence that Hodgkin and Reed-Sternberg cells in Hodgkin disease do not represent cell fusions. Blood *97*, 818–821.
- van Kuppevelt, T.H., Veerkamp, J.H., and Timmermans, J.A. (1995). Immunoquantification of type I, III, IV and V collagen in small samples of human lung parenchyma. Int. J. Biochem. Cell Biol. *27*, 775–782.
- Kyle, R.A., Remstein, E.D., Therneau, T.M., Dispenzieri, A., Kurtin, P.J., Hodnefield, J.M., Larson, D.R., Plevak, M.F., Jelinek, D.F., Fonseca, R., et al. (2007). Clinical course and prognosis of smoldering (asymptomatic) multiple myeloma. N. Engl. J. Med. *356*, 2582–2590.
- Lajoie, V., Lemieux, B., Sawan, B., Lichtensztejn, D., Lichtensztejn, Z., Wellinger, R., Mai, S., and Knecht, H. (2015). LMP1 mediates multinuclearity through downregulation of shelterin proteins and formation of telomeric aggregates. Blood *125*, 2101–2110.
- Lam, N., and Sugden, B. (2003). CD40 and its viral mimic, LMP1: similar means to different ends. Cell. Signal. *15*, 9–16.
- Lammerding, J., Schulze, P.C., Takahashi, T., Kozlov, S., Sullivan, T., Kamm, R.D., Stewart, C.L., and Lee, R.T. (2004). Lamin A/C deficiency causes defective nuclear mechanics and mechanotransduction. J. Clin. Invest. *113*, 370–378.
- Landgren, O., Kyle, R.A., Pfeiffer, R.M., Katzmann, J.A., Caporaso, N.E., Hayes, R.B., Dispenzieri, A., Kumar, S., Clark, R.J., Baris, D., et al. (2009). Monoclonal gammopathy of undetermined significance (MGUS) consistently precedes multiple myeloma: a prospective study. Blood *113*, 5412–5417.
- de Lange, T. (2005). Shelterin: the protein complex that shapes and safeguards human telomeres. Genes Dev. *19*, 2100–2110.
- de Lange, T., Shiue, L., Myers, R.M., Cox, D.R., Naylor, S.L., Killery, A.M., and Varmus, H.E. (1990). Structure and variability of human chromosome ends. Mol. Cell. Biol. *10*, 518–527.
- Lansdorp, P.M. (2009). Telomeres and disease. EMBO J. *28*, 2532–2540.

- Laplante, M., and Sabatini, D.M. (2012). mTOR signaling in growth control and disease. Cell *149*, 274–293.
- de Las Heras, J.I., Batrakou, D.G., and Schirmer, E.C. (2013). Cancer biology and the nuclear envelope: a convoluted relationship. Semin. Cancer Biol. *23*, 125–137.
- Lattanzi, G., Columbaro, M., Mattioli, E., Cenni, V., Camozzi, D., Wehnert, M., Santi, S., Riccio, M., Del Coco, R., Maraldi, N.M., et al. (2007). Pre-Lamin A processing is linked to heterochromatin organization. J. Cell. Biochem. *102*, 1149–1159.
- Lee, A.J.X., Endesfelder, D., Rowan, A.J., Walther, A., Birkbak, N.J., Futreal, P.A., Downward, J., Szallasi, Z., Tomlinson, I.P.M., Howell, M., et al. (2011). Chromosomal instability confers intrinsic multidrug resistance. Cancer Res. *71*, 1858–1870.
- de Leeuw, R., Gruenbaum, Y., and Medalia, O. (2018). Nuclear Lamins: Thin Filaments with Major Functions. Trends Cell Biol. *28*, 34–45.
- Lengauer, C., Kinzler, K.W., and Vogelstein, B. (1998). Genetic instabilities in human cancers. Nature *396*, 643–649.
- Lepage, C.C., Morden, C.R., Palmer, M.C.L., Nachtigal, M.W., and McManus, K.J. (2019). Detecting Chromosome Instability in Cancer: Approaches to Resolve Cell-to-Cell Heterogeneity. Cancers *11*.
- Levy, M.Z., Allsopp, R.C., Futcher, A.B., Greider, C.W., and Harley, C.B. (1992). Telomere end-replication problem and cell aging. J. Mol. Biol. *225*, 951–960.
- Limon, J.J., and Fruman, D.A. (2012). Akt and mTOR in B Cell Activation and Differentiation. Front. Immunol. *3*, 228.
- Lin, F., and Worman, H.J. (1995). Structural organization of the human gene (LMNB1) encoding nuclear lamin B1. Genomics *27*, 230–236.
- Liu, R., and Xing, M. (2016). TERT promoter mutations in thyroid cancer. Endocr. Relat. Cancer *23*, R143-155.
- Liu, L., Luo, Q., Sun, J., Wang, A., Shi, Y., Ju, Y., Morita, Y., and Song, G. (2017). Decreased nuclear stiffness via FAK-ERK1/2 signaling is necessary for osteopontin-promoted migration of bone marrow-derived mesenchymal stem cells. Exp. Cell Res. *355*, 172–181.
- Livak, K.J., and Schmittgen, T.D. (2001). Analysis of Relative Gene Expression Data Using Real-Time Quantitative PCR and the 2−ΔΔCT Method. Methods *25*, 402–408.
- Lohr, J.G., Stojanov, P., Carter, S.L., Cruz-Gordillo, P., Lawrence, M.S., Auclair, D., Sougnez, C., Knoechel, B., Gould, J., Saksena, G., et al. (2014). Widespread genetic heterogeneity in multiple myeloma: implications for targeted therapy. Cancer Cell *25*, 91–101.
- Louis, S.F., Vermolen, B.J., Garini, Y., Young, I.T., Guffei, A., Lichtensztejn, Z., Kuttler, F., Chuang, T.C.Y., Moshir, S., Mougey, V., et al. (2005). c-Myc induces chromosomal rearrangements through telomere and chromosome remodeling in the interphase nucleus. Proc. Natl. Acad. Sci. U. S. A. *102*, 9613–9618.
- Mai, S., and Garini, Y. (2006). The significance of telomeric aggregates in the interphase nuclei of tumor cells. J. Cell. Biochem. *97*, 904–915.
- Mai, S., and Mushinski, J.F. (2003). c-Myc-induced genomic instability. J. Environ. Pathol. Toxicol. Oncol. Off. Organ Int. Soc. Environ. Toxicol. Cancer *22*, 179–199.

- Mai, S., Hanley-Hyde, J., and Fluri, M. (1996a). c-Myc overexpression associated DHFR gene amplification in hamster, rat, mouse and human cell lines. Oncogene *12*, 277–288.

- Mai, S., Fluri, M., Siwarski, D., and Huppi, K. (1996b). Genomic instability in MycER-activated Rat1A-MycER cells. Chromosome Res. Int. J. Mol. Supramol. Evol. Asp. Chromosome Biol. *4*, 365–371.

- Makarov, V.L., Hirose, Y., and Langmore, J.P. (1997). Long G tails at both ends of human chromosomes suggest a C strand degradation mechanism for telomere shortening. Cell *88*, 657–666.

- Marafioti, T., Hummel, M., Foss, H.D., Laumen, H., Korbjuhn, P., Anagnostopoulos, I., Lammert, H., Demel, G., Theil, J., Wirth, T., et al. (2000). Hodgkin and reed-sternberg cells represent an expansion of a single clone originating from a germinal center B-cell with functional immunoglobulin gene rearrangements but defective immunoglobulin transcription. Blood *95*, 1443–1450.

- Maraldi, N.M., and Lattanzi, G. (2005). Linkage of lamins to fidelity of gene transcription. Crit. Rev. Eukaryot. Gene Expr. *15*, 277–294.

- Márk, Á., Hajdu, M., Váradi, Z., Sticz, T.B., Nagy, N., Csomor, J., Berczi, L., Varga, V., Csóka, M., Kopper, L., et al. (2013). Characteristic mTOR activity in Hodgkin-lymphomas offers a potential therapeutic target in high risk disease – a combined tissue microarray, in vitro and in vivo study. BMC Cancer *13*, 250.

- Markiewicz, E., Dechat, T., Foisner, R., Quinlan, R.A., and Hutchison, C.J. (2002). Lamin A/C binding protein LAP2alpha is required for nuclear anchorage of retinoblastoma protein. Mol. Biol. Cell *13*, 4401–4413.

- Martín-Subero, J.I., Klapper, W., Sotnikova, A., Callet-Bauchu, E., Harder, L., Bastard, C., Schmitz, R., Grohmann, S., Höppner, J., Riemke, J., et al. (2006). Chromosomal breakpoints affecting immunoglobulin loci are recurrent in Hodgkin and Reed-Sternberg cells of classical Hodgkin lymphoma. Cancer Res. *66*, 10332–10338.

- Massini, G., Siemer, D., and Hohaus, S. (2009). EBV in Hodgkin Lymphoma. Mediterr. J. Hematol. Infect. Dis. *1*, e2009013.

- Mattout, A., Dechat, T., Adam, S.A., Goldman, R.D., and Gruenbaum, Y. (2006). Nuclear lamins, diseases and aging. Curr. Opin. Cell Biol. *18*, 335–341.

- McCormack, S.J., Weaver, Z., Deming, S., Natarajan, G., Torri, J., Johnson, M.D., Liyanage, M., Ried, T., and Dickson, R.B. (1998). Myc/p53 interactions in transgenic mouse mammary development, tumorigenesis and chromosomal instability. Oncogene *16*, 2755–2766.

- McDonnell, T.J., and Korsmeyer, S.J. (1991). Progression from lymphoid hyperplasia to high-grade malignant lymphoma in mice transgenic for the t(14; 18). Nature *349*, 254–256.

- McHugh, M.L. (2011). Multiple comparison analysis testing in ANOVA. Biochem. Medica *21*, 203–209.

- McHugh, M.L. (2013). The chi-square test of independence. Biochem. Medica *23*, 143–149.

- Meaburn, K.J., Misteli, T., and Soutoglou, E. (2007). Spatial genome organization in the formation of chromosomal translocations. Semin. Cancer Biol. *17*, 80–90.

- Medema, R.H., and Bos, J.L. (1993). The role of p21ras in receptor tyrosine kinase signaling. Crit. Rev. Oncog. *4*, 615–661.

- de Mel, S., Lim, S.H., Tung, M.L., and Chng, W.-J. (2014). Implications of heterogeneity in multiple myeloma. BioMed Res. Int. *2014*, 232546.
- Menssen, A., Epanchintsev, A., Lodygin, D., Rezaei, N., Jung, P., Verdoodt, B., Diebold, J., and Hermeking, H. (2007). c-MYC delays prometaphase by direct transactivation of MAD2 and BubR1: identification of mechanisms underlying c-MYC-induced DNA damage and chromosomal instability. Cell Cycle Georget. Tex *6*, 339–352.
- Michel, L., Diaz-Rodriguez, E., Narayan, G., Hernando, E., Murty, V.V.V.S., and Benezra, R. (2004). Complete loss of the tumor suppressor MAD2 causes premature cyclin B degradation and mitotic failure in human somatic cells. Proc. Natl. Acad. Sci. U. S. A. *101*, 4459–4464.
- Michels, T.C., and Petersen, K.E. (2017). Multiple Myeloma: Diagnosis and Treatment. Am. Fam. Physician *95*, 373–383.
- Mislow, J.M.K., Kim, M.S., Davis, D.B., and McNally, E.M. (2002). Myne-1, a spectrin repeat transmembrane protein of the myocyte inner nuclear membrane, interacts with lamin A/C. J. Cell Sci. *115*, 61–70.
- Misri, S., Pandita, S., Kumar, R., and Pandita, T.K. (2008). Telomeres, histone code, and DNA damage response. Cytogenet. Genome Res. *122*, 297–307.
- Montero, J.J., López de Silanes, I., Graña, O., and Blasco, M.A. (2016). Telomeric RNAs are essential to maintain telomeres. Nat. Commun. *7*, 12534.
- Moreau, P., San Miguel, J., Sonneveld, P., Mateos, M.V., Zamagni, E., Avet-Loiseau, H., Hajek, R., Dimopoulos, M.A., Ludwig, H., Einsele, H., et al. (2017). Multiple myeloma: ESMO Clinical Practice Guidelines for diagnosis, treatment and follow-up†. Ann. Oncol. *28*, iv52–iv61.
- Moulson, C.L., Fong, L.G., Gardner, J.M., Farber, E.A., Go, G., Passariello, A., Grange, D.K., Young, S.G., and Miner, J.H. (2007). Increased progerin expression associated with unusual LMNA mutations causes severe progeroid syndromes. Hum. Mutat. *28*, 882–889.
- Moyzis, R.K., Buckingham, J.M., Cram, L.S., Dani, M., Deaven, L.L., Jones, M.D., Meyne, J., Ratliff, R.L., and Wu, J.R. (1988). A highly conserved repetitive DNA sequence, (TTAGGG)n, present at the telomeres of human chromosomes. Proc. Natl. Acad. Sci. U. S. A. *85*, 6622–6626.
- Munshi, N.C., Anderson, K.C., Bergsagel, P.L., Shaughnessy, J., Palumbo, A., Durie, B., Fonseca, R., Stewart, A.K., Harousseau, J.-L., Dimopoulos, M., et al. (2011). Consensus recommendations for risk stratification in multiple myeloma: report of the International Myeloma Workshop Consensus Panel 2. Blood *117*, 4696–4700.
- Murnane, J.P. (2012). Telomere dysfunction and chromosome instability. Mutat. Res. *730*, 28–36.
- Nabetani, A., and Ishikawa, F. (2011). Alternative lengthening of telomeres pathway: recombination-mediated telomere maintenance mechanism in human cells. J. Biochem. (Tokyo) *149*, 5–14.
- Nau, K.C., and Lewis, W.D. (2008). Multiple myeloma: diagnosis and treatment. Am. Fam. Physician *78*, 853–859.
- Nečasová, I., Janoušková, E., Klumpler, T., and Hofr, C. (2017). Basic domain of telomere guardian TRF2 reduces D-loop unwinding whereas Rap1 restores it. Nucleic Acids Res. *45*, 12170–12180.

- Neri, P., and Bahlis, N.J. (2013). Genomic instability in multiple myeloma: mechanisms and therapeutic implications. Expert Opin. Biol. Ther. *13 Suppl 1*, S69-82.

- Okamoto, K., Iwano, T., Tachibana, M., and Shinkai, Y. (2008). Distinct roles of TRF1 in the regulation of telomere structure and lengthening. J. Biol. Chem. *283*, 23981–23988.

- Okamoto, K., Bartocci, C., Ouzounov, I., Diedrich, J.K., Yates, J.R., and Denchi, E.L. (2013). A two-step mechanism for TRF2-mediated chromosome-end protection. Nature *494*, 502–505.

- Olivier, M., Hollstein, M., and Hainaut, P. (2010). TP53 mutations in human cancers: origins, consequences, and clinical use. Cold Spring Harb. Perspect. Biol. *2*, a001008.

- O'Neal, J., Gao, F., Hassan, A., Monahan, R., Barrios, S., Kilimann, M.W., Lee, I., Chng, W.J., Vij, R., and Tomasson, M.H. (2009). Neurobeachin (NBEA) is a target of recurrent interstitial deletions at 13q13 in patients with MGUS and multiple myeloma. Exp. Hematol. *37*, 234–244.

- Ottaviani, A., Schluth-Bolard, C., Rival-Gervier, S., Boussouar, A., Rondier, D., Foerster, A.M., Morere, J., Bauwens, S., Gazzo, S., Callet-Bauchu, E., et al. (2009). Identification of a perinuclear positioning element in human subtelomeres that requires A-type lamins and CTCF. EMBO J. *28*, 2428–2436.

- Padmakumar, V.C., Libotte, T., Lu, W., Zaim, H., Abraham, S., Noegel, A.A., Gotzmann, J., Foisner, R., and Karakesisoglou, I. (2005). The inner nuclear membrane protein Sun1 mediates the anchorage of Nesprin-2 to the nuclear envelope. J. Cell Sci. *118*, 3419–3430.

- Paez, J., and Sellers, W.R. (2003). PI3K/PTEN/AKT pathway. A critical mediator of oncogenic signaling. Cancer Treat. Res. *115*, 145–167.

- Paiva, B., Paino, T., Sayagues, J.-M., Garayoa, M., San-Segundo, L., Martin, M., Mota, I., Sanchez, M.-L., Barcena, P., Aires-Mejia, I., et al. (2013). Detailed characterization of multiple myeloma circulating tumor cells shows unique phenotypic, cytogenetic, functional, and circadian distribution profile. Blood *122*, 3591–3598.

- Palm, W., and de Lange, T. (2008). How shelterin protects mammalian telomeres. Annu. Rev. Genet. *42*, 301–334.

- Parekh, V.V., Prasad, D.V.R., Banerjee, P.P., Joshi, B.N., Kumar, A., and Mishra, G.C. (2003). B Cells Activated by Lipopolysaccharide, But Not By Anti-Ig and Anti-CD40 Antibody, Induce Anergy in CD8 [+] T Cells: Role of TGF-β1. J. Immunol. *170*, 5897–5911.

- Park, G.E., Jee, W.-H., Lee, S.-Y., Sung, J.-K., Jung, J.-Y., Grimm, R., Son, Y., Paek, M.Y., Min, C.-K., and Ha, K.-Y. (2018). Differentiation of multiple myeloma and metastases: Use of axial diffusion-weighted MR imaging in addition to standard MR imaging at 3T. PloS One *13*, e0208860.

- Partanen, J.I., Nieminen, A.I., and Klefstrom, J. (2009). 3D view to tumor suppression: Lkb1, polarity and the arrest of oncogenic c-Myc. Cell Cycle Georget. Tex *8*, 716–724.

- Pawlyn, C., Melchor, L., Murison, A., Wardell, C.P., Brioli, A., Boyle, E.M., Kaiser, M.F., Walker, B.A., Begum, D.B., Dahir, N.B., et al. (2015). Coexistent hyperdiploidy does not abrogate poor prognosis in myeloma with adverse cytogenetics and may precede IGH translocations. Blood *125*, 831–840.

- Porro, A., Feuerhahn, S., Delafontaine, J., Riethman, H., Rougemont, J., and Lingner, J. (2014). Functional characterization of the TERRA transcriptome at damaged telomeres. Nat. Commun. *5*, 5379.

- Portis, T., Dyck, P., and Longnecker, R. (2003). Epstein-Barr Virus (EBV) LMP2A induces alterations in gene transcription similar to those observed in Reed-Sternberg cells of Hodgkin lymphoma. Blood *102*, 4166–4178.
- Postepska-Igielska, A., Krunic, D., Schmitt, N., Greulich-Bode, K.M., Boukamp, P., and Grummt, I. (2013). The chromatin remodelling complex NoRC safeguards genome stability by heterochromatin formation at telomeres and centromeres. EMBO Rep. *14*, 704–710.
- Prokocimer, M., Davidovich, M., Nissim-Rafinia, M., Wiesel-Motiuk, N., Bar, D.Z., Barkan, R., Meshorer, E., and Gruenbaum, Y. (2009). Nuclear lamins: key regulators of nuclear structure and activities. J. Cell. Mol. Med. *13*, 1059–1085.
- Putiri, E.L., and Robertson, K.D. (2011). Epigenetic mechanisms and genome stability. Clin. Epigenetics *2*, 299–314.
- Qi, R., Xu, N., Wang, G., Ren, H., Li, S., Lei, J., Lin, Q., Wang, L., Gu, X., Zhang, H., et al. (2015). The lamin-A/C-LAP2α-BAF1 protein complex regulates mitotic spindle assembly and positioning. J. Cell Sci. *128*, 2830–2841.
- Rajkumar, S.V. (2016). Myeloma today: Disease definitions and treatment advances. Am. J. Hematol. *91*, 90–100.
- Rajkumar, S.V., Dispenzieri, A., and Kyle, R.A. (2006). Monoclonal gammopathy of undetermined significance, Waldenström macroglobulinemia, AL amyloidosis, and related plasma cell disorders: diagnosis and treatment. Mayo Clin. Proc. *81*, 693–703.
- Rajkumar, S.V., Dimopoulos, M.A., Palumbo, A., Blade, J., Merlini, G., Mateos, M.-V., Kumar, S., Hillengass, J., Kastritis, E., Richardson, P., et al. (2014). International Myeloma Working Group updated criteria for the diagnosis of multiple myeloma. Lancet Oncol. *15*, e538-548.
- Raz, V., Carlotti, F., Vermolen, B.J., van der Poel, E., Sloos, W.C.R., Knaän-Shanzer, S., de Vries, A.A.F., Hoeben, R.C., Young, I.T., Tanke, H.J., et al. (2006). Changes in lamina structure are followed by spatial reorganization of heterochromatic regions in caspase-8-activated human mesenchymal stem cells. J. Cell Sci. *119*, 4247–4256.
- Raz, V., Vermolen, B.J., Garini, Y., Onderwater, J.J.M., Mommaas-Kienhuis, M.A., Koster, A.J., Young, I.T., Tanke, H., and Dirks, R.W. (2008). The nuclear lamina promotes telomere aggregation and centromere peripheral localization during senescence of human mesenchymal stem cells. J. Cell Sci. *121*, 4018–4028.
- Re, D., Müschen, M., Ahmadi, T., Wickenhauser, C., Staratschek-Jox, A., Holtick, U., Diehl, V., and Wolf, J. (2001a). Oct-2 and Bob-1 deficiency in Hodgkin and Reed Sternberg cells. Cancer Res. *61*, 2080–2084.
- Re, D., Benenson, E., Beyer, M., Gresch, O., Draube, A., Diehl, V., and Wolf, J. (2001b). Cell fusion is not involved in the generation of giant cells in the Hodgkin-Reed Sternberg cell line L1236. Am. J. Hematol. *67*, 6–9.
- Rengstl, B., Rieger, M.A., and Newrzela, S. (2014). On the origin of giant cells in Hodgkin lymphoma. Commun. Integr. Biol. *7*, e28602.
- Reunert, J., Wentzell, R., Walter, M., Jakubiczka, S., Zenker, M., Brune, T., Rust, S., and Marquardt, T. (2012). Neonatal progeria: increased ratio of progerin to lamin A leads to progeria of the newborn. Eur. J. Hum. Genet. EJHG *20*, 933–937.
- Righolt, C.H., Guffei, A., Knecht, H., Young, I.T., Stallinga, S., van Vliet, L.J., and Mai, S. (2014). Differences in nuclear DNA organization between lymphocytes, Hodgkin and Reed-

Sternberg cells revealed by structured illumination microscopy. J. Cell. Biochem. *115*, 1441–1448.

- Righolt, C.H., Knecht, H., and Mai, S. (2016). DNA Superresolution Structure of Reed-Sternberg Cells Differs Between Long-Lasting Remission Versus Relapsing Hodgkin's Lymphoma Patients: DNA S TRUCTURE I ɴ P RE -T REATMENT H ODGKIN'S L YMPHOMA. J. Cell. Biochem. *117*, 1633–1637.

- Röber, R.A., Sauter, H., Weber, K., and Osborn, M. (1990). Cells of the cellular immune and hemopoietic system of the mouse lack lamins A/C: distinction versus other somatic cells. J. Cell Sci. *95 ( Pt 4)*, 587–598.

- Rocha-Perugini, V., and González-Granado, J.M. (2014). Nuclear envelope lamin-A as a coordinator of T cell activation. Nucl. Austin Tex *5*, 396–401.

- Rockwood, L.D., Torrey, T.A., Kim, J.S., Coleman, A.E., Kovalchuk, A.L., Xiang, S., Ried, T., Morse, H.C., and Janz, S. (2002). Genomic instability in mouse Burkitt lymphoma is dominated by illegitimate genetic recombinations, not point mutations. Oncogene *21*, 7235–7240.

- Röllig, C., Knop, S., and Bornhäuser, M. (2015). Multiple myeloma. Lancet Lond. Engl. *385*, 2197–2208.

- Rouse, J., and Jackson, S.P. (2002). Interfaces between the detection, signaling, and repair of DNA damage. Science *297*, 547–551.

- Sage, J., Miller, A.L., Pérez-Mancera, P.A., Wysocki, J.M., and Jacks, T. (2003). Acute mutation of retinoblastoma gene function is sufficient for cell cycle re-entry. Nature *424*, 223–228.

- Sakthivel, K.M., and Sehgal, P. (2016). A Novel Role of Lamins from Genetic Disease to Cancer Biomarkers. Oncol. Rev. *10*, 309.

- San-Miguel, J.F., and Mateos, M.-V. (2011). Can multiple myeloma become a curable disease? Haematologica *96*, 1246–1248.

- Sansregret, L., Vanhaesebroeck, B., and Swanton, C. (2018). Determinants and clinical implications of chromosomal instability in cancer. Nat. Rev. Clin. Oncol. *15*, 139–150.

- Scheibe, M., Arnoult, N., Kappei, D., Buchholz, F., Decottignies, A., Butter, F., and Mann, M. (2013). Quantitative interaction screen of telomeric repeat-containing RNA reveals novel TERRA regulators. Genome Res. *23*, 2149–2157.

- Schoeftner, S., and Blasco, M.A. (2008). Developmentally regulated transcription of mammalian telomeres by DNA-dependent RNA polymerase II. Nat. Cell Biol. *10*, 228–236.

- Schwarzer, R., Dörken, B., and Jundt, F. (2012). Notch is an essential upstream regulator of NF-κB and is relevant for survival of Hodgkin and Reed-Sternberg cells. Leukemia *26*, 806–813.

- Seyfried, T.N., and Huysentruyt, L.C. (2013). On the origin of cancer metastasis. Crit. Rev. Oncog. *18*, 43–73.

- Sfeir, A., Kosiyatrakul, S.T., Hockemeyer, D., MacRae, S.L., Karlseder, J., Schildkraut, C.L., and de Lange, T. (2009). Mammalian telomeres resemble fragile sites and require TRF1 for efficient replication. Cell *138*, 90–103.

- Shields, J.D., Kourtis, I.C., Tomei, A.A., Roberts, J.M., and Swartz, M.A. (2010). Induction of lymphoidlike stroma and immune escape by tumors that express the chemokine CCL21. Science *328*, 749–752.
- Shimi, T., Kittisopikul, M., Tran, J., Goldman, A.E., Adam, S.A., Zheng, Y., Jaqaman, K., and Goldman, R.D. (2015). Structural organization of nuclear lamins A, C, B1, and B2 revealed by superresolution microscopy. Mol. Biol. Cell *26*, 4075–4086.
- Singh, R.K., Gutman, M., Bucana, C.D., Sanchez, R., Llansa, N., and Fidler, I.J. (1995). Interferons alpha and beta down-regulate the expression of basic fibroblast growth factor in human carcinomas. Proc. Natl. Acad. Sci. U. S. A. *92*, 4562–4566.
- Smith, E.D., Garza-Gongora, A.G., MacQuarrie, K.L., and Kosak, S.T. (2018a). Interstitial telomeric loops and implications of the interaction between TRF2 and lamin A/C. Differ. Res. Biol. Divers. *102*, 19–26.
- Smith, E.R., Capo-chichi, C.D., and Xu, X.-X. (2018b). Defective Nuclear Lamina in Aneuploidy and Carcinogenesis. Front. Oncol. *8*, 529.
- Smith-Garvin, J.E., Koretzky, G.A., and Jordan, M.S. (2009). T cell activation. Annu. Rev. Immunol. *27*, 591–619.
- Spann, T.P., Goldman, A.E., Wang, C., Huang, S., and Goldman, R.D. (2002). Alteration of nuclear lamin organization inhibits RNA polymerase II-dependent transcription. J. Cell Biol. *156*, 603–608.
- Stadelmann, B., Khandjian, E., Hirt, A., Lüthy, A., Weil, R., and Wagner, H.P. (1990). Repression of nuclear lamin A and C gene expression in human acute lymphoblastic leukemia and non-Hodgkin's lymphoma cells. Leuk. Res. *14*, 815–821.
- Stein, H. (2001). Down-regulation of BOB.1/OBF.1 and Oct2 in classical Hodgkin disease but not in lymphocyte predominant Hodgkin disease correlates with immunoglobulin transcription. Blood *97*, 496–501.
- Stetler-Stevenson, W.G. (1999). Matrix metalloproteinases in angiogenesis: a moving target for therapeutic intervention. J. Clin. Invest. *103*, 1237–1241.
- Sun, X., Huang, J., Homma, T., Kita, D., Klocker, H., Schafer, G., Boyle, P., and Ohgaki, H. (2009). Genetic alterations in the PI3K pathway in prostate cancer. Anticancer Res. *29*, 1739–1743.
- Swerdlow, S.H., Campo, E., Pileri, S.A., Harris, N.L., Stein, H., Siebert, R., Advani, R., Ghielmini, M., Salles, G.A., Zelenetz, A.D., et al. (2016). The 2016 revision of the World Health Organization classification of lymphoid neoplasms. Blood *127*, 2375–2390.
- Szczerbal, I., Foster, H.A., and Bridger, J.M. (2009). The spatial repositioning of adipogenesis genes is correlated with their expression status in a porcine mesenchymal stem cell adipogenesis model system. Chromosoma *118*, 647–663.
- Taddei, A. (2007). Active genes at the nuclear pore complex. Curr. Opin. Cell Biol. *19*, 305–310.
- Taylor, A.M., Shih, J., Ha, G., Gao, G.F., Zhang, X., Berger, A.C., Schumacher, S.E., Wang, C., Hu, H., Liu, J., et al. (2018). Genomic and Functional Approaches to Understanding Cancer Aneuploidy. Cancer Cell *33*, 676-689.e3.
- Teng, M.W.L., Swann, J.B., Koebel, C.M., Schreiber, R.D., and Smyth, M.J. (2008). Immune-mediated dormancy: an equilibrium with cancer. J. Leukoc. Biol. *84*, 988–993.

- Testa, J.R., and Bellacosa, A. (2001). AKT plays a central role in tumorigenesis. Proc. Natl. Acad. Sci. U. S. A. *98*, 10983–10985.
- Thompson, S.L., and Compton, D.A. (2011). Chromosomes and cancer cells. Chromosome Res. Int. J. Mol. Supramol. Evol. Asp. Chromosome Biol. *19*, 433–444.
- Toma, P., Granata, C., Rossi, A., and Garaventa, A. (2007). Multimodality imaging of Hodgkin disease and non-Hodgkin lymphomas in children. Radiogr. Rev. Publ. Radiol. Soc. N. Am. Inc *27*, 1335–1354.
- Torlakovic, E., Tierens, A., Dang, H.D., and Delabie, J. (2001). The transcription factor PU.1, necessary for B-cell development is expressed in lymphocyte predominance, but not classical Hodgkin's disease. Am. J. Pathol. *159*, 1807–1814.
- Tutton, S., Azzam, G.A., Stong, N., Vladimirova, O., Wiedmer, A., Monteith, J.A., Beishline, K., Wang, Z., Deng, Z., Riethman, H., et al. (2016). Subtelomeric p53 binding prevents accumulation of DNA damage at human telomeres. EMBO J. *35*, 193–207.
- Uzoh, C.C., Perks, C.M., Bahl, A., Holly, J.M.P., Sugiono, M., and Persad, R.A. (2009). PTEN-mediated pathways and their association with treatment-resistant prostate cancer. BJU Int. *104*, 556–561.
- Vafa, O., Wade, M., Kern, S., Beeche, M., Pandita, T.K., Hampton, G.M., and Wahl, G.M. (2002). c-Myc can induce DNA damage, increase reactive oxygen species, and mitigate p53 function: a mechanism for oncogene-induced genetic instability. Mol. Cell *9*, 1031–1044.
- Vaillant, M., and Olliaro, P. (2007). Geometric least squares means ratios for the analysis of Plasmodium falciparum in vitro susceptibility to antimalarial drugs. Malar. J. *6*, 156.
- Van Ly, D., Low, R.R.J., Frölich, S., Bartolec, T.K., Kafer, G.R., Pickett, H.A., Gaus, K., and Cesare, A.J. (2018). Telomere Loop Dynamics in Chromosome End Protection. Mol. Cell *71*, 510-525.e6.
- Van Wier, S., Braggio, E., Baker, A., Ahmann, G., Levy, J., Carpten, J.D., and Fonseca, R. (2013). Hypodiploid multiple myeloma is characterized by more aggressive molecular markers than non-hyperdiploid multiple myeloma. Haematologica *98*, 1586–1592.
- Vander Heiden, M.G., Cantley, L.C., and Thompson, C.B. (2009). Understanding the Warburg effect: the metabolic requirements of cell proliferation. Science *324*, 1029–1033.
- Vaux, D.L., Cory, S., and Adams, J.M. (1988). Bcl-2 gene promotes haemopoietic cell survival and cooperates with c-myc to immortalize pre-B cells. Nature *335*, 440–442.
- Vermolen, B.J., Garini, Y., Mai, S., Mougey, V., Fest, T., Chuang, T.C.-Y., Chuang, A.Y.-C., Wark, L., and Young, I.T. (2005). Characterizing the three-dimensional organization of telomeres. Cytom. Part J. Int. Soc. Anal. Cytol. *67*, 144–150.
- Vigouroux, C., and Bonne, G. (2002). Laminopathies: One Gene, Two Proteins, Five Diseases…. In Nuclear Envelope Dynamics in Embryos and Somatic Cells, P. Collas, ed. (Boston, MA: Springer US), pp. 153–172.
- Volpert, O.V., Dameron, K.M., and Bouck, N. (1997). Sequential development of an angiogenic phenotype by human fibroblasts progressing to tumorigenicity. Oncogene *14*, 1495–1502.
- Voss, B., Rauterberg, J., Allam, S., and Pott, G. (1980). Distribution of Collagen Type I and Type III and of two Collagenous Components of Basement Membranes in the Human Liver. Pathol. - Res. Pract. *170*, 50–60.

- Wang, J., Xie, L.Y., Allan, S., Beach, D., and Hannon, G.J. (1998). Myc activates telomerase. Genes Dev. *12*, 1769–1774.
- Wang, Y., Jiang, J., He, L., Gong, G., and Wu, X. (2019). Effect of lamin-A expression on migration and nuclear stability of ovarian cancer cells. Gynecol. Oncol. *152*, 166–176.
- Warburg, O. (1956a). On respiratory impairment in cancer cells. Science *124*, 269–270.
- Warburg, O. (1956b). On the origin of cancer cells. Science *123*, 309–314.
- Wazir, U., Ahmed, M.H., Bridger, J.M., Harvey, A., Jiang, W.G., Sharma, A.K., and Mokbel, K. (2013). The clinicopathological significance of lamin A/C, lamin B1 and lamin B receptor mRNA expression in human breast cancer. Cell. Mol. Biol. Lett. *18*, 595–611.
- Weaver, B.A.A., and Cleveland, D.W. (2009). The role of aneuploidy in promoting and suppressing tumors. J. Cell Biol. *185*, 935–937.
- Weber-Matthiesen, K., Deerberg, J., Poetsch, M., Grote, W., and Schlegelberger, B. (1995). Numerical chromosome aberrations are present within the CD30+ Hodgkin and Reed-Sternberg cells in 100% of analyzed cases of Hodgkin's disease. Blood *86*, 1464–1468.
- Wei Dai, Y.Y. (2014). Genomic Instability and Cancer. J. Carcinog. Mutagen. *05*.
- Wein, F., and Küppers, R. (2016). The role of T cells in the microenvironment of Hodgkin lymphoma. J. Leukoc. Biol. *99*, 45–50.
- Weinberg, R.A. (1995). The retinoblastoma protein and cell cycle control. Cell *81*, 323–330.
- Weinrich, S.L., Pruzan, R., Ma, L., Ouellette, M., Tesmer, V.M., Holt, S.E., Bodnar, A.G., Lichtsteiner, S., Kim, N.W., Trager, J.B., et al. (1997). Reconstitution of human telomerase with the template RNA component hTR and the catalytic protein subunit hTRT. Nat. Genet. *17*, 498–502.
- Werb, Z. (1997). ECM and cell surface proteolysis: regulating cellular ecology. Cell *91*, 439–442.
- Wheeler, L.A., Trifonova, R., Vrbanac, V., Basar, E., McKernan, S., Xu, Z., Seung, E., Deruaz, M., Dudek, T., Einarsson, J.I., et al. (2011). Inhibition of HIV transmission in human cervicovaginal explants and humanized mice using CD4 aptamer-siRNA chimeras. J. Clin. Invest. *121*, 2401–2412.
- Willis, N.D., Cox, T.R., Rahman-Casañs, S.F., Smits, K., Przyborski, S.A., van den Brandt, P., van Engeland, M., Weijenberg, M., Wilson, R.G., de Bruïne, A., et al. (2008). Lamin A/C Is a Risk Biomarker in Colorectal Cancer. PLoS ONE *3*, e2988.
- Wolf, K., Te Lindert, M., Krause, M., Alexander, S., Te Riet, J., Willis, A.L., Hoffman, R.M., Figdor, C.G., Weiss, S.J., and Friedl, P. (2013). Physical limits of cell migration: control by ECM space and nuclear deformation and tuning by proteolysis and traction force. J. Cell Biol. *201*, 1069–1084.
- Wood, A.M., Rendtlew Danielsen, J.M., Lucas, C.A., Rice, E.L., Scalzo, D., Shimi, T., Goldman, R.D., Smith, E.D., Le Beau, M.M., and Kosak, S.T. (2014). TRF2 and lamin A/C interact to facilitate the functional organization of chromosome ends. Nat. Commun. *5*, 5467.
- Worman, H.J., and Bonne, G. (2007). "Laminopathies": a wide spectrum of human diseases. Exp. Cell Res. *313*, 2121–2133.
- Wright, W.E., and Shay, J.W. (1992). The two-stage mechanism controlling cellular senescence and immortalization. Exp. Gerontol. *27*, 383–389.

- Wu, Z., Wu, L., Weng, D., Xu, D., Geng, J., and Zhao, F. (2009). Reduced expression of lamin A/C correlates with poor histological differentiation and prognosis in primary gastric carcinoma. J. Exp. Clin. Cancer Res. CR *28*, 8.

- Yadav, S.K., Feigelson, S.W., Roncato, F., Antman-Passig, M., Shefi, O., Lammerding, J., and Alon, R. (2018). Frontline Science: Elevated nuclear lamin A is permissive for granulocyte transendothelial migration but not for motility through collagen I barriers. J. Leukoc. Biol. *104*, 239–251.

- Yang, L., Pang, Y., and Moses, H.L. (2010). TGF-beta and immune cells: an important regulatory axis in the tumor microenvironment and progression. Trends Immunol. *31*, 220–227.

- Ye, J.Z.-S., Hockemeyer, D., Krutchinsky, A.N., Loayza, D., Hooper, S.M., Chait, B.T., and de Lange, T. (2004). POT1-interacting protein PIP1: a telomere length regulator that recruits POT1 to the TIN2/TRF1 complex. Genes Dev. *18*, 1649–1654.

- Yu, Wang, Tammur, Tamm, Punab, Rangel-Pozzo, and Mai (2019). Distinct Nuclear Organization of Telomeresand Centromeres in Monoclonal Gammopathyof Undetermined Significance and Multiple Myeloma. Cells *8*, 723.

- Yuan, T.L., and Cantley, L.C. (2008). PI3K pathway alterations in cancer: variations on a theme. Oncogene *27*, 5497–5510.

- Zhang, C., Lee, H.J., Shrivastava, A., Wang, R., McQuiston, T.J., Challberg, S.S., Pollok, B.A., and Wang, T. (2018). Long-Term In Vitro Expansion of Epithelial Stem Cells Enabled by Pharmacological Inhibition of PAK1-ROCK-Myosin II and TGF-β Signaling. Cell Rep. *25*, 598-610.e5.

*cancers*

**MDPI**

*Article*

# Distinct 3D Structural Patterns of Lamin A/C Expression in Hodgkin and Reed-Sternberg Cells

**Fabio Contu [1,2,†], Aline Rangel-Pozzo [1,†], Peter Trokajlo [1], Landon Wark [1], Ludger Klewes [1], Nathalie A. Johnson [3], Tina Petrogiannis-Haliotis [3], John G. Gartner [4], Yuval Garini [5], Roberta Vanni [2] , Hans Knecht [3] and Sabine Mai [1,*]**

1   Cell Biology, Research Institute of Oncology and Hematology, University of Manitoba, CancerCare Manitoba, Winnipeg, MB R3E 0V9, Canada; fabio.contu89@gmail.com (F.C.); Aline.RangelPozzo@umanitoba.ca (A.R.-P.); umtrokaj@myumanitoba.ca (P.T.); lando.wark@gmail.com (L.W.); Ludger.Klewes@umanitoba.ca (L.K.)
2   Department of Biomedical Sciences, Unit of Biology and Genetics, University of Cagliari, 09042 Cagliari, Italy; vanni@unica.it
3   Division of Hematology and Division of Pathology, Department of Medicine, Jewish General Hospital, McGill University, Montréal, QC H3G 2M1, Canada; nathalie.johnson@mcgill.ca (N.A.J.); tina.haliotis@mcgill.ca (T.P.-H.); hans.knecht@mcgill.ca (H.K.)
4   Department of Pathology, University of Manitoba, Winnipeg, MB R3E 0W2, Canada; John.Gartner@umanitoba.ca
5   Physics Department & Institute of Nanotechnology, Bar Ilan University, Ramat Gan 5290002, Israel; Yuval.Garini@biu.ac.il
*   Correspondence: sabine.mai@umanitoba.ca; Tel.: +1-(204)-787-2135
†   These authors contributed equally to this paper.

**Abstract:** Classical Hodgkin's lymphoma (cHL) is a B-Cell lymphoma comprised of mononuclear Hodgkin cells (H) and bi- to multi-nucleated Reed-Sternberg (RS) cells. Previous studies revealed that H and RS cells express lamin A/C, a component of the lamina of the nuclear matrix. Since no information was available about the three-dimensional (3D) expression patterns of lamin A/C in H and RS cells, we analyzed the 3D spatial organization of lamin in such cells, using 3D fluorescent microscopy. H and RS cells from cHL derived cell lines stained positive for lamin A/C, in contrast to peripheral blood lymphocytes (PBLs), in which the lamin A/C protein was not detected or weak, although its presence could be transiently increased with lymphocyte activation by lipopolysaccharide (LPS). Most importantly, in H and RS cells, the regular homogeneous and spherically shaped lamin A/C pattern, identified in activated lymphocytes, was absent. Instead, in H and RS cells, lamin staining showed internal lamin A/C structures, subdividing the nuclei into two or more smaller compartments. Analysis of pre-treatment cHL patients' samples replicated the lamin patterns identified in cHL cell lines. We conclude that the investigation of lamin A/C protein could be a useful tool for understanding nuclear remodeling in cHL.

**Keywords:** Hodgkin's Lymphoma; Reed-Sternberg cells; Lamin A/C patterns; 3D imaging; Lymphocytes; nuclear architecture

---

## 1. Introduction

Classical Hodgkin's lymphoma (cHL) is characterized by two tumor cell populations: mononuclear Hodgkin cells (H) and bi- to multi-nucleated Reed-Sternberg cells (RS), which are the diagnostic cells of this lymphoma. H and RS cells represent only 1–5% of the total lymph node cells [1]. H cells originate from crippled, pre-apoptotic germinal center B cells [2] that have been

rescued from apoptosis by cellular transformation events [3,4]. RS cells originate from H cells through a process of multinucleation due to incomplete cytokinesis [5]. Transition from H to RS cell has also been correlated with an aberrant number of mitotic spindles, increased numbers of centrosomes, altered 3D telomere organization and telomere loss [6]. Advanced telomere loss and aggregation result in RS cells presenting telomere-poor 'ghost' nuclei, which interfere with endomitosis [7]. Super resolution microscopy (3D-structured illumination microscopy, 3D-SIM) investigation showed that the nuclear DNA structure is significantly changed in H and RS cells when compared to normal primary lymphocytes, with a significant increase in the amount of DNA-free or DNA-poor nuclear spaces defined by the absence of 4',6-diamidino-2-phenylindole (DAPI)-staining [8,9]. The number of DAPI-free spaces is increased in cancer cells during the transition from H to RS cells [8].

Lamins are type V intermediate filament (IF) proteins, which are the principal component of the lamina of the nuclear matrix. Two types of lamin have been described in human cells: B-type lamins, encoded by the *LMNB1* gene for lamin B1 [10] and the *LMNB2* gene for lamin B2 [11], and A-type lamins, encoded by the *LMNA* gene, the alternative splicing of which produces lamin A and lamin C [12]. Lamin B1 and lamin B2 are constitutively expressed and necessary for cell survival [13]. Lamin A/C expression differs from cell to cell and is usually limited to differentiated cells and not found in proliferating cells [14]. Lamin proteins are involved in a myriad of nuclear processes, including DNA replication, RNA transcription, cell differentiation and mitosis [15]. In particular, lamin A/C plays a crucial role in the regulation of mitotic spindle assembly and positioning [16].

Resting human and mouse T lymphocytes express lamin A/C, and its presence is transiently and considerably increased upon T cell activation [17]. Lamin A/C expression has been found to be down-regulated in different cancer types, like small cell lung cancers [18], colon cancers [19] and nodal diffuse large B-cell lymphoma [20]. On the other hand, squamous cell carcinoma and basal cell carcinoma are characterized by an up-regulation of lamin A/C [21]. Investigation of lamin A/C expression in neuroblastoma [22] and in prostate cancer [23] has been proven to be a reliable biomarker of cancer aggressiveness.

The first investigation of lamin proteins in reactive lymph nodes and cHL samples showed that lamin A/C was not expressed in CD20+ non-neoplastic B lymphocytes, but that it was expressed by a large population of CD30+ cells, in nine patients with nodular sclerosis Hodgkin's lymphoma [24].

To our knowledge, no data have been reported on 3D lamin A/C protein expression patterns in the H and RS cells of cHL patients and their relation to the process of multinucleation, namely the transition of cellular architecture from H to RS cells. Also, no data was reported on B lymphocyte lamin A/C expression following activation.

In this study, we investigated the three-dimensional (3D) spatial distribution of lamin A/C in three different cHL derived cell lines, in resting and stimulated purified peripheral blood lymphocytes (PBLs); and in 12 primary paraffin-embedded pre-treatment lymph node samples from patients diagnosed with cHL. Our findings reveal, for the first time, the presence of an aberrant lamin A/C structure in H and RS cells, which is distinct from that seen in normal lymphocytes.

## 2. Results

### 2.1. Lamin A/C and Lamin B1 in Hodgkin Lymphoma Derived Cell Lines and PBLs

To assess lamin A/C positivity in H and RS cells we performed immunostaining for lamin A/C and lamin B1 in three cHL-derived cell lines and normal lymphocytes. Immunohistochemical analysis revealed that H and RS cells from all the HL-derived cell lines stained for both lamin A/C (Figure 1A–C) and lamin B1 (Figure S1A–E).

As healthy controls, we used both lipopolysaccharide (LPS)-activated and resting normal B lymphocytes (Figure 2A–C). Resting PBLs showed weak to no positivity for lamin A/C expression (Figure 2D), while they were positive for lamin B1 (Figure S2A–D). However, lamin A/C expression increased after B cell activation with LPS (Figure 2E).
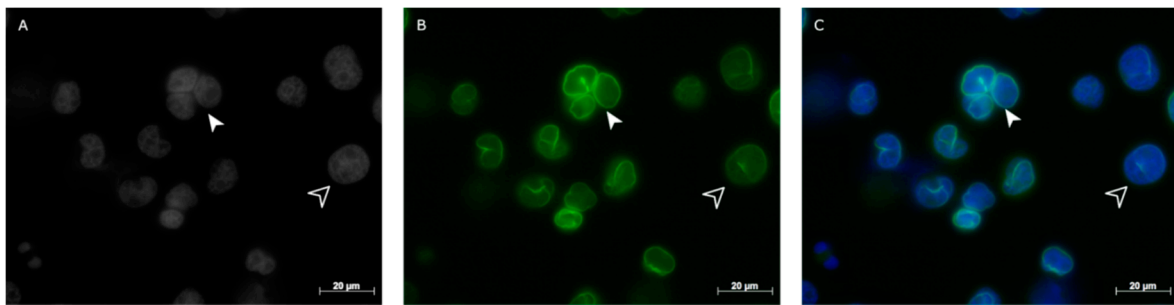
**Figure 1.** Example of lamin A/C protein staining in cells from Hodgkin's lymphoma (HDLM-2). (**A**) Two-dimensional (2D) image of nuclei stained with 4′,6-diamidino-2-phenylindole (DAPI)-(gray scale); (**B**) 2D image of anti-lamin A/C antibody immunostaining (green); (**C**) 2D merged image showing both mono-nuclear H (empty arrowhead) and bi- to multi-nuclear RS cells (solid arrowhead) expressing lamin A/C.
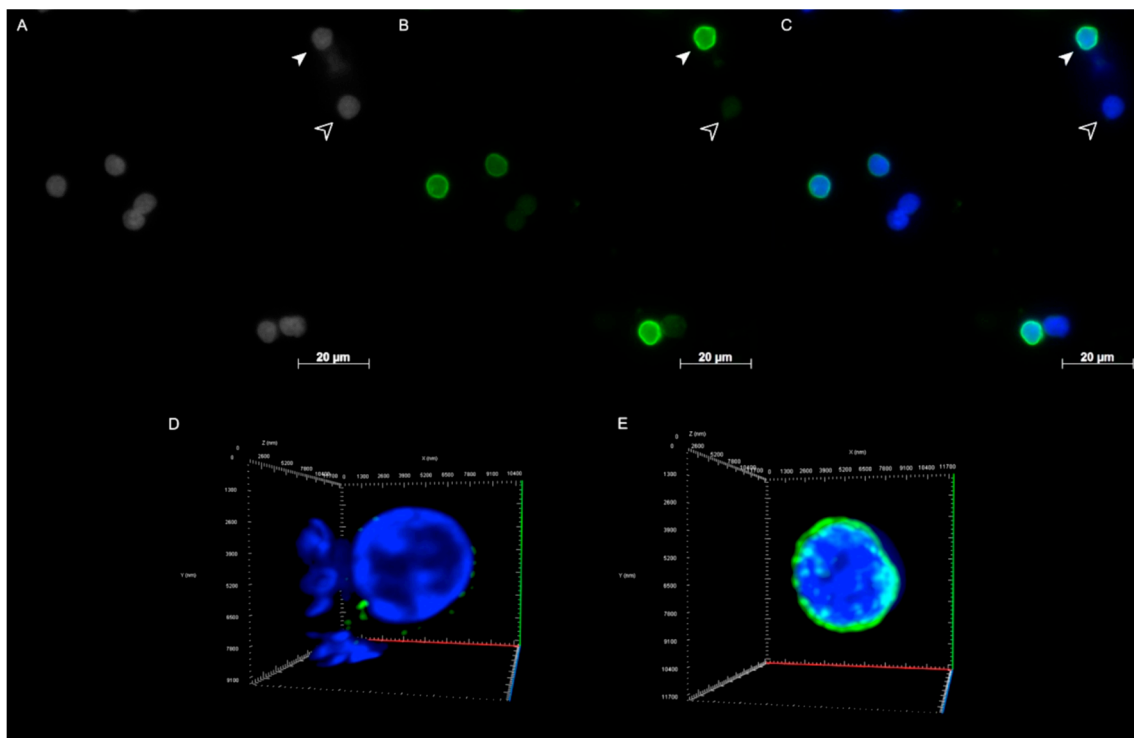


**Figure 2.** Lamin A/C immunostaining of resting and LPS-activated lymphocytes from peripheral blood (PB) of a healthy donor. (**A**) 2D image of nuclei stained with DAPI (gray scale); (**B**) 2D image of anti-lamin A/C antibody immunostaining (green); (**C**) 2D merged image showing activated lymphocytes with a higher fluorescence intensity lamin A/C signal (solid arrowhead) compared to resting cells (empty arrowhead). Complete 3D reconstitution of a resting (**D**) and an activated (**E**) lymphocyte.

## 2.2. Lamin A/C and Lamin B1 3D Spatial Distribution Patterns in Hodgkin Lymphoma Derived Cell Lines and PBLs

The lamin A/C 3D spatial distribution in resting PBLs was characterized by points of protein accumulation (Figure 2D). The lamin A/C pattern in activated lymphocytes appears as a regular sphere surrounding the nucleus (Figure 2E). The regular pattern is replaced in H and RS cells by a more irregular one, characterized by the presence of internal lamin A/C structures, dividing the 3D structure into multiple compartments not seen in the normal lymphocytes.

We identified five different types of lamin A/C patterns for H cells (0, A, B, C and D), and four for the RS cells (bi-nuclear, tri-nuclear, tetra-nuclear and multi-nuclear) (Table 1; Table S1). Quantitative analysis of the identified patterns for both H and RS cells was performed investigating the ratio of the external total lamin A/C intensity ($I_e$) on the internal total lamin A/C intensity ($I_i$) (Table 2).

**Table 1.** Means and frequencies of the lamin A/C 3D pattern observed in cHL-derived cell line HDLM-2. 30 H and 30 RS cells from three independent experiments were analyzed using the deconvoluted 3D reconstructions and divided according to the lamin A/C 3D pattern shown.

| Lamin A/C Pattern | Mean $\pm$ SD | Percentage |
|---|---|---|
| Hodgkin Cell Pattern 0 | 5 $\pm$ 3 | 15.48% |
| Hodgkin Cell Pattern A | 10 $\pm$ 1 | 29.15% |
| Hodgkin Cell Pattern B | 14.67 $\pm$ 4.51 | 42.16% |
| Hodgkin Cell Pattern C | 4.33 $\pm$ 3.51 | 11.63% |
| Hodgkin Cell Pattern D | 0.67 $\pm$ 1.15 | 1.59% |
| Bi-nuclear Reed-Sternberg | 19.67 $\pm$ 8.74 | 57.66% |
| Tri-nuclear Reed-Sternberg | 7.33 $\pm$ 0.58 | 22.27% |
| Tetra-nuclear Reed-Sternberg | 3.33 $\pm$ 1.15 | 10.29% |
| Multi-nuclear Reed-Sternberg | 3 $\pm$ 4.36 | 9.79% |

**Table 2.** Quantitative analysis of lamin A/C patterns in H and RS cells. 30 H and 30 RS cells of the cHL-derived cell line HDLM-2 from three independent experiments were analyzed. Total external lamin A/C signal intensity ($I_e$) was divided by the total internal lamin A/C signal intensity ($I_i$) to obtain a ratio. Resulting ratios and S.D. are shown.

| Lamin A/C Pattern | $I_e/I_i$ | S.D. |
|---|---|---|
| Hodgkin Cell Pattern 0 | 1.88 | 1.17 |
| Hodgkin Cell Pattern A | 2.65 | 1.15 |
| Hodgkin Cell Pattern B | 3.65 | 2.12 |
| Hodgkin Cell Pattern C | 4.02 | 2.66 |
| Hodgkin Cell Pattern D | 5.43 | 0.04 |
| Bi-nuclear Reed-Sternberg | 2.96 | 1.07 |
| Tri-nuclear Reed-Sternberg | 3.57 | 1.26 |
| Tetra-nuclear Reed-Sternberg | 4.50 | 3.37 |
| Multi-nuclear Reed-Sternberg | 4.55 | 2.95 |

The lamin A/C patterns were observed in all three HL-derived cell lines analyzed in this study. H cells were divided into groups based on how the lamin A/C 3D internal structures divided the nucleus (Figure 3A–E, Videos S1–S5). Pattern 0 has similar architecture to that found in LPS-activated normal B cells (Figure 3A). Pattern A is characterized by the presence of small internal structures and by the irregular 3D profile of lamin A/C (Figure 3B). In Pattern B, C, and D, the aberrant lamin A/C staining divides the 3D structure of mono-nuclear H cells into two, three and four different compartments, defined by internal lamin structures (Figure 3C–E). Mononuclear cells expressing pattern B constituted a majority (42.16%), followed by patterns A (29.15%), 0 (15.48%), C (11.63%) and D (1.59%). The pattern classification for H cells described increasing complexity of the internal lamin A/C structure and the quantitative analysis reflected this change as the $I_e/I_i$ ratio increased.

RS cells were divided into different groups according to the numbers of total nuclei, all covered by a spherical lamin surface. However, lamin A/C showed a more irregular pattern when compared to the mononuclear H cells. Anomalous lamin A/C features observed in H cells were also present (Figure 3F–H, Videos S6–S8). Bi-nuclear RS cells were found to be the most frequent (57.66%) in the RS cell population analyzed, followed by tri- (22.27%), tetra- (10.29%) and multi-nuclear (9.79%) RS cells. In RS cells as the pattern classification complexity of the lamin A/C structures increases from bi- to multi-nuclear, the quantitative analysis reflects this change with an increasing $I_e/I_i$ ratio.

Investigation of lamin B1 3D spatial distribution revealed the presence of the same types of patterns identified for lamin A/C in all the three HL-derived cell lines (Figure S1D,E), which were, however, observed with different frequencies (Table S2). The differences were statistically significant (respectively, H: *p* = 0.0002; RS: *p* = 0.006).
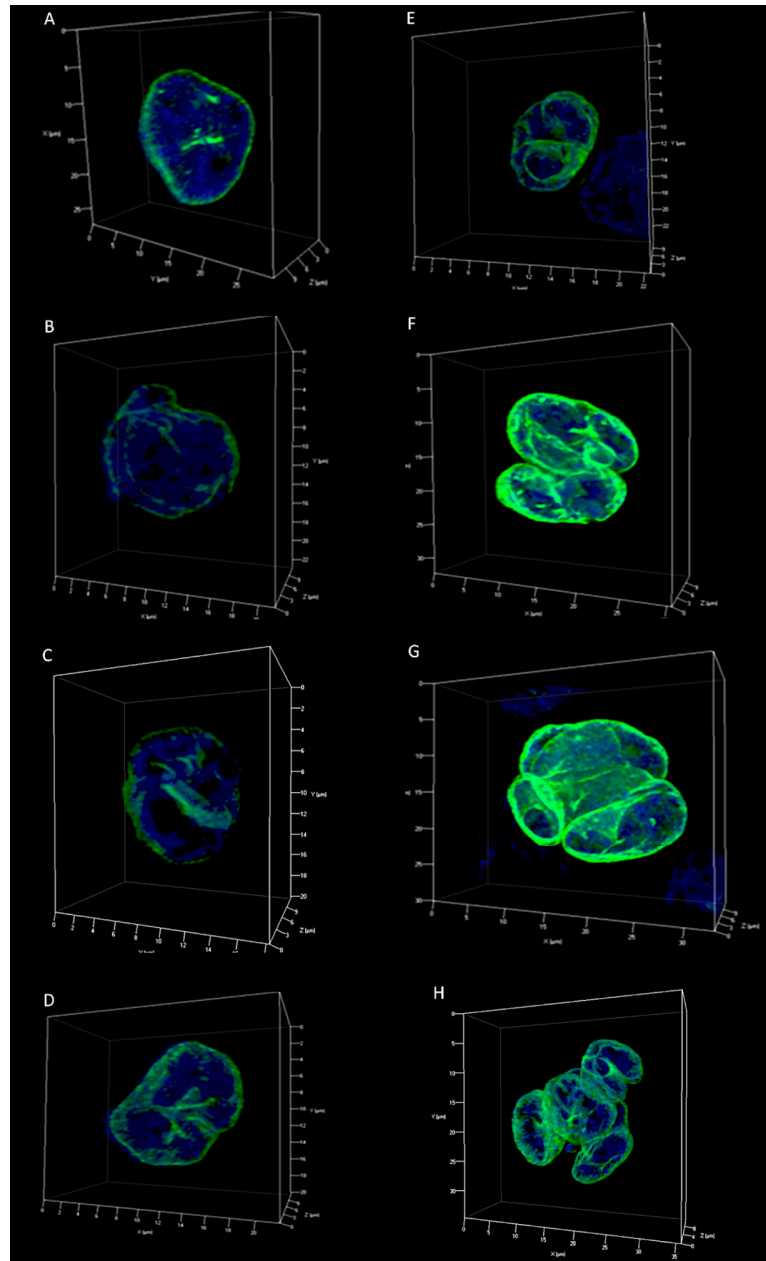


**Figure 3.** Lamin A/C patterns in 3D reconstructions of H and RS nuclei from HDLM-2. (**A**–**E**) H cells patterns according to how the internal lamin structures divide the 3D structure of lamin A/C: (**A**) pattern 0, characterized by a 3D pattern similar to the regular pattern of the LPS-activated lymphocytes, showing, however, localized accumulation of the lamin A/C; (**B**) pattern A, characterized by the irregular lamin A/C 3D distribution and the presence of invaginations due to short internal lamin structures; (**C**) pattern B, characterized by a single long internal lamin A/C 3D structure, which divides the nucleus into 2 different compartments; (**D**) pattern C, characterized by 3D multiple internal lamin structures which divide the nucleus into 3 different compartments; (**E**) pattern D, characterized by 3D division of the nucleus into 4 different compartments. (**F**–**H**) RS cells patterns according to the number of nuclei: (**F**), bi-nuclear RS cell; (**G**) tetra-nuclear RS cell; (**H**) multi-nuclear RS cell.

*2.3. Hodgkin's Lymphoma Patient Samples and Reactive Tonsils Samples*

Twelve primary diagnostic classical Hodgkin's lymphoma pre-treatment lymph node biopsy tissue sections were immunostained for lamin A/C. CD30 positivity was used to recognize H and RS (Figure S3A–C). Immunohistochemical analysis revealed that the majority of the non-neoplastic lymphocytes in the lymph node were lamin A/C negative, while all H and RS cells stained positively for lamin A/C. However, the lamin A/C fluorescent signal was not consistent throughout the patients' samples. The levels of the lamin A/C fluorescent signal was assessed as follows: (i) $-/-$ (poor), patient samples with weak fluorescent signals, in which it was impossible to evaluate lamin A/C 3D spatial distribution of H and RS cells; (ii) $-/+$ (average), patient samples with strong lamin A/C staining and clear 3D spatial distribution in a limited number of H and RS cells; (iii) +++ (high), patient samples with strong lamin A/C staining and clear 3D spatial distribution in most of the H and RS cells (Table 3). H and RS cells from patient samples with high lamin A/C fluorescent signal intensity presented the irregular 3D lamin A/C staining pattern characterized by internal lamin structures and points of protein accumulation (Figure 4). The different lamin A/C patterns observed in the H and RS cells of the Hodgkin cell lines were also identified in the H and RS cells of patient samples (Figure 4D,E). The majority of H cells expressed pattern 0 (45.71%) or pattern A (34.29%). Patterns B (14.29%) and C (5.71%) were rarely observed.

**Table 3.** Clinical data of patients diagnosed with cHL. Abbreviations: ABVD—doxorubicin, bleomycin, vinblastine, dacarbazine; CHLVPP—chlorambucil, vinblastine, procarbazine, prednisone; EBV—Epstein Barr Virus.

| Case | Gender | Age at Diagnosis | Stage | Type of Chemotherapy | Relapse | EBV Status | Lamin A/C Fluorescent Signal |
|------|--------|------------------|-------|----------------------|---------|------------|------------------------------|
| 1 | Male | 24 | IV | ABVD | N | − | −/− |
| 2 | Female | 55 | III | ABVD | Y | − | −/+ |
| 3 | Female | 25 | I | ABVD | N | + | −/− |
| 4 | Male | 55 | III | ABVD | Y | − | +++ |
| 5 | Male | 47 | I | ABVD | N | + | +++ |
| 6 | Female | 75 | IV | ABVD | N | − | −/+ |
| 7 | Male | 22 | II | ABVD | N | − | +++ |
| 8 | Male | 19 | II A | ABVD | N | − | −/+ |
| 9 | Male | 50 | III A | ABVD | N | − | +++ |
| 10 | Male | 37 | I A | ABVD | N | + | +++ |
| 11 | Male | 85 | III | CHLVPP | Y | − | −/− |
| 12 | Male | 28 | IA | ABVD | N | − | −/+ |

To assess lamin A/C spatial distribution in the germinal center (GC) lymphocytes, precursors of the H cells, five reactive tonsils biopsy tissue sections were immunostained for lamin A/C. Immunohistochemical analysis of the GC revealed weak-to-no positivity for lamin A/C (Figure S4A–C). Analysis of the centrocytes within the dark zone (DZ) of the GC confirmed the absence of lamin A/C staining (Figure S4D–G).
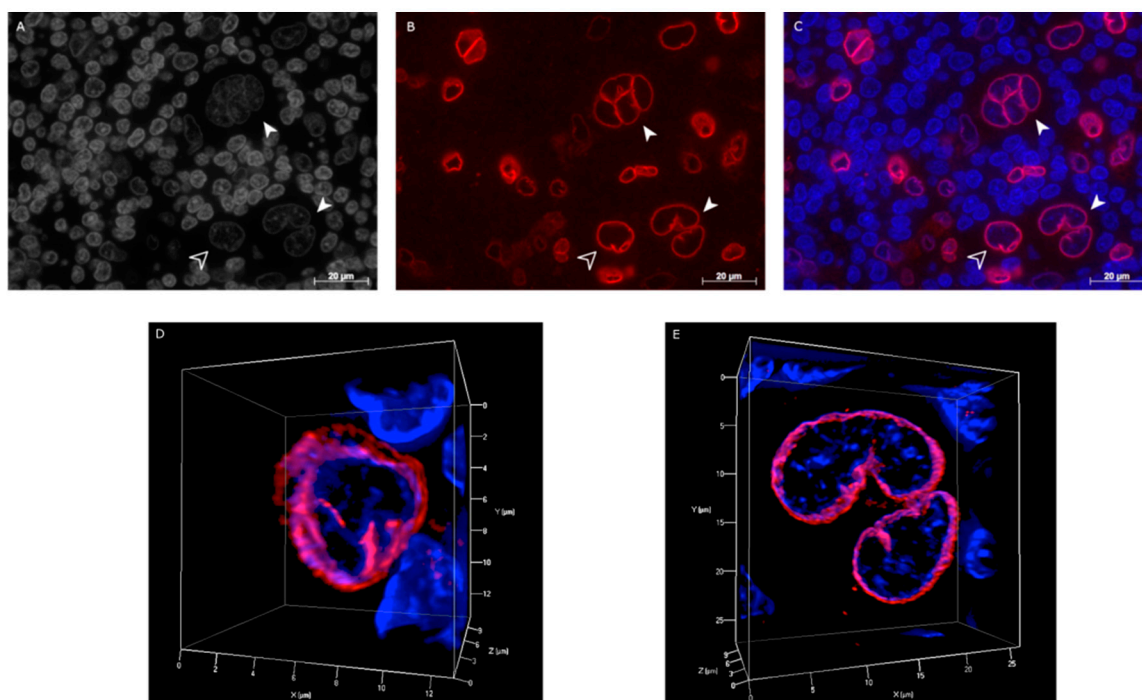
**Figure 4.** Example of lamin A/C expression in primary Hodgkin's lymphoma paraffin-embedded pre-treatment lymph node tissues from patients diagnosed with cHL. (**A**) 2D image of nuclei stained with DAPI (gray scale); (**B**) 2D image of anti-lamin A/C antibody immunostaining (red); (**C**) 2D merged image showing H (empty arrowhead) and RS (solid arrowhead) cells positively stained for lamin A/C. 3D reconstruction of patient-derived mono-nuclear Hodgkin (H) (**D**), and bi-nuclear (RS) cells (**E**), presenting the same patterns of irregular lamin A/C 3D structure characterized by internal lamin structures and points of protein accumulation, similar to those seen in the HL derived cell lines.

## 2.4. Co-Localization of Lamin A/C and Telomeres in H and RS Cells

To investigate the interaction of lamin A/C and telomeres, we combined the immuno-staining for lamin A/C with telomere quantitative fluorescent in situ hybridization (Q-FISH). The deconvolved 3D cell reconstructions of 30 H and 30 RS cells from three independent experiments were loaded on ImageJ (NIH, Bethesda, MD, USA) and analyzed through the TANGO (Sorbonne University, Paris, France) plug-in [25,26]. The overlapping percentage of the Cy3 signals of the telomeres and the fluorescein isothiocyanate (FITC) signal of the internal lamin A/C structures was examined by putting the generated data through a binary logic gate: a value of 0 was assigned by the software when no overlap was detected between a telomere signal and lamin A/C; a value of 1 was assigned when overlap was detected. The analysis revealed that only a minority of the telomeres co-localized with lamin A/C in the H cells (mean 33.06%; S.D. 0.08) and in the RS cells (mean 38.11%; S.D. 0.07) respectively.

## 2.5. Silencing of Lamin A/C mRNA and 3D Telomere Structure Analysis

In order to explore the effect of lamin A/C silencing in the HDLM-2 cells in terms of multinucleation process and genomic instability, we transfected the HDLM-2 cells with siRNA lamin A/C and non-targeting siRNA (Scramble) in three different concentrations for 24 h, 48 h and 72 h. Lamin A/C silencing was evaluated by Western Blot (WB) (Figure 5) which revealed a decrease in lamin A/C expression after 24 h with an even greater decrease after 96 h compared to control cells (non-targeting siRNA named as Scramble and cells without transfection named as control). After 96 h, the expression of lamin A/C was down-regulated by about 70% (Figure 5), and the number of RS cells decreased from 48.37 to 25% in the HDLM2 siRNA lamin A/C when compared to the Scramble. Subsequent time points of 120 h and 144 h were investigated to understand the complete kinetics

of siRNA-mediated lamin A/C silencing and its effects in the 3D nuclear organization of telomeres (Figure 6). After 96 h, the degradation of complementary lamin A/C mRNA molecules started to decrease as shown in Figure 5. To analyze the effects of siRNA on the 3D nuclear organization of telomeres we combined the immuno-staining for lamin A/C with Q-FISH.
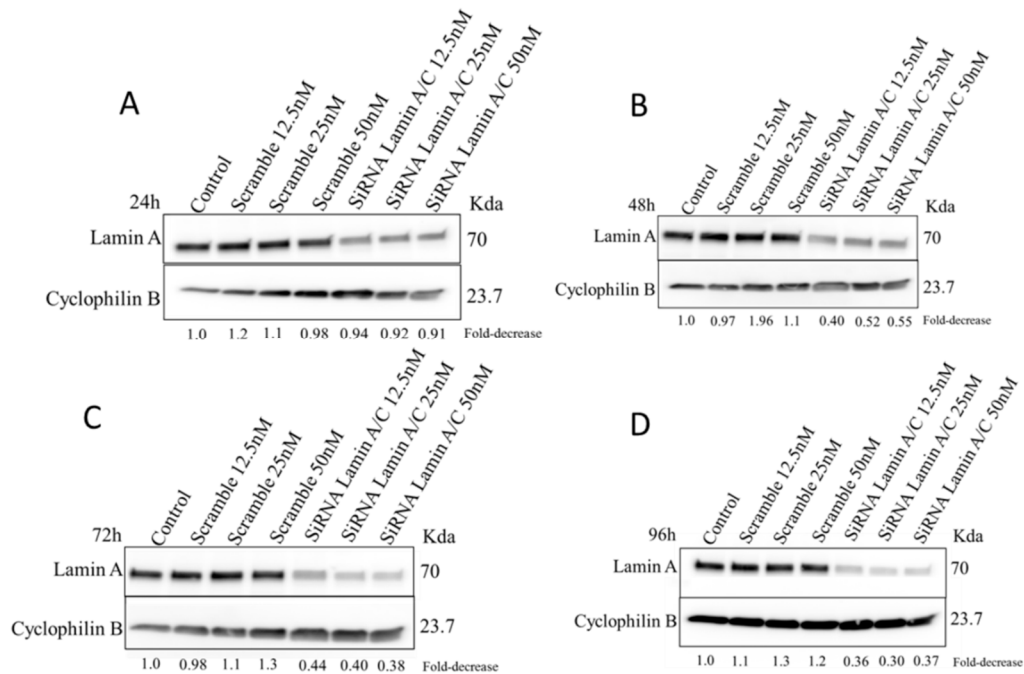


**Figure 5.** siRNA silencing of lamin A/C in HDLM-2. Lamin A/C expression was monitored by Western Blot after siRNA lamin A/C transfection in different concentration (12.5 nM, 25 nM and 50 nM) for 24 h (**A**), 48 h (**B**), 72 h (**C**) and 96 h (**D**). siRNA Scramble was used as a negative control and Cyclophilin B was used as a loading control. The fold-decrease for the siRNA is relative to the negative control (Scramble for each concentration) and the Scramble is relative to control without transfection (Control). These experiments were performed in triplicate using cells from different passages.
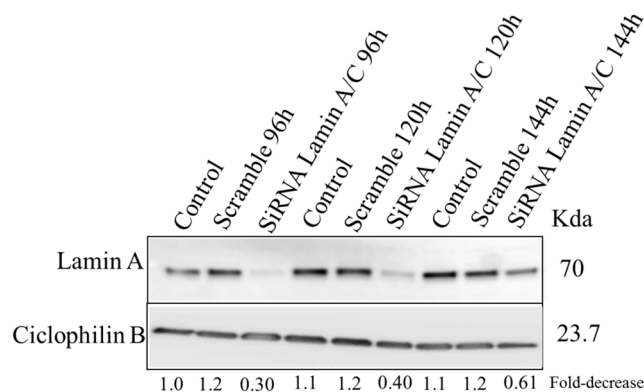


**Figure 6.** Investigation of siRNA silencing of lamin A/C in HDLM-2 for additional time points. Lamin A/C expression was monitored by Western Blot after siRNA lamin A/C transfection for 96 h, 120 h and 144 h (50 nM). siRNA Scramble was used as a negative control and Cyclophilin B was used as a loading control. The fold-decrease for the siRNA is relative to the negative control (Scramble for each concentration) and the Scramble is relative to control without transfection (Control). These experiments were performed in triplicate using cells in different passages.

Nuclei of 30 H and 30 RS cells transfected with siRNA lamin A/C were used for the telomere analysis. Scramble H and RS cells were used as controls. siRNA treated H cells, after 96 h, were characterized by a decrease in the average telomere signal intensity ($p = 0.0119$), and by changes in the overall telomere spatial organization, as demonstrated by an increased a/c ratio, when compared to the control ($p = 0.0079$). The increased a/c ratio was also observed after 120 h ($p = 0.0038$) and 144 h ($p = 0.0015$). siRNA treated RS cells, after 96 h, were characterized by an increase in the total number of telomeres ($p = 0.0013$), an increase in number of telomere aggregates ($p = 0.0073$), an increase in nuclear volume ($p < 0.0001$), and a decrease in average telomere signal intensity ($p = 0.0006$) when compared to the Scramble control. The nuclear volume was still increased after 120 h ($p < 0.0001$) and 144 h ($p = 0.0057$).

Moreover, the comparison among the 96 h, 120 h and 144 h time points revealed other telomere related abnormalities. In siRNA treated H cells, while both the total number of signals ($p = 0.0308$) and the total number of aggregates ($p = 0.0473$) increase from 96 h to 144 h, the average telomere intensity ($p = 0.0081$), the total telomere signal intensity ($p = 0.0311$), the a/c ratio ($p < 0.0001$) and the nuclear volume ($p < 0.0001$) decrease from 96 h to 144 h. Total number of telomere signals ($p = 0.0280$) and the total number of telomere aggregates ($p = 0.0208$) are found to be increased also in siRNA treated RS cells after 144 h when compared to 96 h, and the average telomere intensity ($p = 0.0002$), the total telomere signal intensity ($p = 0.0318$) and the nuclear volume ($p = 0.0027$) decrease as observed in the H cells. Prolonged downregulation of lamin A/C induced genomic instability in both H and RS cells, suggesting a prominent role of lamin A/C in the maintenance of telomere 3D spatial organization.

### 2.6. DNA Structure and Stucture of DNA-Poor Spaces in siRNA Treated HL Cell Line

Structured illumination microscopy (SIM) of 30 H and 30 RS cells from three independent siRNA lamin A/C samples (50 ng, 96 h) (Figure 7B,E respectively) and Scramble controls (Figure 7A,D respectively) were used to compare the 3D structural organization of the nuclear DNA of the two experimental arms. We used a granulometry-based measurement technique to quantify both the DNA structure and the structure of DNA-free space inside interphase nuclei [8]. The cumulative distributions of structure sizes (Figure 7C,F) have been plotted. Two-sided, two-sample Kolmogorov–Smirnov test showed that although the size distribution of both the DNA structure ($p = 0.26$) and DNA-free space ($p = 0.37$) was not significantly different between siRNA transfected H cells and Scramble H cells, the comparison between siRNA transfected RS cells and Scramble RS cells showed a difference. Both the DNA structure ($p < 0.001$) and structure of the DNA-free space ($p < 0.001$) contained finer structure for siRNA lamin A/C cells, suggesting a prominent role of lamin A/C in the nuclear architecture maintenance.
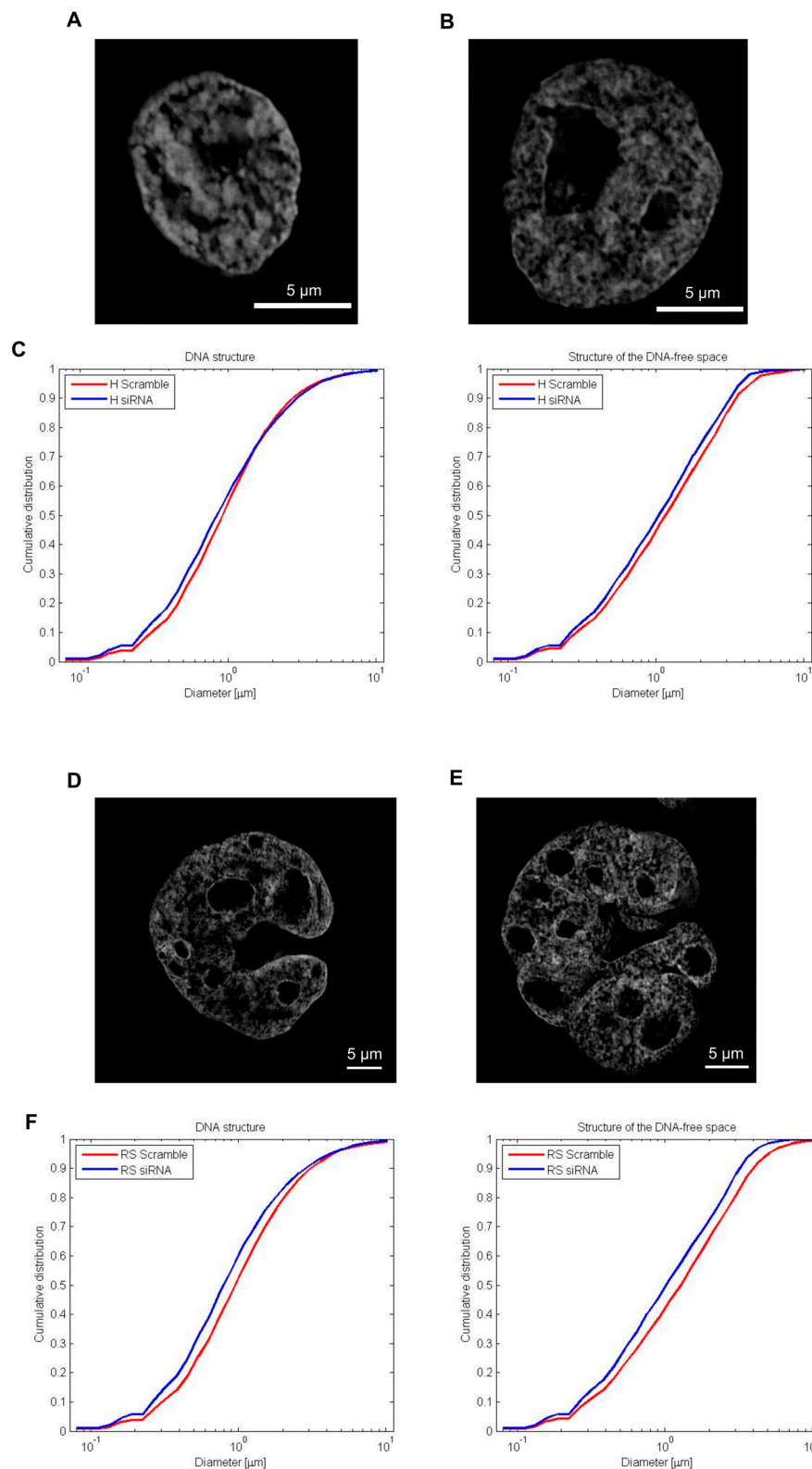
**Figure 7.** Granulometry analysis of siRNA lamin A/C cells and Scramble cells: (**A**) SIM image of Scramble H cell; (**B**) SIM image of siRNA H cell; (**C**) Measurements of the size distribution of DNA structure and structure of the DNA-free space in SIM images of Hoechst (33258) stained nuclei of 30 H cells from three independent experiments; (**D**) SIM image of Scramble RS cell; (**E**) SIM image of siRNA RS cell; (**F**) Measurements of the size distribution of DNA structure (H: $p = 0.26$; RS: $p < 0.001$) and structure of the DNA-free space (H: $p = 0.37$; RS: $p < 0.001$) in SIM images of Hoechst (33258) stained nuclei of 30 RS cells from three independent experiments. Two-sided, two-sample Kolmogorov–Smirnov test was used to determine statistical significance.

## 3. Discussion

Our study is the first one to describe different lamin A/C 3D nuclear organizational patterns leading to progressively complex nuclear matrix compartmentalization by laminar structures in H and RS cells in cHL-derived cell lines and in patients' diagnostic pre-treatment lymph nodes that are distinct from what is seen in normal lymphocytes, and in non-neoplastic (inflammatory) lymphocytes in the same lymph nodes.

H and RS cells from classical Hodgkin's lymphoma-derived cell lines showed high lamin A/C expression. In contrast, isolated resting PBLs were lamin A/C negative or presented weak lamin A/C staining. Immunohistochemical analysis confirmed that LPS-activated B cells stained positively for lamin A/C and were used as a control for H and RS cells from HL-derived cell lines.

It has been demonstrated that dysregulation of lamin A/C can affect DNA transcription, replication and repair, inducing genomic instability which leads to cancer progression [27–29]. Lamin A/C, in fact, plays a role in mitosis by regulating mitotic spindle assembly and positioning [16]. Since RS cells are characterized by an increased number of mitotic spindles, and incomplete spindles are regularly detected [6], lamin A/C could be involved in the multinucleation process. In order to verify the role of lamin A/C in this process, we performed silencing experiments of the lamin A/C mRNA through siRNA transfection. The number of RS cells after 96 h was found to be decreased. It has been demonstrated that telomere loss and aggregation in RS cells interferes with the endomitotic process [7]. Telomere analysis through the different time points showed that siRNA treated H and RS cells were characterized by an increased genomic instability, with an increase in the number of short telomeres and telomere aggregates, revealing that lamin A/C is crucial for the multinucleation process. In addition, silencing of lamin A/C led to a progressive disruption of nuclear DNA organization in siRNA lamin A/C treated cells when compared to the control, suggesting that lamin A/C plays an important role in determining the nuclear structure.

Our findings indicated that H and RS cells had an irregular lamin 3D distribution pattern compared to the 3D structure of lamin A/C in LPS-activated lymphocytes, which displayed a continuous spherical protein matrix surrounding the nucleus. Specifically, H and RS cells were characterized by the presence of lamin A/C invaginations, points of protein accumulation, and internal lamin structures that subdivide the nuclei into multiple compartments. According to the organization of the internal structures and number of resulting sub-compartments, we defined five different groups for the H cells (0-A-B-C-D), and four different groups for the Reed-Sternberg cells (bi-nuclear, tri-nuclear, tetra-nuclear and multi-nuclear). Pattern 0 of H cells is morphologically similar to the regular one characteristic of LPS-activated lymphocytes, except for localized accumulation of lamin A/C. Pattern A is characterized by an irregular lamin A/C 3D spatial distribution and the presence of invaginations and short internal lamin structures. Pattern B presents one long lamin internal structure, which divides the H cell nuclei into two distinct compartments. We supposed that this lamin A/C compartmentalization could anticipate the transition of a mono-nuclear H to a bi-nuclear RS cell, making lamin A/C a useful tool to predict the future behavior of the cell. Pattern C is characterized by the presence of multiple internal lamin structures which divide the cell into three different portions, either foreshadowing a transition from H to tri-nuclear RS cell or indicating that this is an end-stage H cell unable to perform further nuclear division. Pattern D shows a division into four different regions and could either anticipate a transition from a mono-nuclear H to tetra-nuclear RS cell, or again indicate an end-stage H-cell no longer capable of dividing.

To investigate the above hypothesis, we divided the H and RS cells from three independent experiments (90 cells total for each cell type) into different groups according to which specific pattern they showed. The obtained percentages are consistent with the hypothesis that a significant proportion of mono-nuclear H-cells is still capable of progression to RS-cells [30]. However, considering that likely not every mono-nuclear H cell will complete the transition to a RS cell [6], lamin A/C may be a useful tool in predicting the future behavior of an H cell and, therefore, of the neoplastic population of any given patient on the whole.

The analysis of the HL patient samples confirmed the presence of the patterns we observed in the Hodgkin cell lines, with most of the H cells expressing patterns similar to the one of the activated lymphocytes. More complex ones, like pattern B or pattern C, were observed with lower frequency. Though in histological slide preparations the thickness of the cut is 5 μm, and, therefore, never includes the whole nuclear volume of H- and RS-cells, our collective data suggest that the observed differences in lamin A/C spatial organization is likely to be linked to an alternative, aberrant remodeling of the lamin A/C protein in H and RS cells, as compared to normal lymphocytes. However, a larger cohort of patients will be required to confirm the distribution of lamin A/C patterns among the H and RS cell population in the lymph node.

It is known that lamin A/C plays a crucial role in maintenance of genome organization, since it is responsible for chromosomal crosslinking and chromosomal anchoring by binding to the telomeres via the shelterin protein TRF2 (telomere repeat binding factor 2) [31,32]. cHL is, however, characterized by genomic instability [8,33,34], and it has been previously demonstrated that 3D direct telomere-TRF2 interaction is severely disrupted in H- and RS-cells [35]. In order to explore whether the telomeres of H and RS cells would bind to the internal lamin A/C structure, we performed immuno-staining for lamin A/C combined with telomere Q-FISH. Our results revealed that lamin is binding the telomeres in a low percentage in both cell types. Future studies on the direct interaction between lamin A/C and TRF2 will be necessary to understand if lamin A/C is actively involved in disruption of the telomere-TRF2 interaction process.

In summary, our results show that lamin A/C spatial organization may be instrumental in the transition from mononuclear H- to bi- and multi-nucleated RS-cells and that the technology of 3D analysis holds the potential for becoming an invaluable predictive tool in the clinical management of this complex disease. However, live cell imaging for visualization of lamin will be necessary to follow not only the formation of the internal lamin A/C structures but to confirm their impact in the multinucleation process.

## 4. Materials and Methods

### 4.1. Lymphocyte Isolation and Stimulation

Peripheral blood lymphocytes (PBLs) were isolated from peripheral blood from healthy donors through Ficoll-gradient centrifugation (Ficoll-Paque$^{TM}$ Plus, 17-1440-02, GE Healthcare, Little Chalfont, UK). Blood was diluted with PBS (3.5:1) and settled with a ratio of 1.5:1 on Ficoll. The obtained buffy coat was collected and washed twice in a PBS solution. Stimulation of B-lymphocytes was obtained culturing PBLs with 50μM of Lipopolysaccharides (LPS) (SIGMA, L2630, St. Louis, MO, USA) for 72 h. Isolated resting and LPS-activated PBLs were then placed onto poly-l-lysine (SIGMA, p8920, St. Louis, MO, USA) coated slides.

### 4.2. Cell Lines

Three different EBV-negative cHL derived cell lines were used for this study: Nodular Sclerosis cHL derived cell lines HDLM-2 and L-428, and Mixed Cellularity cHL derived cell line L-1236 (DSMZ, Braunschweig, Germany). The HDLM-2 and L-428 cell lines were grown in RPMI-1640 medium, supplemented with 20% fetal bovine serum (FBS), 1% L-glutamine, 1% sodium pyruvate, and 1% penicillin–streptomycin (reagents from Invitrogen/Gibco, Burlington, ON, Canada). The L-1236 cell line was grown in RPMI-1640 medium, supplemented with 10% FBS, 1% L-glutamine, 1% sodium pyruvate, and 1% penicillin–streptomycin. Cells were incubated at 37 °C with 5% $CO_2$ in a humidified atmosphere. Fresh slides were prepared before every experiment spreading the cells onto poly-L-lysine coated slides.

*4.3. Immunohistochemistry*

Primary Anti-Lamin A (rabbit polyclonal, ab26300, Abcam Ltd., Cambridge, UK) and secondary Goat Anti-rabbit Alexa 488 (Molecular Probes, Waltham, MA, USA) antibodies were used for immunohistochemical analysis of lamin A/C at a dilution of 1:200 and 1:500 respectively in 4%BSA/4× SSC blocking solution. Primary Anti-Lamin B1 (rabbit polyclonal, ab16048, Abcam Ltd. UK) and secondary Goat Anti-rabbit Cy3 (AP187C, Sigma Chemical, St. Louis, MO, USA) antibodies were used for immunohistochemical analysis of lamin B1 at a dilution of 1:200 and 1:500 respectively in 4%BSA/4× SSC blocking solution. The cells were fixed in 3.7% formaldehyde/1× PBS and permeabilized with 0.1% Triton-X 100. 1× PBS washes were performed to wash the solutions off. Slides were then incubated with primary antibody for 45 min at 37 °C, humidified atmosphere. 1× PBS washes were performed to wash away the extra primary antibody. Incubation with secondary antibody was performed for 30 min at 37 °C, humidified atmosphere. 1× PBS washes were performed to wash away the extra antibody. DNA of the nuclei was counterstained with DAPI. Vectashield was used as mounting medium to prevent photo-bleaching of the sample.

*4.4. Lamin A/C Patterns Quantitative Analysis*

The quantitative measurements of the lamin A/C patterns have been performed on the cHL derived cell line HDLM-2, on 30 H and 30 RS cells from three independent experiments. 2D images of H and RS cells representing the identified pattern were selected and used for the quantitative analysis on ZEN Blue Version 2.3 Software (Carl Zeiss, Jena, Germany). The Draw Spline Contour tool of ZEN was used to manually select two distinct areas: (i) the external lamin A/C fluorescent signal ($I_e$) and (ii) the internal lamin A/C fluorescent signal ($I_i$). Total external lamin A/C signal intensity and total internal lamin A/C signal intensity were calculated. A ratio of the resulting intensities ($I_e/I_i$) was calculated for every cell. The obtained ratios from cells having the same pattern were averaged and compared with the ratios obtained for the other patterns.

*4.5. cHL Patient Samples*

We analyzed 12 primary Hodgkin's lymphoma paraffin embedded pre-treatment lymph node samples from patients diagnosed with cHL. The patients' information are summarized in Table 3. The patients were consented to participate into this research, which was approved by the research ethics board at the Jewish General Hospital in Montreal (protocol 16-016).

Formalin-fixed, paraffin-embedded tissue slides (5 μm thickness) were deparaffinized at room temperature in xylene until the paraffin was completely dissolved away, and then placed in 100% ethanol. The slides were subsequently rehydrated in a descending gradient of ethanol-water solutions to 50% ethanol, and transferred to PBS before fixation in 3.7% formaldehyde/1× PBS. The immuno-staining protocol for lamin A/C applied was the same one used for the Hodgkin derived cell lines, with the addition of an antigen-retrieval treatment before the permeabilization in Triton-X. For this step, we incubated the slides in the Target Retrieval Solution (DAKO, S1700, Santa Clara, CA, USA) for 20 min at 90 °C, and then 20 min at room temperature (RT).

*4.6. Immuno-Staining for Lamin A/C/Telo-Q-FISH*

The combined quantitative 3D lamin A/C-telomere immuno Q-FISH protocol used in this study has been previously described by Knecht and Mai in 2017 [36]. In addition to the immuno-staining procedure, Q-FISH was performed using Cy3- labeled peptide nucleic acid (PNA) probe (Dako, Glostrup, Denmark). Slides were placed in 70% formamide/10 mM, then washed in 0.1× SSC at 55 °C. An additional wash in 2× SSC/0.05% Tween 20 was performed. A second incubation with primary and secondary antibodies was performed before DAPI counterstaining.

### 4.7. siRNA Silencing and Western Blot

Lamin A/C expression was monitored by Western Blot after siRNA lamin A/C transfection in different concentration (12.5 nM, 25 nM and 50 nM) for 24 h (Figure 5A), 48 h (Figure 5B), 72 h (Figure 5C) and 96 h (Figure 5D). siRNA lamin A/C transfection with 50 nM was also performed on two additional time points—120 h and 144 h (Figure 6)—to investigate the complete kinetics of siRNA-mediated lamin A/C silencing. siRNA Scramble was used as a negative control and Cyclophilin B was used as a loading control. The fold-decrease for the siRNA is relative to the negative control (Scramble for each concentration) and the Scramble is relative to control without transfection (Control). All numbers are indicated under each column. These experiments were performed in triplicate using cells from different passages.

### 4.8. 3D Image Acquisition

3D conventional imaging of 30 H, 30 RS, and 30 Lymphocytes was performed using ZEISS Axio Imager.Z2 (Carl Zeiss, Toronto, ON, Canada) with a cooled AxioCam HR B&W, FITC, Cy3 and DAPI filters in combination with a Planapo 63x/1.4 oil objective lens (Carl Zeiss). 60 z-stacks were imaged for every fluorophore of every cell with a 200 nm step among the stacks. Images were obtained using AxioVision 4.8 (Carl Zeiss), deconvolved using the constrained iterative restoration algorithm with Theoretical PSF and Clip Normalization, and rendered using the Maximum Module.

The automated image acquisition of interphase nuclei was performed using the ScanView system [Applied Spectral Imaging (ASI)], using a Zeiss Imager Z2 microscope with a Basler CCD camera. For scanning purposes, the microscope was equipped with a motorized nine-slide stage (Märzhäuser, Wetzlar, Germany). The 3D-images were acquired with dry $40\times$ objective and a $0.6\times$ c-mount (Olympus, Tokyo, Japan) taking 9 focal planes per cell. The axial sampling distance between planes, Dz, was 300 nm. Exposure times were constant at 1 ms (DAPI) and 100 ms (FITC) throughout the experiments. The tissue sample mode with cell circularity setting of 1.4 was used to enable segmentation of touching cells and cell detection. Cells touching the border of the field of view were excluded. Approximately 1000 were scanned and analyzed. For data acquisition and analysis the software modules GenASIs and SpotScan were used.

3D SIM imaging was performed using Zeiss PS.1 Elyra microscopy system equipped with 63x 1.4 NA objective lens and IXon 885 EMCCD Camera (Andor, Oxford, UK). Images were acquired using 1.518 refractive index (RI) immersion oil. 405 nm laser was used for excitation of the DAPI channel. SIM grating period of 28 μm was used. The step between z-planes ($\Delta z$), was set at 0.091 μm. The images were reconstructed with ZEN 2012 black edition software (Carl Zeiss, Jena, Germany) with Noise filter set to $-3.0$ and deactivation of the Baseline Cut option. Pixel size resulted 40 nm in the reconstructed image.

### 4.9. Image Analysis

For co-localization of lamin A/C and telomeres, following deconvolution of the images, a minimum of 30 H and 30 RS cells from three independent experiments on the HDLM-2 cell line were processed using NIH Image J Software (version 1.52e) and Tools for Analysis of Nuclear Genome Organization (TANGO) software (version 0.97) [25,26]. All structures were segmented using the stock segmentation; background was subtracted for Cy3 signals with subtract background 2D. Signal quantification was performed for FITC (lamin A/C) and Cy3 (telomere) signals and simple geometric measurements were taken for the nuclei and Cy3 signals. Co-localization was determined through the overlap between FITC signal of lamin A/C and Cy3 signal of the telomeres.

For telomeres' analysis of siRNA treated cells and controls, deconvolved images were converted into TIFF files and exported for 3D analysis using the TeloView software program (version 2.0, 3D Signatures Inc., Toronto, ON, Canada) [37]. TeloView has been used for the analysis of the following parameters: (i) total number of telomeres' signals; (ii) total number of telomeres' aggregates; (iii) a/c

ratio, which represents the cell cycle-dependent nuclear telomere distribution, where values close to 1 indicate cells are in G0/G1 phase, while values bigger than 1 are in S/G2 state; (iv) nuclear volume; (v) average telomeres' signal intensity; (vi) total telomeres' signal intensity.

The granulometry analysis of the DNA structure, DNA-free space and all computations were performed using the DIPimage toolbox for Matlab (version R2012a, MathWorks, Natick, MA, USA) as described by Righolt et al. in 2014 [8].

*4.10. Statistical Analysis*

Chi-square ($\chi^2$) test was used to assess the differences among the frequencies observed for the different patterns in H and RS cells. The telomeric parameters (number of telomeres, number of telomere aggregates, nuclear volume, a/c ratio, average and total telomere signal intensity) were compared between siRNA treated and Scramble H and RS cells, and among siRNA treated H and RS cells from different time points using a nested factorial analysis of variance (ANOVA) or two way ANOVA. Multiple comparisons using the least-square means tests followed in which interaction effects between two factors were found to be significant. Two-sided, two-sample Kolmogorov–Smirnov test was used to determine statistical significance of the differences measured in the granulometry analysis. Significance levels were set at $p = 0.05$.

## 5. Conclusions

Lamin A/C spatial distribution in H and RS cells from cHL is characterized by an aberrant shape and the presence of internal lamin structures and points of protein accumulation. These internal structures subdivide the nuclei into different sub-compartments. Due to the involvement of lamin A/C in regulating mitosis, these new findings suggest a potential role of lamin A/C in the multinucleation process from H to RS cells.

## References

1. Swerdlow, S.H.; Campo, E.; Pileri, S.A.; Harris, N.L.; Stein, H.; Siebert, R.; Advani, R.; Ghielmini, M.; Salles, G.A.; Zelenetz, A.D.; et al. The 2016 revision of the World Health Organization classification of lymphoid neoplasms. *Blood* **2016**, *127*, 2375–2390. [CrossRef] [PubMed]

2.  Küppers, R.; Rajewsky, K.; Zhao, M.; Simons, G.; Laumann, R.; Fischer, R.; Hansmann, M.L. Hodgkin disease: Hodgkin and Reed-Sternberg cells picked from histological sections show clonal immunoglobulin gene rearrangements and appear to be derived from B cells at various stages of development. *Proc. Natl. Acad. Sci. USA* **1994**, *91*, 10962–10966. [CrossRef] [PubMed]

3.  Bohle, V.; Döring, C.; Hansmann, M.-L.; Küppers, R. Role of early B-cell factor 1 (EBF1) in Hodgkin lymphoma. *Leukemia* **2013**, *27*, 671–679. [CrossRef] [PubMed]

4.  Izban, K.F.; Ergin, M.; Huang, Q.; Qin, J.Z.; Martinez, R.L.; Schnitzer, B.; Ni, H.; Nickoloff, B.J.; Alkan, S. Characterization of NF-kappaB expression in Hodgkin's disease: Inhibition of constitutively expressed NF-κB results in spontaneous caspase-independent apoptosis in Hodgkin and Reed-Sternberg cells. *Mod. Pathol.* **2001**, *14*, 297–310. [CrossRef] [PubMed]

5.  Drexler, H.G.; Gignac, S.M.; Hoffbrand, A.V.; Minowada, J. Formation of multinucleated cells in a Hodgkin's-disease-derived cell line. *Int. J. Cancer* **1989**, *43*, 1083–1090. [CrossRef] [PubMed]

6.  Knecht, H.; Sawan, B.; Lichtensztejn, D.; Lemieux, B.; Wellinger, R.J.; Mai, S. The 3D nuclear organization of telomeres marks the transition from Hodgkin to Reed-Sternberg cells. *Leukemia* **2009**, *23*, 565–573. [CrossRef] [PubMed]

7.  Knecht, H.; Sawan, B.; Lichtensztejn, Z.; Lichtensztejn, D.; Mai, S. 3D Telomere FISH defines LMP1-expressing Reed-Sternberg cells as end-stage cells with telomere-poor "ghost" nuclei and very short telomeres. *Lab. Investig.* **2010**, *90*, 611–619. [CrossRef] [PubMed]

8.  Righolt, C.H.; Guffei, A.; Knecht, H.; Young, I.T.; Stallinga, S.; van Vliet, L.J.; Mai, S. Differences in nuclear DNA organization between lymphocytes, Hodgkin and Reed-Sternberg cells revealed by structured illumination microscopy. *J. Cell. Biochem.* **2014**, *115*, 1441–1448. [CrossRef] [PubMed]

9.  Righolt, C.H.; Knecht, H.; Mai, S. DNA Superresolution Structure of Reed-Sternberg Cells Differs Between Long-Lasting Remission Versus Relapsing Hodgkin's Lymphoma Patients. *J. Cell. Biochem.* **2016**, *117*, 1633–1637. [CrossRef] [PubMed]

10. Lin, F.; Worman, H.J. Structural organization of the human gene (LMNB1) encoding nuclear lamin B1. *Genomics* **1995**, *27*, 230–236. [CrossRef] [PubMed]

11. Höger, T.H.; Zatloukal, K.; Waizenegger, I.; Krohne, G. Characterization of a second highly conserved B-type lamin present in cells previously thought to contain only a single B-type lamin. *Chromosoma* **1990**, *99*, 379–390. [CrossRef] [PubMed]

12. Fisher, D.Z.; Chaudhary, N.; Blobel, G. cDNA sequencing of nuclear lamins A and C reveals primary and secondary structural homology to intermediate filament proteins. *Proc. Natl. Acad. Sci. USA* **1986**, *83*, 6450–6454. [CrossRef] [PubMed]

13. Harborth, J.; Elbashir, S.M.; Bechert, K.; Tuschl, T.; Weber, K. Identification of essential genes in cultured mammalian cells using small interfering RNAs. *J. Cell Sci.* **2001**, *114*, 4557–4565. [PubMed]

14. Willis, N.D.; Cox, T.R.; Rahman-Casañs, S.F.; Smits, K.; Przyborski, S.A.; van den Brandt, P.; van Engeland, M.; Weijenberg, M.; Wilson, R.G.; de Bruïne, A.; et al. Lamin A/C Is a Risk Biomarker in Colorectal Cancer. *PLoS ONE* **2008**, *3*, e2988. [CrossRef] [PubMed]

15. Gruenbaum, Y.; Goldman, R.D.; Meyuhas, R.; Mills, E.; Margalit, A.; Fridkin, A.; Dayani, Y.; Prokocimer, M.; Enosh, A. The nuclear lamina and its functions in the nucleus. *Int. Rev. Cytol.* **2003**, *226*, 1–62. [PubMed]

16. Qi, R.; Xu, N.; Wang, G.; Ren, H.; Li, S.; Lei, J.; Lin, Q.; Wang, L.; Gu, X.; Zhang, H.; et al. The lamin-A/C-LAP2α-BAF1 protein complex regulates mitotic spindle assembly and positioning. *J. Cell Sci.* **2015**, *128*, 2830–2841. [CrossRef] [PubMed]

17. González-Granado, J.M.; Silvestre-Roig, C.; Rocha-Perugini, V.; Trigueros-Motos, L.; Cibrián, D.; Morlino, G.; Blanco-Berrocal, M.; Osorio, F.G.; Freije, J.M.P.; López-Otín, C.; et al. Nuclear envelope lamin-A couples actin dynamics with immunological synapse architecture and T cell activation. *Sci. Signal* **2014**, *7*, ra37. [CrossRef] [PubMed]

18. Broers, J.L.; Raymond, Y.; Rot, M.K.; Kuijpers, H.; Wagenaar, S.S.; Ramaekers, F.C. Nuclear A-type lamins are differentially expressed in human lung cancer subtypes. *Am. J. Pathol.* **1993**, *143*, 211–220. [PubMed]

19. Moss, S.F.; Krivosheyev, V.; de Souza, A.; Chin, K.; Gaetz, H.P.; Chaudhary, N.; Worman, H.J.; Holt, P.R. Decreased and aberrant nuclear lamin expression in gastrointestinal tract neoplasms. *Gut* **1999**, *45*, 723–729. [CrossRef] [PubMed]

20. Agrelo, R.; Setien, F.; Espada, J.; Artiga, M.J.; Rodriguez, M.; Pérez-Rosado, A.; Sanchez-Aguilera, A.; Fraga, M.F.; Piris, M.A.; Esteller, M. Inactivation of the lamin A/C gene by CpG island promoter hypermethylation in hematologic malignancies, and its association with poor survival in nodal diffuse large B-cell lymphoma. *J. Clin. Oncol.* **2005**, *23*, 3940–3947. [CrossRef] [PubMed]

21. Tilli, C.M.L.J.; Ramaekers, F.C.S.; Broers, J.L.V.; Hutchison, C.J.; Neumann, H.A.M. Lamin expression in normal human skin, actinic keratosis, squamous cell carcinoma and basal cell carcinoma. *Br. J. Dermatol.* **2003**, *148*, 102–109. [CrossRef] [PubMed]

22. Maresca, G.; Natoli, M.; Nardella, M.; Arisi, I.; Trisciuoglio, D.; Desideri, M.; Brandi, R.; D'Aguanno, S.; Nicotra, M.R.; D'Onofrio, M.; et al. LMNA knock-down affects differentiation and progression of human neuroblastoma cells. *PLoS ONE* **2012**, *7*, e45513. [CrossRef] [PubMed]

23. Skvortsov, S.; Schäfer, G.; Stasyk, T.; Fuchsberger, C.; Bonn, G.K.; Bartsch, G.; Klocker, H.; Huber, L.A. Proteomics profiling of microdissected low- and high-grade prostate tumors identifies Lamin A as a discriminatory biomarker. *J. Proteome Res.* **2011**, *10*, 259–268. [CrossRef] [PubMed]

24. Jansen, M.P.; Machiels, B.M.; Hopman, A.H.; Broers, J.L.; Bot, F.J.; Arends, J.W.; Ramaekers, F.C.; Schouten, H.C. Comparison of A and B-type lamin expression in reactive lymph nodes and nodular sclerosing Hodgkin's disease. *Histopathology* **1997**, *31*, 304–312. [CrossRef] [PubMed]

25. Ollion, J.; Cochennec, J.; Loll, F.; Escudé, C.; Boudier, T. TANGO: A generic tool for high-throughput 3D image analysis for studying nuclear organization. *Bioinformatics* **2013**, *29*, 1840–1841. [CrossRef] [PubMed]

26. Natarajan, S.; Begum, F.; Gim, J.; Wark, L.; Henderson, D.; Davie, J.R.; Hombach-Klonisch, S.; Klonisch, T. High Mobility Group A2 protects cancer cells against telomere dysfunction. *Oncotarget* **2016**, *7*, 12761–12782. [CrossRef] [PubMed]

27. Huang, S.; Risques, R.A.; Martin, G.M.; Rabinovitch, P.S.; Oshima, J. Accelerated telomere shortening and replicative senescence in human fibroblasts overexpressing mutant and wild-type lamin A. *Exp. Cell Res.* **2008**, *314*, 82–91. [CrossRef] [PubMed]

28. Gonzalo, S. DNA Damage and Lamins. In *Cancer Biology and the Nuclear Envelope*; Schirmer, E.C., de las Heras, J.I., Eds.; Springer: New York, NY, USA, 2014; Volume 773, pp. 377–399. ISBN 978-1-4899-8031-1.

29. Gonzalez-Suarez, I.; Redwood, A.B.; Perkins, S.M.; Vermolen, B.; Lichtensztejin, D.; Grotsky, D.A.; Morgado-Palacin, L.; Gapud, E.J.; Sleckman, B.P.; Sullivan, T.; et al. Novel roles for A-type lamins in telomere biology and the DNA damage response pathway. *EMBO J.* **2009**, *28*, 2414–2427. [CrossRef] [PubMed]

30. Rengstl, B.; Kim, S.; Döring, C.; Weiser, C.; Bein, J.; Bankov, K.; Herling, M.; Newrzela, S.; Hansmann, M.-L.; Hartmann, S. Small and big Hodgkin-Reed-Sternberg cells of Hodgkin lymphoma cell lines L-428 and L-1236 lack consistent differences in gene expression profiles and are capable to reconstitute each other. *PLoS ONE* **2017**, *12*, e0177378. [CrossRef] [PubMed]

31. Bronshtein, I.; Kepten, E.; Kanter, I.; Berezin, S.; Lindner, M.; Redwood, A.B.; Mai, S.; Gonzalo, S.; Foisner, R.; Shav-Tal, Y.; et al. Loss of lamin A function increases chromatin dynamics in the nuclear interior. *Nat. Commun.* **2015**, *6*, 8044. [CrossRef] [PubMed]

32. Wood, A.M.; Rendtlew Danielsen, J.M.; Lucas, C.A.; Rice, E.L.; Scalzo, D.; Shimi, T.; Goldman, R.D.; Smith, E.D.; Le Beau, M.M.; Kosak, S.T. TRF2 and lamin A/C interact to facilitate the functional organization of chromosome ends. *Nat. Commun.* **2014**, *5*, 5467. [CrossRef] [PubMed]

33. Knecht, H.; Righolt, C.; Mai, S. Genomic Instability: The Driving Force behind Refractory/Relapsing Hodgkin's Lymphoma. *Cancers (Basel)* **2013**, *5*, 714–725. [CrossRef] [PubMed]

34. Guffei, A.; Sarkar, R.; Klewes, L.; Righolt, C.; Knecht, H.; Mai, S. Dynamic chromosomal rearrangements in Hodgkin's lymphoma are due to ongoing three-dimensional nuclear remodeling and breakage-bridge-fusion cycles. *Haematologica* **2010**, *95*, 2038–2046. [CrossRef] [PubMed]

35. Knecht, H.; Johnson, N.A.; Haliotis, T.; Lichtensztejn, D.; Mai, S. Disruption of direct 3D telomere–TRF2 interaction through two molecularly disparate mechanisms is a hallmark of primary Hodgkin and Reed–Sternberg cells. *Lab. Investig.* **2017**, *97*, 772–781. [CrossRef] [PubMed]

36. Knecht, H.; Mai, S. The Use of 3D Telomere FISH for the Characterization of the Nuclear Architecture in EBV-Positive Hodgkin's Lymphoma. *Methods Mol. Biol.* **2017**, *1532*, 93–104. [CrossRef] [PubMed]

37. Chuang, T.C.Y.; Moshir, S.; Garini, Y.; Chuang, A.Y.-C.; Young, I.T.; Vermolen, B.; van den Doel, R.; Mougey, V.; Perrin, M.; Braun, M.; et al. The three-dimensional organization of telomeres in the nucleus of mammalian cells. *BMC Biol.* **2004**, *2*, 12. [CrossRef] [PubMed]